Estimating Catchment Sediment Yield:

Development of the GIS-based CALSITE model

Dr P A Bradbury
N J Lea
Dr P Bolton

Report OD 125
April 1993

HR Wallingford

Registered Office: HR Wallingford Ltd. Howbery Park, Wallingford, Oxfordshire, OX10 8BA, UK
Telephone: 0491 35381 International + 44 491 35381 Telex: 848552 HRSWAL G.
Facsimile: 0491 32233 International + 44 491 32233 Registered in England No. 1622174

Contract

This report describes work carried out as part of the Overseas Development Unit's (ODU) research programme funded by the Overseas Development Administration of the British Government's Foreign and Commonwealth Office, through its Engineering Division headed by Mr T D Pike. The ODU is part of HR Wallingford Limited, and is headed by Dr K Sanmuganathan. The ODU's research on erosion control is headed by Dr P Bolton. The work described in this report is part of this research was undertaken in collaboration with the National Irrigation Agency of the Philippines, whose representative was Mr R L Baloloy. The HR job number was TPS 112/64

Mr N J Lea was responsible for initial development of the CALSITE and HR_CASCADE software models described in this report. Dr P A Bradbury was the principal author of this report and undertook model validation and further software developments. Dr P Bolton was Project Manager for this study and guided the development of physical concepts of the model.

Prepared by Peter A. Bradbury (name) Senior Scientist (Job title)

Approved by K. Sanmuganathan HEAD/ODU.

Date 13/9/93

Summary

Estimating Catchment Sediment Yield:
Development of the GIS-based CALSITE model

Dr P A Bradbury
N J Lea
Dr P Bolton

Report OD 125
April 1993

This report provides details of the initial developments of the CALibrated SImulation of Transport Erosion (CALSITE) model, which is designed to enable the prediction of soil erosion and sedimentation within a catchment. It presents details of the theoretical concepts of the model and the results of the initial testing of the software for the Magat catchment in Luzon, Philippines.

The CALSITE model combines a soil erosion model, currently the Universal Soil Loss Equation (USLE), with sediment routing techniques in order to determine sediment delivery. The model uses Geographical Information System (GIS) technology to enable the spatial variation of soil erosion to be analysed, so that areas of high soil erosion can be identified and the effects of soil conservation programmes or land use change can be visualised. Sediment yield estimates may be calibrated each time the model is run by using observed sediment measurements from within the catchment.

Version I of the CALSITE model was configured for use in the Philippines and relies upon data analysed on a specific GIS. The model is currently being generalised for use in Sri Lanka and Thailand on Standard IBM/PC compatibles without the requirement for specific GIS software of hardware.

For further information on CALSITE please contact:

Dr. Peter A Bradbury
Overseas Development Unit
HR Wallingford Limited
Howbery Park
Wallingford
Oxfordshire OX10 8BA

tel +44 491 835381
fax +44 491 826352

Contents

Contents continued

Contents *continued*

Figures

Appendices

1 Introduction

1.1 Overview of the Work Programme

The Overseas Development Unit (ODU) of HR Wallingford Ltd, UK and the National Irrigation Administration (NIA), Government of the Philippines have been undertaking a programme of collaborative work since 1984. The aim of this work was to develop methods to quantify the effectiveness of reforestation in controlling sediment yield within the Magat catchment of Central Luzon, and to predict future sediment deposition in a large, recently constructed reservoir.

The work programme has enabled the development and testing of techniques for the field measurement of sediment discharge from several river sites in the catchment, as described by Dickinson et al. (1990) and Dickinson and Reid (1993). Techniques for the computer modelling of soil erosion and sediment delivery have been developed in parallel with the field measurements using a geographical information system (GIS) for the combined analysis of different types of map data. As a result of these studies version 1.0 of the CALSITE software package was delivered to NIA, in February 1992, enabling the modelling of the effects of changing land use within the Magat catchment on the sediment yield of the catchment into the reservoir. This report describes the methodology of the sediment delivery model and provides some examples of its predictive capabilities.

1.2 The Study Area

The Magat catchment is located approximately 350km north of Manilla in North Central Luzon, the Philippines, as shown in Figure 1.1. The catchment is bounded on three sides by major mountain systems which have high relief and steeply dissected topography. The Magat River originates at an elevation of 1200m and flows through a broad alluvial valley in a north-easterly direction as shown in Figure 1.1.

Rainfall in the Philippines is dominated by two tropical monsoon seasons: November to April and June to November. Seventy percent of the annual rainfall in the Magat catchment falls during the June to November 'south-east' monsoon period usually in the form of a few very intensive storms or typhoons. Average annual rainfall for the catchment has been estimated at 2500mm, but may reach 4000mm in the highest mountains.

Catchment soils are generally shallow, acidic and of a fine loamy to clayey texture. An assessment undertaken in the mid-1970s indicated that land use and vegetation within the catchment consisted of primary and secondary forest (42%), scrubland and grassland (36%), agricultural crops such as rice (21%) and other uses such as settlement and water bodies (1%) (NIA & Engineering Consultants Inc., 1978). A classification of Landsat MSS satellite data of 1987, which was undertaken by HR as a part of this study, resulted in similar land cover statistics: primary forest 16%, secondary forest 31%, open grassland 32%, rice cultivation 15%, settlement, water bodies and other uses 6%. Uncontrolled logging operations, overgrazing, shifting cultivation and severe fires in the catchment have resulted in severe to excessive erosion in a large proportion of the catchment.

In 1975 the Magat River Multipurpose Project (MRMP) was set up by NIA to harness water in the catchment for irrigation and power generation. The main component of the MRMP was the construction of the Magat Dam between

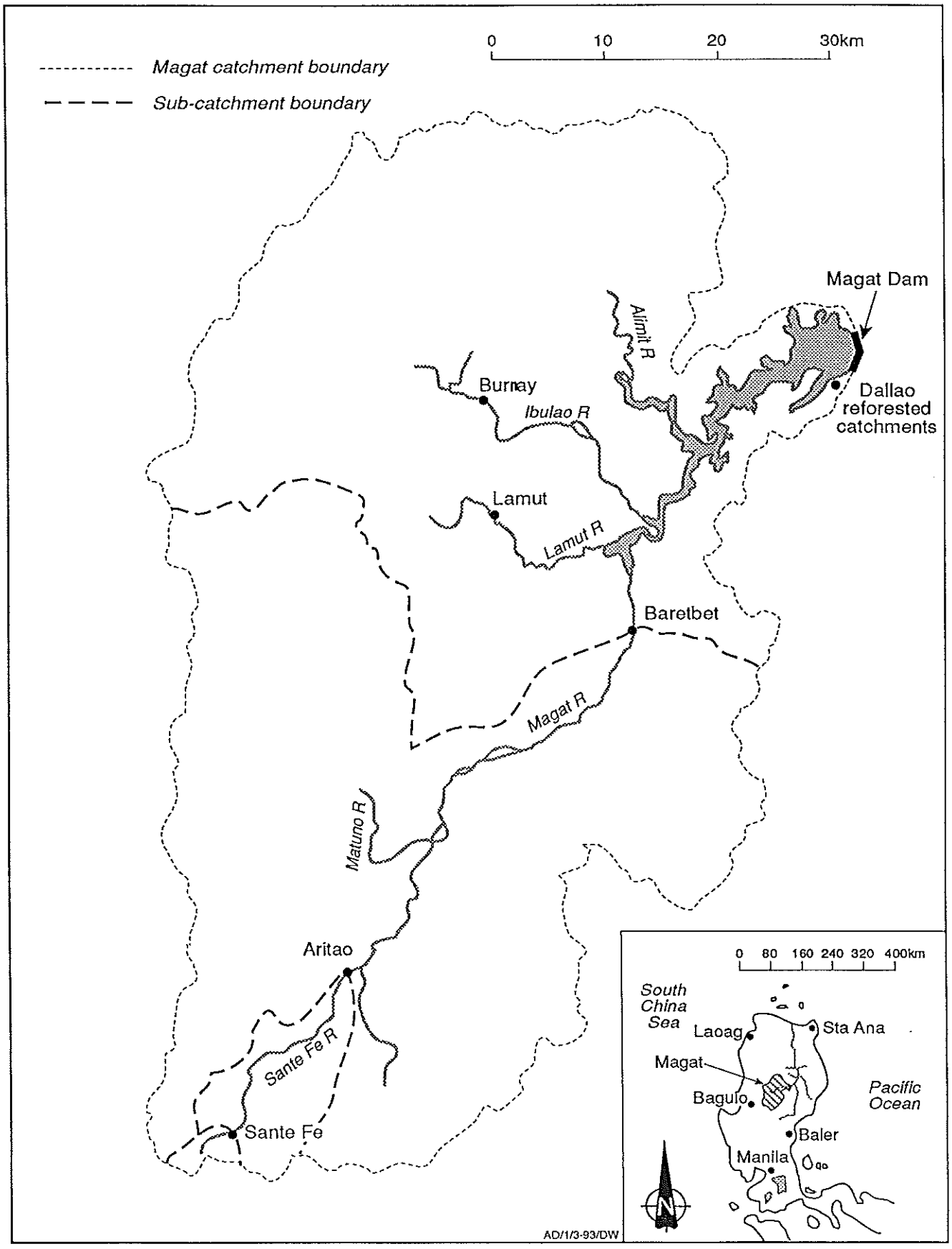

Figure 1.1 Location Map of Magat Catchment, Luzon, Philippines

1975 and 1982 which has resulted in the formation of a large reservoir in the north east of the catchment, as shown in Figure 1.1, holding up to 1090 X $10^6 m^3$ of water.

A feasibility study carried out in 1976 estimated that sediment would be deposited into the reservoir at the rate of 20 t ha^{-1} yr^{-1} giving a design life expectancy of 100 years (NIA & Engineering Consultants Inc., 1978). Doubt was cast on this estimate when a hydrographic survey of the reservoir carried out in 1984, 32 months after the completion of the dam construction, calculated the rate of sedimentation as 38 t ha^{-1} yr^{-1}. Unfortunately this figure was in error due to a misunderstanding over the date at which impoundment began. A reassessment of results from the 1984 survey and a subsequent survey in 1988/89 is presented in Appendix 1 and shows a mean sediment yield at the reservoir of approximately 24 t $ha^{-1}yr^{-1}$ over a 7 year period.

In order to reduce soil erosion and consequent reservoir sedimentation a reforestation programme was initiated in 1982 using Ipil Ipil, Yemane and Japanese Acacia species. Measurements of the sediment yield from two small reforested sub-catchments, taken between 2 and 6 years after tree planting, indicated that soil loss was less than 0.6 t ha^{-1} yr^{-1} (Amphlett and Dickinson, 1989).

1.3 Programme for the Field Measurement of Sediment Discharge

During the initial stages of the collaborative work the above hydrographic survey of the reservoir was undertaken and sediment yield was measured from the two small reforested catchments at Dallao, near to Magat Dam (Woolridge, 1986; Amphlett and Dickinson, 1989). The results of both these surveys, which are outlined above, indicated the great potential of reducing soil erosion by reforestation.

Between 1986 and 1991 sediment discharge measurements were taken for three sites along the Magat and Santa Fe Rivers, representing three nested sub-catchments, as shown in Figure 1.3. These measurements were undertaken in order to provide information for the study of sediment transport and delivery processes. They also provide a useful set of measurements for assessing the effects of different types of land use on soil erosion. The sedimentation data for the years 1986 to 1988 have been analysed and are reported in Dickinson et al (1990). Sediment measurements for the years 1986 to 1991 are reported in Dickinson and Reid (1993) and are reviewed here.

Sediment samples were taken using a system of pump sampling, developed over several years by HR (Brabben et al., 1991). The technique involves the lowering of a pipe and attached sinker weight into a river from a cableway or bridge, then extracting river water at various depths using a pump installed on the river bank.

Table 1.1 summarises the sediment yield estimates for the three sub-catchments for the years 1986 to 1988.

Table 1.1 Sediment Yield Observations in t $ha^{-1}yr^{-1}$ (After Dickinson and Reid, 1993)

Site	Aritao	Baretbet	Burnay	Lamut	Santa Fe
Area (km^2)	144	2149	28.6	17.9	15.0
Year	Soil Loss (t/ha)				
1986	22.0	(17.0-33.5)[1]	-	-	39.7
1987	0.6	4.0	-	-	1.5
1988	(3.5-7.0)[2]	20.8	-	-	5.4
1989	-	(0.3-0.4)	-	4.1	(12.7-29.6)
1990	-	(19.7-26.0)	(5.5-8.8)	13.1	-
1991	-	(5.0-7.0)	-	-	41.3
Average	9.3	13.2	7.2	8.6	21.8

[1] = Uncertainty due to problem of choosing gradient of sand concentration rating curve

[2] = Uncertainty due to unknown change time between discharge ratings

1.4 Objectives of Sediment Yield Modelling

The prediction of sediment yield in developing countries is usually difficult because of the lack of suitable data and an appropriate predictive technique. Although numerous techniques have been developed to predict soil erosion and sediment delivery, as described in Chapter 2, they are normally either very simplistic and unrealistic, based on only one or two factors, or are extremely complex, requiring data which are not easily available in developing countries. Most of the predictive techniques have also been developed in climatic and geomorphological zones which are very different to those generally found in developing countries.

Early formulae for the calculation of soil erosion were designed to be applied either to individual sites or to the whole catchment using data averaged over the catchment. The development of computer models in the 1970s allowed soil erosion within a catchment to be analysed in more detail, either by dividing the area with a regular grid and calculating the erosion for each grid cell or 'pixel', or by dividing the catchment into sub-catchments. As noted above, such computer models have largely been inappropriate for use in developing countries.

The objective of this study is to develop a computer model of sediment delivery which is suitable for use in developing countries with a limited data set. The following types of data are generally available and may be used for such a model:

i) a topographic map;
ii) a soil map;
iii) a land use map or remotely sensed data for the production of such a map;
iv) total annual rainfall measurements for a sufficient number of sites within and near to the catchment for spatial variability in rainfall to be assessed;
v) direct measurements of annual sediment load at several locations in the catchment over several years.

In the model described in this report, data items i) to iv) are input to a GIS, using scanning or digitising devices, then processed to produce an estimate of the soil erosion generated by each pixel. These estimates are referred to as 'source erosion' which is represented as a 'source erosion' map. Digital elevation data within the GIS are then used to calculate the routes of overland flow within the catchment and to estimate the delivery ratio of each pixel.

The delivery ratio, DR_p, may be defined for an individual pixel as:

$$DR_p = \frac{\text{Sediment from the source pixel reaching a specified catchment outlet}}{\text{Sediment eroded at the source pixel}} \qquad \text{Equation 1.1}$$

A map showing the variation in DR_p over the catchment is used in conjunction with the map of soil erosion at source to provide a map of 'transported erosion'. The term 'transported erosion' was newly proposed for this work. It is used to indicate the amount of material eroded from each pixel which reaches a specified catchment outlet; in this case the individual contribution of each pixel to the sediment discharge into the reservoir. Values of transported erosion, therefore, depend upon the choice of catchment outlet. At this stage the transported erosion values may be summed and the total calibrated using the available field measurements of sediment discharge (item v) to produce more realistic absolute values.

A map of source erosion is useful in highlighting areas of severe soil erosion for the planning of a soil conservation programme. Similarly a map of transported erosion is useful in planning catchment management with regard to the potential for reducing the sediment load in rivers at specified points downstream. The model can be used not only to estimate the proportion of the reservoir sediment currently being produced from a specific site but also to predict the likely reduction in sediment yield resulting from proposed catchment management or soil conservation measures. Conversely the increase in sediment yield caused by changes in land use, such as deforestation, increased grazing or fires, or the effects of abnormal rainfall regimes can be predicted by the model.

The model may also be a useful aid for the prediction of the expected life of a reservoir, in terms of the time taken for the reservoir to fill to an unusable level. Although the model could be used in the absence of field measurements of sediment discharge to produce an estimate of expected life, the resulting estimates are likely to be very inaccurate, due to the inherent

inaccuracies of available erosion predictors. The calibration of the estimates using field measurements of sediment discharge for one or more year is therefore essential. If, for example, reliable sediment discharge measurements were only available for the year 1985 then the model estimates could be calibrated using these values in conjunction with rainfall and land use information for the same year. Any known variations in rainfall and land use in subsequent years could be input to the model and used to produce modified sediment discharge estimates for such years. The predictions of future discharge values could similarly be made based upon average rainfall conditions and expected land use. It should be stressed, however, that the errors inherent in sediment discharge measurements and erosion prediction result in large margins of potential error even in estimates produced from a calibrated model.

The main objective of the model is therefore to provide information to aid the planning and management of a soil conservation programme within a catchment. It should enable the identification of priority areas for soil conservation and predict the effects of natural or man-made environmental changes on soil erosion and sediment delivery. The model may also be useful in obtaining more reliable estimates of the design life of a reservoir when used in conjunction with limited field measurements of sediment discharge.

1.5 Report Structure

The main purposes of this report are to explain the methodology of the model and to provide some examples of its predictive capabilities.

Existing soil erosion and sediment delivery models are briefly discussed in Chapter 2. Chapter 3 presents an outline of the methodology of the model and its computer implementation. The main stages of the model are then described in the order that they are undertaken.

Chapter 4 explains how the topographic and soil maps, remotely sensed data, rainfall data and sediment discharge measurements are processed to provide input data for the calculation of source erosion. The method used to calculate soil erosion is described in Chapter 5 and the resulting map or image is illustrated. Chapter 6 discusses the techniques used to produce an image showing the change in sediment delivery ratio over the whole of the catchment. This image is combined with the source erosion image to produce a transported erosion image showing the amount of eroded soil which reaches the reservoir from every location within the catchment, as described and illustrated in Chapter 7. The method of calibrating transported erosion using field measurements is also described in Chapter 7.

Chapter 8 reviews the results of the model for both the existing land use situation and for possible land use and rainfall scenarios within the Magat basin. Chapter 9 summarises the model as a whole and makes some suggestions for future developments.

2 An overview of existing models

2.1 Introduction

Numerous techniques have been developed to predict the soil loss from land or the consequent sediment deposition in water bodies. The ability to predict soil erosion aids land managers in choosing crops and management techniques that keep soil erosion within tolerable limits. Techniques for the estimation of sediment yield are used by engineers to estimate the design life of reservoirs and other hydraulic structures and to plan programmes to protect them from sedimentation effects.

The earliest predictive tools for soil erosion and sedimentation consisted of fairly simple formulae or nomographs, based upon empirical studies, that were designed for the prediction of soil loss at the site level. Many of these early formulae have been used or adapted for use within more recently developed 'models' of soil erosion or sedimentation. The term 'model' has tended to be used since the 1970s in place of 'theory' or 'formula', as discussed by Philip (1991), and implies an attempt to simulate the natural processes of reality, often by simplifying them. In recent years quite complex physically-based erosion models have been developed with the aim of increasing our understanding of the nature and interaction of environmental processes, as well as providing a predictive ability. However, the term model may equally be applied to the simplest of empirical formulae.

Models may be classified hierarchically according to the system shown in Figure 2.1, based upon a classification system suggested by Becker and Serban (1990). The initial distinction in modelling is between 'deterministic' and 'stochastic' models. Whereas deterministic models presume that a certain set of events lead to a uniquely definable outcome, stochastic models presuppose the outcome to be uncertain and are structured to accommodate this uncertainty (Addiscott, 1993). Few soil erosion or sediment yield models adopt a stochastic approach, although such an approach would be valid given that many of the factors used to predict soil erosion are uncertain, notably rainfall.

Deterministic models may be sub-divided into three types: 'empirical', 'conceptual' and 'physically-based'. It should be noted that some authors use the term 'deterministic' to refer only to 'physically-based' models. An empirical or 'black-box' model, is based solely on the statistical relationships between different environmental factors, that have been established from field observations and experiments, without any regard for how or why such relationships occur. A physically-based model is based upon physical laws and attempts to model individual physical processes. The distinction between empirical and physically-based models is not clear cut. Between the two extremes are models which are based upon concepts about physical laws but rely on empirical data. These are termed 'conceptual' models. Physically-based models are often developed with the aid of empirical data, either by making use of laws which themselves were derived empirically, or by using empirical data to test and modify the final version of the model.

Physically-based models are seen as more useful than empirical models because they can provide a greater understanding of processes and enable parameter values to be set using established physical properties. The development of physically-based soil erosion and sedimentation models is,

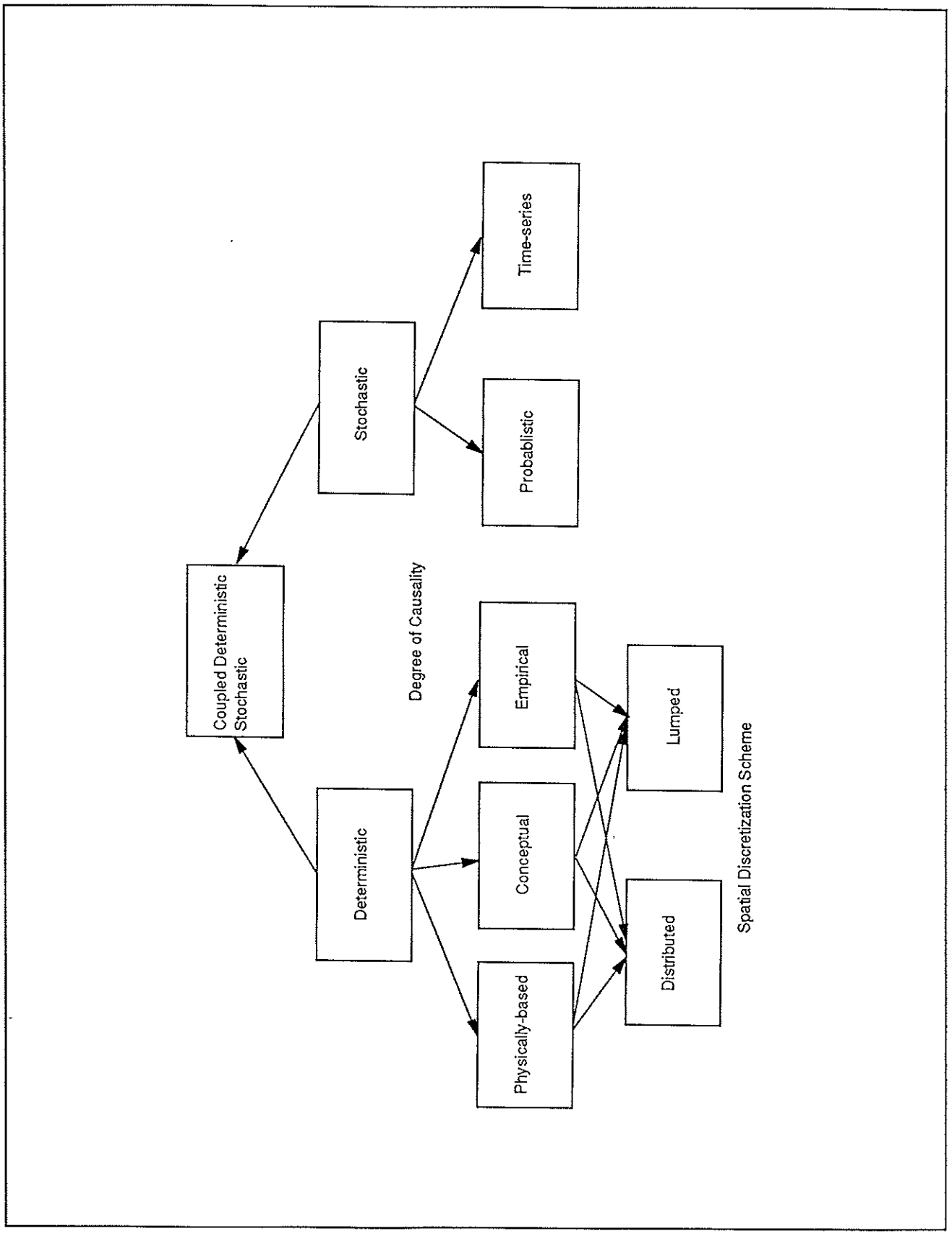

Figure 2.1 A Classification of Models

however, still in its infancy and it may be several years before they are used as predictive tools. Those which have been developed tend to be very complex and demanding in terms of input data parameters and computer processing time. Furthermore few physically-based models have been validated with observed data for a wide range of environments. Empirical models and formulae tend to be simple to use and have often been tried and tested in a number of different environments.

Models may be further subdivided into 'lumped' and 'distributive' on the basis of the type of spatial unit used. Initial attempts at estimating soil erosion over the whole of a catchment were based upon 'lumped' parameter values which, it was hoped, represented average values for the whole of the catchment. Models which consider the spatial variation or distribution of environmental conditions within a catchment are termed 'distributive'. Such models are likely to be more realistic than lumped models, as spatial variations in environmental conditions are often marked. They also provide useful information for resource planning within a catchment and enable the effects of different types of development to be assessed and compared. Distributive models require the overlay of many 'layers' of spatial data, usually within a Geographic Information System (GIS). Frequently input data to 'distributive' models are provided on a 'raster' basis in the form of a grid of rectangular cells or pixels. Beven (1989) considers that such 'subgrid lumping' can provide measurement problems and, in the case of physically-based models, conceptual problems. The approximation of parameters over space is inevitable in catchment modelling and occurs when point data are interpolated or averaged, when remotely-sensed and map data are used as input and often within a GIS to enable different types of data to be overlain.

The increasing use of computers since the late 1970s has led to two notable trends in modelling. Firstly the development of GIS techniques has enabled distributive models to become a useful tool for catchment and regional planning. Secondly the increasing power of computers has enabled more complex physically-based models to be developed.

In summary, the state-of-the-art of technology and our understanding of erosion processes allows soil erosion and sediment yield to be modelled and predicted at the catchment level on personal computers using proven statistical models and often fairly limited input data. Although many physically-based models have been developed over recent years we have not yet reached the stage when they have been sufficiently validated and easily adapted for practical use. Therefore, an alternative modelling approach, such as described in this report, is needed.

2.2 Historical Developments

A major catalyst to soil erosion research was the Dust Bowl crisis of the 1930s in mid-western USA. Large areas of land were subject to severe erosion as a result of unsuitable arable cultivations. This resulted in loss of soil fertility and high reservoir siltation rates. Experimental research was initiated, based upon small run-off plots, to determine soil erosion rates under a range of physical and agricultural conditions. This work led to the development of the Universal Soil Loss Equation (USLE) (Wischmeier and Smith, 1958) which has enabled land managers, in the USA and elsewhere, to estimate existing soil erosion on a field by field basis and to choose, where necessary, alternative crops or management techniques when predicted erosion rates are unacceptable. It

should be noted that the USLE was developed for use on arable, gently sloping land and in a region where the climate is fairly temperate.

The early soil erosion research that took place in the USA formed the basis for several soil conservation programmes throughout the world. As the USLE was based only upon data from the USA it has to be modified for sites where climatic, geomorphic and land use conditions are different to those of the USA. In response, some soil conservation programmes in tropical countries conducted their own soil erosion research and modified the USLE to make it more applicable to their own conditions. The Soil Loss Estimator of Southern Africa or SLEMSA (Elwell, 1980) is one such adaptation of the USLE.

The USLE is essentially an empirical formula designed to predict soil erosion on a field by field basis for detailed land use planning. Attempts were made to use it to estimate erosion at catchment scale but to simplify the calculations, reduced variability was assumed. Some techniques were also developed from the 1960s onwards, such as the Fournier Equation (Fournier, 1960), for estimating soil erosion, using data which were averaged or 'lumped' over the whole catchment. As a result it was not possible to identify the locations within the catchment where soil erosion was most intense. It was not until the development of GIS technology in the 1970s and 1980s when formulae such as the USLE could be rigorously applied for catchment planning.

Formulae for the determination of overland flow and sediment yield were developed, mainly in the 1970s, based upon flow and sediment measurements and upon experimental data from laboratory flumes and canal sections. Walling (1983) reviews several formulae which have been developed to determine the delivery ratio based upon geomorphological and hydrological parameters of a catchment. Such types of formulae have been incorporated into some soil erosion models so that sediment yield estimates can also be made over a catchment. Thus by calculating the product of source erosion and the delivery ratio at each point within a catchment, sediment yield values may be obtained and the contribution of different locations within the catchment to sediment yields may be assessed. The computer models CREAMS (USDA, 1980) and AGNPS (Young et al., 1987) are two examples of the use of USLE and a delivery ratio within a GIS.

In parallel to the development of relatively simple, largely statistically based, formulae and GIS-based models for field and catchment erosion prediction, several workers made use of computer technology to develop more complex physically-based mathematical models. Many of these models are reviewed by White (1987).

The Stanford Watershed Model (Crawford and Lindley, 1966) is a computer-based hydrological model which has been used for predicting sediment loads (Negev, 1967; David and Beer, 1975a, 1975b). David and Beer (1975a, 1975b) attempted to break down soil erosion into splash, sheet, rill and gully erosion rather than use empirical data for soil erosion as whole. More recently in the USA, physically-based erosion models have been developed such as RUNOFF (Borah, 1989) and KYERMO (Hirschi and Barfield, 1988) as research models rather than practical tools. Currently in the USA a major project called the Water Erosion Prediction Project (WEPP) is being undertaken with the aim of providing a physically-based sediment yield model, based upon an IBM PC/AT, that will replace the use of USLE by land managers (Lafflen et al., 1991).

In Europe, Kirkby (1974) has developed physically-based formulae for the determination of overland flow and sediment yield. Morgan et al. (1986) have developed a physically-based erosion model which has been validated for 67 sites in 12 countries. A physically-based hydrological model known as System Hydrologique Europeen or SHE has been developed over several years by organisations in The Netherlands, UK, France and Denmark (Abbot et al., 1986) and has recently been adapted to provide sediment transport information (Bathurst, 1992).

The following sections review a number of different types of soil erosion and sediment yield prediction techniques and some of the computer-based catchment models which are currently available. Tables 2.1 and 2.2 summarise the details of a number of erosion prediction techniques and models. It was considered beyond the scope of this report to describe in detail each technique, however references are provided for further reading.

2.3 Techniques of Soil Erosion Prediction

The USLE and the SLEMSA techniques, listed in Table 2.1, are designed for use by land managers in the field or office to predict on-site soil erosion.

The USLE equation is based upon the statistical analysis of about 10 000 plot-years of experiments in central USA. The output from the equation is an estimate of long term average sheet and rill erosion. The equation has the general form:

$$E_a = R \times K \times LS \times C \times P \qquad \text{Equation 2.1}$$

where

E_a = estimated average annual soil loss;
R = rainfall erosivity;
K = soil erodibility;
LS = slope length and steepness factor;
C = cropping and management factor;
P = conservation practice factor.

Precise definitions of these variables are given in Wischmeier and Smith (1958; 1978) and many text books. Once the existing soil erosion of a site has been estimated the effects of changing crop type and management on soil erosion may be determined. Such changes may result in lower values for the C and P factors (obtained from tables), and, where the construction of terraces are considered, may result in lower L and S values.

The USLE is an empirical relationship that has been established between 6 environmental factors. It could be argued that the USLE has some physical basis as the equation assumes that soil erosion is due to a combination of rainfall erosivity, soil erodibility, site and management factors. One deficiency of the USLE is that, as mentioned previously, it is based upon experimental data from arable land in mid-western USA. Furthermore it does not take into account the contribution of gully and channel erosion to sedimentation.

The SLEMSA technique is based upon statistical data gathered in Zimbabwe and consists of three sub-models to account for soil loss estimation from bare soil (RK), slope steepness and length (RX) and crop type and cropping practices (RC). Average annual soil erosion is then determined by the following equation:

Table 2.1 Soil Erosion / Sediment Yield Models - Manual

Name	Inputs	Output	Reference
Universal Soil Loss Equation (USLE)	Slope length, steepness, rainfall intensity, soil erodibility, cropping management	Average annual soil loss	Wischmeier & Smith (1978)
Soil Loss Estimator for Southern Africa	Slope length, steepness, rainfall energy, soil erodibility, land use	Average annual soil loss	Elwell (1978)
Fournier equation	Slope, mean height, monthly & annual rainfall	Mean suspended sediment yield	Fournier (1960)
Soil erosion design curve	Slope, mean height, monthly & annual rainfall, USDA soil type, land use	Mean suspended sediment yield	Al Kadhimi (1982)
Kirkby overland flow formula	Annual & mean rainfall / day, soil water storage capacity	Annual overland flow	Kirkby (1974)
Kirkby sediment yield method	Slope, elevation, overland flow	Sediment yield	Kirkby (1974)
Fleming sediment yield method	Catchment area, land use, annual discharges	Annual suspended sediment load	Fleming (1969)
Douglas suspended yield model	Effective precipitation	Mean annual sediment yield	Douglas (1967)
Douglas sediment load model	Relief/length ratio, rainfall seasonality & volume, % forest, bifurcation ratio	Mean annual sediment load	Douglas (1968)

Table 2.2 Soil Erosion / Sediment Yield Models - Computer

Name	Inputs	Output	Reference
Stanford watershed model	Area, slope, hourly and daily rainfall, potential evaporation, storage infiltration, interflow, stream characteristics, solar radiation, min/max temperatures	Runoff hydrographics for individual events	Crawford & Linsley (1966)
Negev model	Hourly rainfall, Runoff from Stanford model	Daily suspended sediment loads	Negev (1967)
David & Beer model	Not known Runoff from Stanford model	Daily suspended sediment loads	David & Beer (1957a, 1975b)
Gupta & Solomon model	Topography, hourly rainfall, soil type, land use & cover, no., length & order of streams, daily temps	Runoff & sediment yield	Gupta & Solomon (1977)
WASCH model	Not known	Erosion and sediment yield	Bruce et al. (1975)
Smith model	Not known	Water and sediment hydrographs through a storm	Smith (1977)
Strathclyde sediment erosion-transport-deposition models	Topography, hourly or daily rainfall, potential evaporation, soil type, vegetation type & densities	Erosion and sediment and water yield	Fleming & Walker (1976)
CSU model	Not known	Erosion, sediment yield, particle size distribution of eroded sediment	Li (1977)
ANSWERS model	Not known	Erosion and sediment yield hydrographs for single events	Beasley (1977)

OD 125 16/04/93

Table 2.2 (continued) Soil Erosion / Sediment Yield Models - Computer

Name	Inputs	Outputs	Reference
CREAMS (Chemical Runoff and Erosion from Agricultural Management Systems)	Not known (Soil erosion based on ULSE)	Erosion, sediment yield, particle size distribution of sediment	USDA (1980)
Institute of Hydrology (IoH) model	Rainfall intensity, evaporation	Runoff hydrographs for individual events	Moore & Clarke, (1983)
EPIC (Erosion Productivity Impact Calculator) model	Not known	Effect of erosion on crop yield. Estimates sediment yield	Williams et al. (1982)
SPUR (Simulation of Production and Utilisation of Rangelands)	Channel/distribution of slopes, daily rainfall, soil type, land cover 7 area, solar radiation, min/max temperatures	Optimum management systems for rangeland	Wight (1983)
KYERMO (Kentucky Erosion Model)	Slope, surface roughness, rainfall intensity, soil type	Runoff and sediment transport	Hirschi & Barfield (1988)
RUNOFF model	Rainfall intensity, raindrop diameter, soil type, vegetation cover density	Soil erosion, sediment transport	Borah (1989)
SMODERP (Simulation Model of Surface Runoff and Erosion Process)	Rainfall, soil type, vegetation type, crop management, slope steepness & length	Surface runoff & permissible slope length	Holy et al (1989)

Table 2.2 (Continued) Soil Erosion / Sediment Yield Models - Computer

Name	Inputs	Output	Reference
AGNPS (Agricultural Non-Point Source Pollution Model)	Land use, soil type, slope steepness & length, aspect, rainfall amount & intensity	Soil erosion by particle size class, pollutants	Young et al (1987)
GAMES	Rainfall, soil erodibility land-management, surface roughness, slope steepness & length, hydraulic condition	Soil erosion, sediment delivery at site and catchment level	Cooke et al (1985)
THEPROM	Soil type, rainfall erosivity, slope steepness & length	Soil erosion & productivity index values	Biot (1990)
SHE (Systeme Hydrologique Europeen)	Rainfall, evapotranspiration, vegetation, drainage, topography, soil moisture	Run-off hydrographs	Abbot et al (1986)
SHETRAN-UK	Based upon SHE	Run-off, sediment transport, contaminant migration	Bathurst (1992)

E_a = RK x RX x RC Equation 2.2

As with USLE, tables and equations presented in detail in Elwell (1980) are used to determine the contribution of each environmental parameter to the average soil loss.

Whilst empirical techniques for soil erosion assessment, such as the USLE, relate environmental parameters to overall erosion values obtained from plot measurements, conceptual and physically-based models attempt to sub-divide erosion into its constituent processes: splash, sheet, rill and/or gully erosion. Figure 2.2 shows how Meyer and Wischmeier (1969) break down soil erosion into detachment by rainfall and by runoff. Morgan et al. (1986) relate splash erosion to rainfall intensity using the physical relationship established by Meyer (1981) which has been modified to take account of the effects of soil and crop type. The ANSWERS model of Beasley et al (1980) calculate soil detachment by rainfall and runoff using empirical relationships with factors used by the USLE.

Foster (1990) summarises the different processes being modelled as a part of the WEPP work programme. These processes consist of splash erosion in the inter rill areas, detachment by overland flow in the rill areas and detachment by channel flow in gullied land and along river banks. No physically-based soil erosion model appears to have yet successfully modelled all of the above processes.

2.4 Techniques of Sediment Yield Prediction

In common with erosion modelling most sediment yield models are deterministic rather than stochastic. Some stochastic sediment yield models have been developed, e.g. Murota and Hashino (1969) and Woolhiser and Todorovic (1974), which provide information on the time variability of sediment yield phenomena. Deterministic sediment yield models may be subdivided into empirical, conceptual and physically-based, as shown in Figure 2.1. Neibling and Foster (1977) provide early examples of each of these types of models:

i) Empirical - those which relate sediment yield to morphological characteristics of the catchment as a whole;

ii) Conceptual - those which use the USLE as the basis for soil erosion prediction then modify erosion estimates to take into account the delivery ratio;

iii) Physically-based - those which have separate components for each erosion and sediment transport process.

Empirical equations for determining the sediment delivery ratio are reviewed by Walling (1983). These use morphological factors such as: relief (or altitudinal range), length, area, bifurcation ratio and drainage density. Table 2.3 provides details of the several formulae which have been derived. Small steep catchments generally have higher delivery ratios than larger and more gently sloping catchments, where a higher proportion of eroded material is redeposited. The delivery ratio may be multiplied by an estimate of soil erosion per unit area to provide estimates of sediment yield. Some empirical techniques are available for determining sediment yield directly from catchment characteristics (Niebling and Foster, 1977).

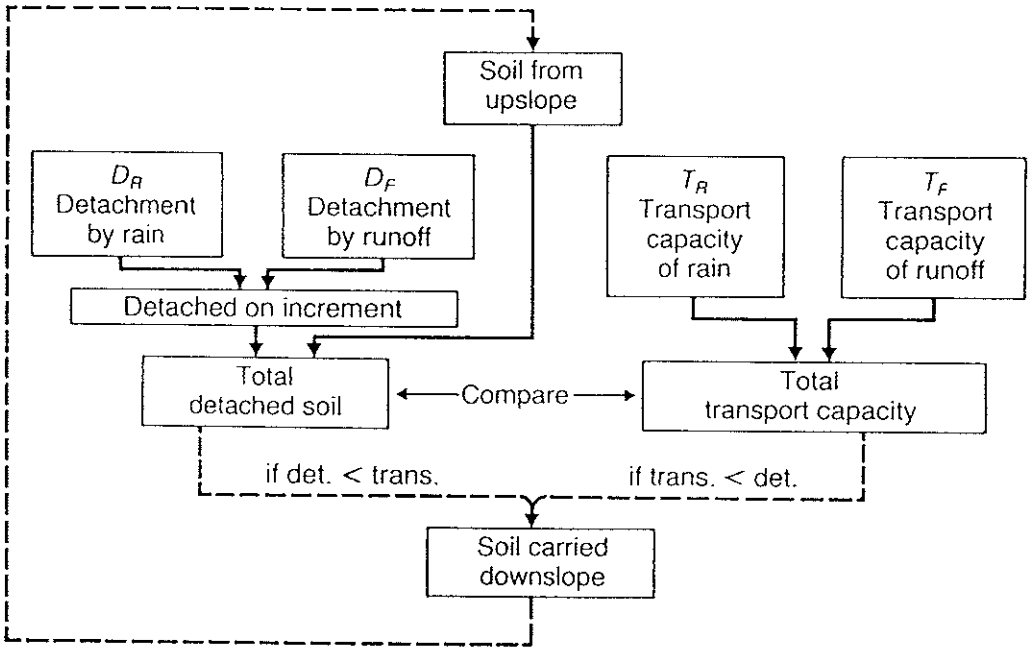

$D_R = k_1 A I^2$

$D_F = k_2 A S^{2/3} Q_w^{2/3}$

$T_R = k_3 S I$

$T_F = k_4 S^{5/3} Q_w^{5/3}$

Where A = area, I = rainfall intensity,

S = ground slope ($\sin \theta$),

Q_w = runoff

Figure 2.2 Flow chart for modelling processes of soil erosion by Water (after Meyer and Wischmeier, 1969)

Fournier (1960) developed an empirical relationship which was designed to enable sediment yield of the catchment to be predicted from monthly and annual rainfall amount and catchment slope and shape. Although the technique has been used to estimate sediment yield (e.g. Russell, 1981) it can only make very approximate estimates since it does not take into account the effects of soil and vegetation characteristics and it uses a rather crude estimate of rainfall erosivity (i.e. (monthly rainfall)^2/annual rainfall). A similar technique for erosion prediction at the catchment level has since been developed by Al Kadhami (1982) known as the 'soil erosion design curve'. This empirical technique enables erosion rates and sediment yields to be predicted from average values for the whole catchment of slope, rainfall, soil type, farming practice and disturbance.

Williams (1975) and Foster (1982) developed the Modified USLE or MUSLE to calculate annual sediment yield (Y_a) due to sheet-rill erosion at the outlet of a small catchment using the following modification of USLE, which basically replaces rainfall erosivity with an estimate of overland flow:

$$Y_a = 9.05\ (V_a.Q_p)^{0.56}.K.LS.C.P \qquad \text{Equation 2.3}$$

where V_a = annual runoff volume,
Q_p = peak runoff, and
K, LS, C, P = USLE factors listed above.

Some distributive sediment yield models, such as CREAMS, GAMES and AGNPS, calculate the erosion rate by the USLE then convert these values to sediment yield by multiplying by delivery ratio values for each spatial unit of the model. Such models have mainly been configured to analyse a database of field cells or units, rather than being implemented on a GIS.

Distributive models of sediment yield need to determine the volume and distribution of overland and channel flow within a catchment that will transport eroded material. Kirkby (1974) calculates annual overland flow rates using a formula which determines the daily rainfall in excess of soil water storage capacity. A kinematic routing algorithm is sometimes used to determine the paths of overland flow within a watershed (e.g. Smith (1977) and Li (1977)).

The AGNPS model uses the empirical USLE formula to calculate soil erosion within each grid cell of a catchment then a physically-based routing equation derived to progressively determine the amount of sediment which is deposited or discharged downstream (Young et al., 1989). This equation uses an estimate of the effective transport capacity of runoff which is a function of channel flow velocity.

Meyer and Wischmeier (1969) and Morgan et al. (1976) are two early examples of models which determine both erosion and sediment transport using physical bases. Figure 2.2 illustrates the Meyer and Wischmeier (1969) model. Morgan et al. (1976) calculate the transport capacity of overland flow using an equation developed by Kirkby (1974) which depends upon the volume of overland flow, the slope steepness and the effect of crop cover.

One limitation of the two above models is that they are designed for use on field sized areas rather than whole catchments. There are currently very few entirely physically-based distributive models which can model soil erosion and sediment transport within a catchment area. The ANSWERS model (Beasley

et al, 1980) uses physically-based equations for soil erosion by rainfall and overland flow together with a transport capacity equation similar to that of Kirkby (1974). However the model was found to be very sensitive to changes in soil variables when implemented on a GIS and applied to an area of the Netherlands (De Roo et al., 1989). In the USA the WEPP project aims to use a combination of erosion and hydrological models to predict catchment sediment transport (Lafflen et al., 1991).

2.5 Future Modelling Requirements

Current research in soil erosion and sediment transport is focusing upon the development of physically-based models which can provide a greater understanding of the processes involved. Whilst there have been many developments of physically-based models we have not yet reached the stage when they can replace empirical and conceptual models for operational prediction. The current generation of physically-based models have not been sufficiently validated using observed data or are not sufficiently distributive to allow their use as catchment management tools.

The increasing availability and efficiency of GIS technology have resulted in computer modelling being seen as a useful tool for land resource managers, rather than just a preoccupation of research scientists. When erosion and sediment transport models have been installed on GISs land managers are able to examine the implications of different development scenarios. In the USA, conceptual erosion models such as AGNPS have been implemented on a GIS and used to choose agricultural management systems which will minimise soil erosion and water pollution (Prato et al., 1989; Panuska et al., 1991). Similarly in Canada the GAMES model has been found to be useful for targeting agricultural pollution (Dickinson et al., 1986).

There appears to be little current use of GIS-based erosion models for planning in the developing world. De Meijere et al (1988) provide one example of how estimates of soil erosion made on a GIS can be used to determine the suitability for coffee planting in Southern Sumatra, Indonesia. There appears, however, to be considerable scope for the use of the proven erosion and sediment transport models within a GIS environment as an aid to land management in tropical countries where erosion is most severe. The CALSITE model described in the following chapters addresses this need and demonstrates how even a small amount of measured sediment discharge data may be used to improve the reliability of sediment yield prediction.

Table 2.3 Examples of proposed relationships between sediment delivery ratio and catchment characteristics (after Walling, 1983)

Author	Region	Equation
Maner (1958)	Kansas, USA	log DR = 2.962 + 0.869 log R - 0.854 log L
Roehl (1962)	southeastern USA	log DR = 4.5 - 0.23 log 10 A - 0.510 x colog R/L - 2.786 log BR
Williams and Berndt (1972)	Brushy Creek, Texas, USA	$DR = 0.627\ SLP^{0.403}$
Williams (1977)	Texas, USA	$DR = 1.366 \cdot 10^{-11}\ A^{-0.100}\ R/L^{0.363}\ CN^{5.444}$
Mutchler and Bowie (1975)	Pigeon Roost Creek, Mississippi, USA	DR = 0.488 - 0.006 A + 0.010 RO
Mou and Meng (1980)	Dali River Basin Shaanxi, China	DR = 1.29 + 1.37 ln Rc - 0.025 ln A

DR = sediment delivery ration; R = basin relief; L = basin length; A = basin area; R/L = relief/length ratio; BR = bifurcation ratio; SLP = % slope of main stem channel; CN = S.C.S. curve number; RO = annual runoff; Rc = gully density.

Note: Units vary between equations.

3 An overview of CALSITE

3.1 Introduction

The CALSITE model, for the **CAL**ibrated **SI**mulation of Transported Erosion, uses the combination of the USLE and a delivery ratio function to determine the sediment yield from a catchment. The sediment yield values are then calibrated using sediment measurements made at one or more points along the river network. The model enables estimates to be made of sediment yield at any required point within the catchment. In addition the model produces of a map of 'transported erosion' indicating the origins of river sediment. This map may be useful for identifying priority sites for soil conservation measures which are aimed at reducing sediment yield from a catchment.

CALSITE may be classified as a distributed-conceptual-deterministic model, according to the classification system shown in Figure 2.1. It is deterministic because it produces one result from a single set of input data. It is conceptual because it is uses formulae which are based upon general physical concepts but using exponents which have been derived empirically. It is distributed because it considers the spatial variation of soil erosion and sedimentation, and their influencing factors, within the catchment area.

Whilst CALSITE is similar in concept to the distributive sediment yield models based on the USLE, discussed in Section 2.4, there are two fundamental improvements. Firstly the model is implemented on a GIS to enable the spatial variation in erosion and sedimentation to be analysed. Secondly the model uses observed sediment data to calibrate erosion and sediment predictions.

Figure 3.1 shows the input and output data for the CALSITE model. In the descriptions which follow the capabilities of CALSITE Version 1.0 are given. A generalised version is, however, under development in which certain manipulations currently performed by separate software are incorporated.

The model uses rainfall data, remotely sensed data, and digitised topographic and soils maps to determine source soil erosion. Delivery ratio values are determined from a digitised topographic map. The input data needs to be 'pre-processed' prior to being used by the model in order to extract the required environmental characteristic, such as slope or land use, and to geometrically correct all data to the same map base. The output from the model is an image or map of transported erosion together with erosion and sediment yield estimates.

3.2 The GIS Implementation

The CALSITE model is implemented on a 'raster-based' GIS which uses a grid of rectangles or 'pixels' to define the catchment area and to enable the combined analysis of different types of spatial data. The current version of CALSITE is based upon an IBM PC/AT computer with a colour EGA or VGA screen, one Megabyte of internal memory and about 10 Megabytes of disk space.

The map data required for the model, such as topography, soils, land use and rainfall, are converted to 'raster images' whereby average values are determined for each pixel within the catchment, each pixel representing a

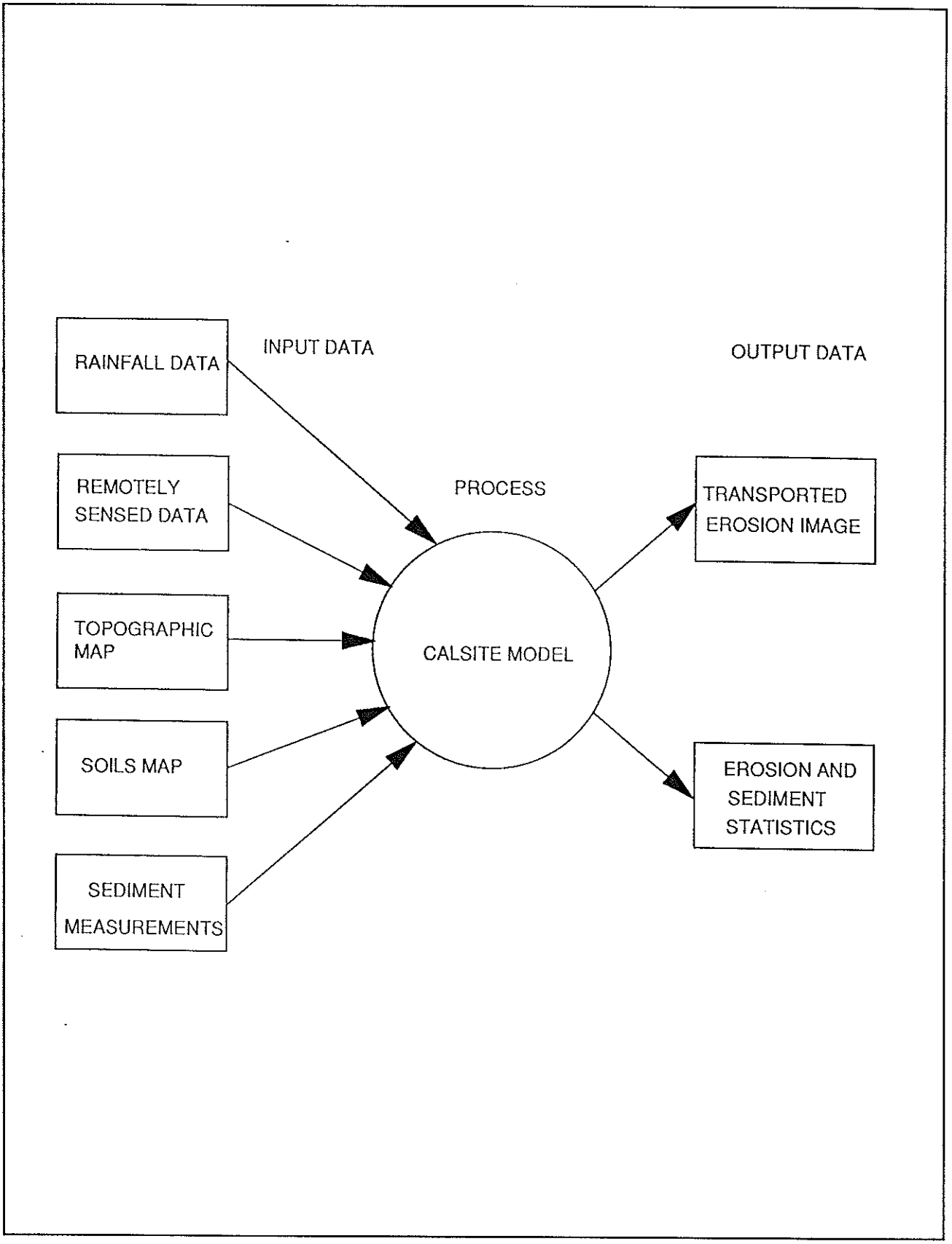

Figure 3.1 CALSITE Model - context data flow diagram

precise area on the ground. The resulting raster images may be displayed on a computer screen using colours to represent ranges of values.

Figure 3.2 shows how the tasks required for the CALSITE model can be sub-divided into the following three processes defined within circles:

i) Pre-processing of input data;

ii) Determination of delivery index;

iii) CALSITE model.

The digital data and maps are pre-processed into digital 'images' of rainfall, land cover, slope and soils for use by the 'Main model', as shown in Figure 3.2. An elevation image, produced by the pre-processing task is used to determine the delivery ratio which is then input to the main model in the form of a delivery map.

The software required to pre-process the input data and to determine the delivery ratio, tasks (i) and (ii) above, is currently based upon a GIS and image processing system called ICONOCLAST, developed by Image Technology Systems of Birmingham, UK. This system enables the digitisation of map data using a video camera, the classification and analysis of satellite imagery using image processing algorithms and the determination of slope and aspect using digital terrain model techniques.

The ICONOCLAST software is designed to be used with a high resolution monitor connected to a PC4000 framestore installed inside the IMB/PC AT computer. This hardware enables up to 4 different types of raster images, 768 by 768 pixels in size, to be stored in computer memory or framestore. Such images may be displayed as colour high resolution images on a special purpose colour monitor and processed rapidly by avoiding hard disk access. Although ICONOCLAST is fast and efficient, the cost of the software and additional hardware required makes it an expensive system and cheaper more flexible GIS alternatives are being investigated for the generalised version of CALSITE being developed.

Whilst the pre-processing of input data was possible using the ICONOCLAST software alone, the determination of sediment delivery is currently based upon software written in-house, called HR_CASCADE, which is designed for use with the ICONOCLAST hardware.

The CALSITE model itself is currently implemented as a stand-alone software package which, although based on GIS principles for the analysis of raster images, does not require to be used in conjunction with the ICONOCLAST GIS or any other commercial GIS. This makes the software package suitable for use as a low-cost soil conservation and land management tool by the land use planner.

The CALSITE package uses 'pull-down' menus to enable the user to display and manipulate raster images or maps which are displayed in colour on a standard EGA or VGA computer monitor, as described in the CALSITE User Manual (ODU, 1992).

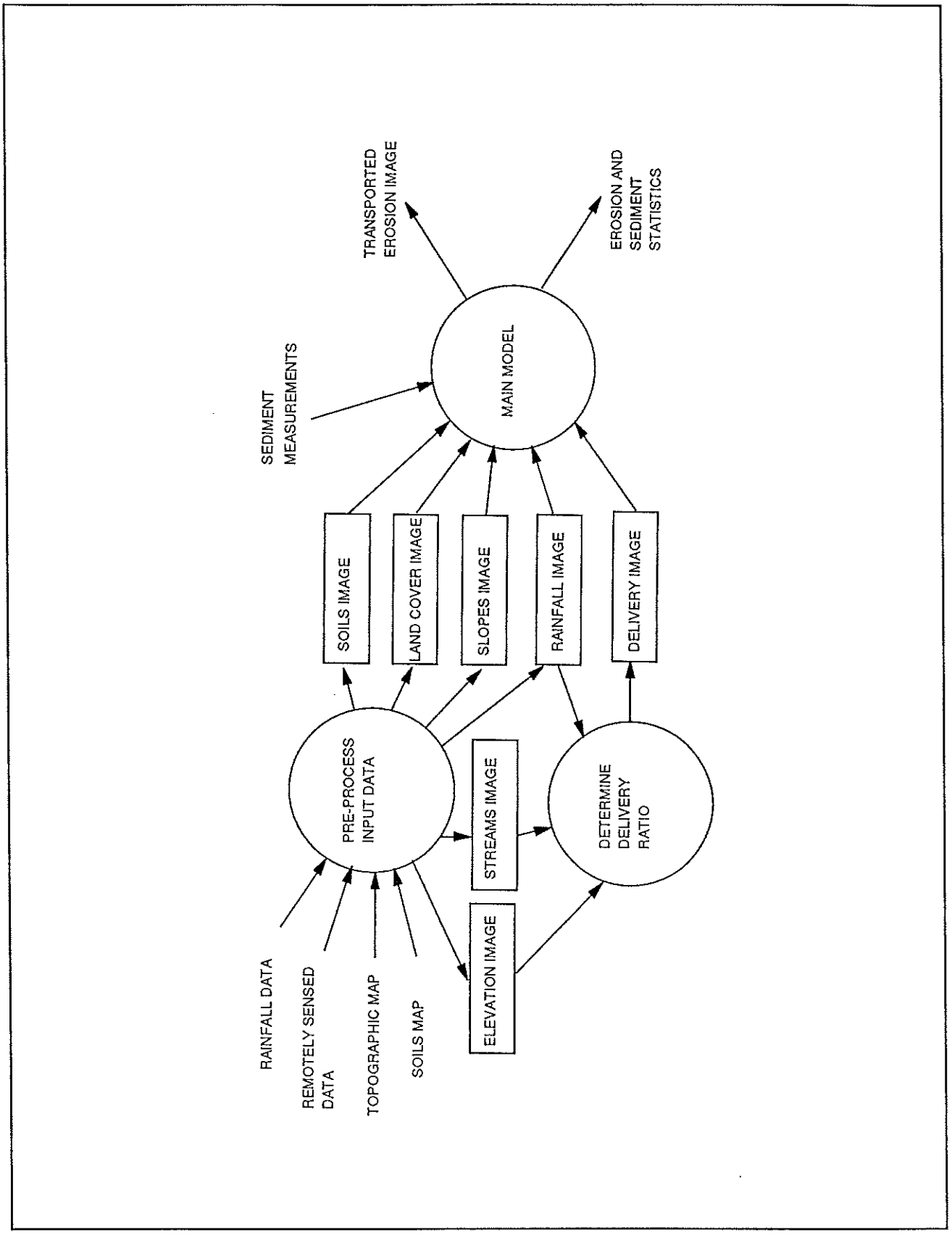

Figure 3.2 CALSITE Model - level 1 data flow diagram

3.3 Input Data and Pre-Processing Requirements

The minimum input data requirements for running the model are, as indicated in Figure 3.1:

i) **Rainfall Data** - for the production of a map showing the distribution of rainfall to be used to determine soil erosion and delivery index. In the case of the Magat catchment, the rainfall measurements were not well distributed spatially and interpolation was, therefore, undertaken using the rainfall-elevation model of Blyth and White (1990).

ii) **A Land Cover Map** - for the determination of soil erosion. This may be obtained from a land use map or from **remotely sensed data**, such as Landsat or SPOT satellite data.

iii) **A Topographic Map** - for the determination of a slope map, to be used to determine soil erosion and delivery index.

iv) **A Soils Map** - for the determination of soil erodibility and its effects on soil erosion.

v) **Sediment Discharge Measurements** - for the calibration of predicted rates of sediment yield and transported erosion.

The amount of pre-processing of the data required depends to some extent on the type of maps and input data that are available. In all cases it is necessary to digitise any paper maps using either a digitising tablet, scanner or a video camera. Digital data must be converted to the appropriate format for use by the CALSITE software. Furthermore all data sets must be geometrically rectified to a common map base in order that, for example, soils information can be overlain with land cover information.

Figure 3.3 shows how the pre-processing operations can be broken down into the following five tasks shown in circles. Each task is designed to produce input image data for the CALSITE model, and in the case of elevation, for the determination of the delivery ratio. The five tasks are:

a) 'determine rainfall' - from rainfall data (and if necessary an elevation image) ;

b) 'determine land cover' - from remotely sensed data (or map data if available);

c) 'determine elevation' - from a topographic map;

d) 'determine slopes' - from an elevation image;

e) 'digitise soils map'.

Chapter 4 describes each of these pre-processing tasks in detail.

For the Magat catchment discussed here, much time and effort was spent in the production of an accurate land cover map from satellite data. For other sites it may be possible to digitise existing land cover maps, or in some instances to make use of digital land cover data sets. However land cover can

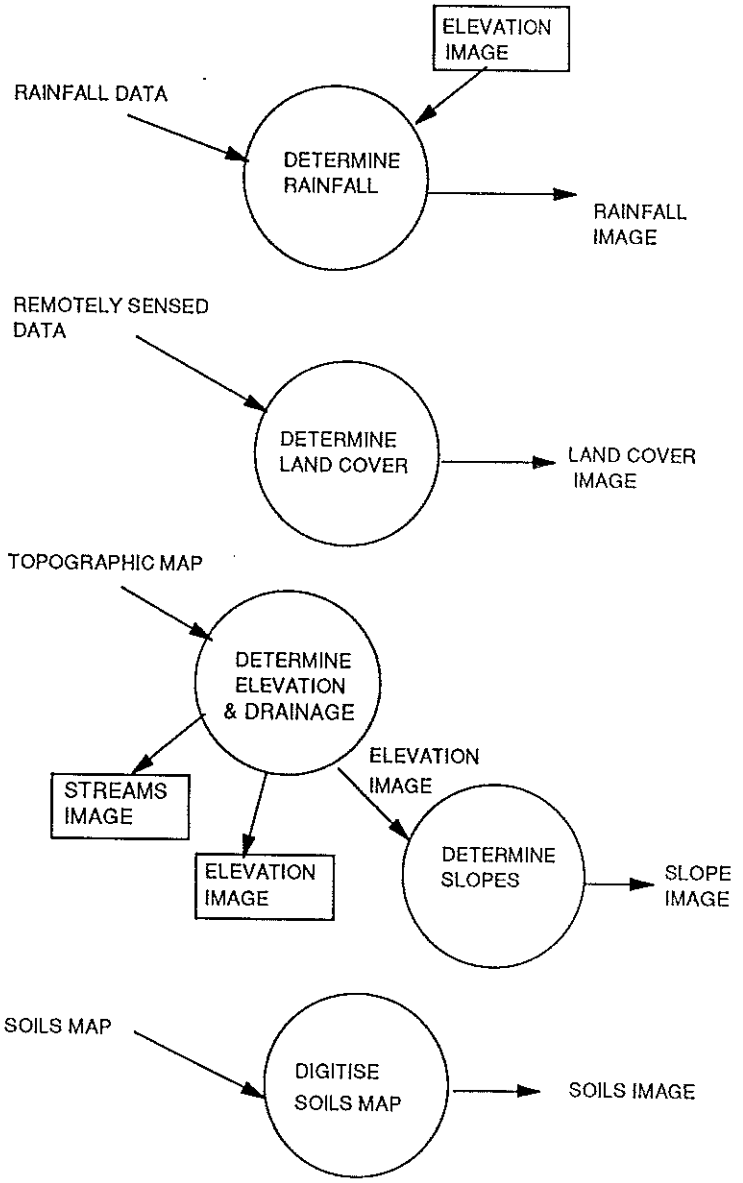

Figure 3.3 Pre-processing - level 2 data flow diagram

change rapidly so maps based on recent data, such as satellite imagery, are preferred.

As a part of the Magat study a topographic and a soils map were video digitised using the ICONOCLAST system. In the case of the soils map the information was converted to the required pixel size and format then coded according to soil erodibility. The topographic map was used to produce a map of slope, for the estimation of source erosion, and a map showing the delivery ratio.

3.4 Determination of Delivery Index

The production of a map showing the variation in delivery index over the catchment area is based on the analysis of a digital elevation data produced from a digitised topographic map. Values of delivery index are subsequently used to calculate the delivery ratio for individual pixels as defined in Equation 1.1. A software package called HR_CASCADE was developed to determine the delivery index. This package is based upon kinematic routing algorithms for overland flow which are applied to the elevation image, as described in Lea (1991).

The calculation of delivery index may be divided into two components: overland redeposition of eroded materials and river and floodplain redeposition. Overland redeposition is dependant on the length and slope of the flow path, and the overland discharge at each pixel (Foster and Meyer, 1975). River and floodplain redeposition is dependant on river channel dimensions and sediment and flow characteristics. The kinematic routing algorithms of HR_CASCADE are designed to enable the determination of the delivery index during the overland flow phase of sediment transport. For the Magat basin Atkinson (1992) has shown that once sediment reaches the river system a high proportion of this sediment will be transported downstream: river and floodplain redeposition is assumed to be negligible. In less mountainous catchments, a separate river sediment routing component may be required within CALSITE to model river and floodplain redeposition.

An index of sediment delivery during the overland flow phase is derived for the whole image by modelling the flow path from each pixel. The transporting capacity of a particular path is calculated as a function of the flow along it and the steepness of the terrain over which it passes. This function, which is described in Chapter 6, results in the production of a delivery image showing 'delivery index' values from 0 to 255. The delivery index (DI) is a measure of the transporting capacity of overland flow, 1 indicating low capacity and 255 indicating very high capacity.

The delivery index values are converted to delivery ratios from 0 to 1 within the CALSITE model using a conversion function which may be user-defined to take account of sediment measurements at various locations within the catchment. This aspect of the model is discussed in more detail in Chapter 6.

3.5 The Main CALSITE Model

3.5.1 Introduction

The main CALSITE model is currently implemented in a stand-alone software package which uses the input image files produced using the ICONOCLAST GIS, as illustrated in Figure 3.2. Field measurements of sediment discharge are used to calibrate the sediment yield and transported erosion estimates which form the main outputs of the model.

Figure 3.4 shows, in circles, the three main stages of the main CALSITE model. These are: the calculation of source soil erosion using the USLE; the calibration of erosion using the delivery image and observed values of soil loss; and the calculation of transported erosion based upon the source erosion and delivery images.

3.5.2 Calculation of Source Erosion

Soil erosion is calculated on a pixel by pixel basis using the following formula based on USLE (Wischmeier and Smith, 1978), for the determination of annual soil erosion (E_a):

$$E_a = R \times K \times LS \times CP \qquad \text{Equation 3.1}$$

where
- R = Rainfall erosivity;
- K = Soil erodibility;
- LS = Slope length and steepness factor;
- CP = A combined cropping management and conservation practice factor;

Some versions of USLE use a separate factor P, a conservation practice factor, whilst others, including CALSITE, modify the C factor to take account of the effects of soil conservation measures.

The four input images to the Calculate Source Erosion process, shown in Figure 3.4, are converted to USLE factor values then multiplied together to provide USLE estimates of annual soil loss. The USLE formula used by the model is therefore:

$$\text{Source Erosion Image} = f(\text{Rainfall Image}) \times f(\text{Soils Image}) \times f(\text{Slope Image}) \times f(\text{Land Use Image}) \qquad \text{Equation 3.2}$$

where f(Image) is a function of the original image.

Computer files containing 'Look Up Tables' or LUTs are used to convert image values to USLE factor scores. Thus for example in the case of a land use image the 'primary forest' class will be assigned the C factor of 0.002, or in the case of the soils image a 'clay-loam' soil will be assigned the K value of 0.26. The CALSITE model software allows the operator to enter and edit the values in the LUTs to enable the choice of factor scores which are appropriate to the conditions under study.

3.5.3 Calculation of calibrated transported erosion

The contribution made to annual sediment yield by each pixel within a catchment is termed 'transported erosion' (TE) and is calculated by the following equation:

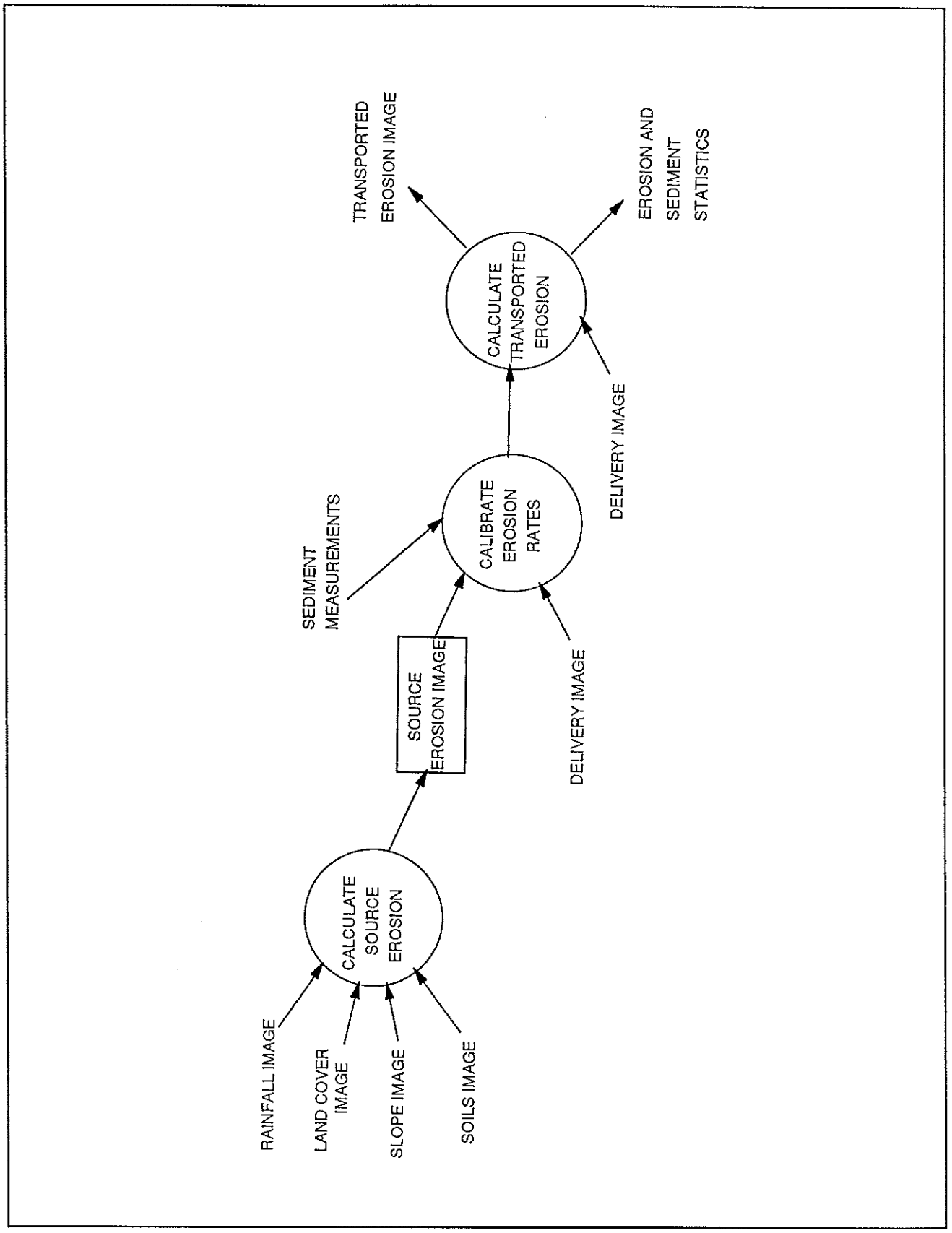

Figure 3.4 Main model - level 2 data flow diagram

$$TE = SE \times f(DI_p) \times k \qquad \text{Equation 3.3}$$

where:

SE	=	Source Erosion (from USLE);
DI_p	=	Delivery Index for a given pixel;
$f(DI_p)$	=	Calibrated Delivery Ratio;
k	=	Scaling Constant.

DI_p is described in Section 3.4 and defined in Chapter 6. The actual pixel delivery, as defined in Equation 1.1 applied to the outlet from the entire catchment, is the product of k times the calibrated delivery ratio, $f(DI_p)$.

The principal source of uncertainty in determining transported erosion is the proportion of source erosion which reaches the river system. The observed sediment yield measurements are therefore used to calibrate the delivery index values by minimising the variation between observed and predicted sediment.

The calculation of source erosion is designed to provide estimates in $t\ ha^{-1}\ yr^{-1}$ of soil loss on a pixel basis, based upon the USLE and experimental work undertaken in the Philippines. Should the overall magnitude of the soil erosion estimates be incorrect over the catchment as a whole the CALSITE model scales the transported erosion estimates using the Scaling Constant k in Equation 3.3.

An image showing the transported erosion of each pixel is displayed on the screen in order to enable the identification of areas which contribute greatly to reservoir sediment deposition. By editing the land-cover image the effects of land use change and land management practices may be modelled. Similarly the effects of different rainfall regimes on rates of sedimentation may be analysed.

The current version of the CALSITE software enables reports to be printed showing the mean annual transported erosion per 10 km or per 1 km grid square. Sediment yield values may also be predicted for user defined sub-catchments.

4 Pre-processing of input data

4.1 Input Data Used

The five types of input or source data used for the CALSITE model were outlined in Section 3.3 and shown in Figure 3.3. Four of these types are geographically distributed data from the Magat catchment area and their uses in CALSITE are described in this chapter and may be summarised below. The fifth type is annual sediment discharge data described in Chapter 8.

a) Rainfall data - annual rainfall data for the Consuelo meteorological station in the Magat catchment were used in conjunction with elevation data derived from a topographic map (see item c) and a rainfall-elevation model (Blyth and White, 1990) to produce an image showing rainfall distribution (Section 4.4).

b) Remotely sensed data - Landsat Multi-Spectral Scanner imagery on magnetic tape, dated 17 March 1987, was used in conjunction with field data on land use and vegetation cover to produce a land cover image (Section 4.5).

c) Topographic map - the 1:500 000 scale Tactical Pilotage Map (TPM) of Northern Luzon was digitised in order to produce an elevation image by means of the digital elevation model (DEM) software in ICONOCLAST. This image was used for the determination of slope, to provide overlaid flow paths and an image of the drainage network and for the interpolation of rainfall values (Section 4.6).

d) Soils map - the 1: 50 000 scale reconnaissance soil maps of the Bureau of Soils, Philippines dated 1978 were digitised to provide a soils image (Section 4.7).

4.2 Geometric Rectification

The image files used by the CALSITE model need to be geometrically rectified to a common map projection and coordinate system in order that they may be overlain. This may be achieved by identifying 'ground control points' on each image, for which map coordinates are known, and geometrically transforming the image to fit them.

In the case of the Magat catchment study the image data were rectified to latitude and longitude coordinates in degrees and minutes so that for example pixel (70,135) in each image corresponded to latitude 16 degrees 10' North and longitude 121 degrees East, where pixel (0,0) represents the bottom left of the image and each pixel represents 1/12th of a minute of both latitude and longitude. A single pixel therefore represents 150.8 m in the X direction and 154.9 m in the Y direction, and 2.36 ha in area. The overall size of the images used for the Magat catchment is 500 pixels in the X direction and 700 pixels in the Y direction.

4.3 Image Data Storage

Geometrically rectified images, each 500 by 700 pixels in size, are used to store 8-bit integer values (between 0 and 255) which describe the rainfall, soils, slope and land cover of the catchment. In order to convert the arbitrary integer values into meaningful values, in the case of the continuous variables, rainfall and slope, files containing 'look up tables' or LUTs which represent a chosen transformation function are used. Such LUTs provide a real value for each pixel value from 0 to 255, for example the LUT may convert the pixel value 100 in a rainfall image to an annual rainfall of 2345 mm.

In the case of discontinuous variables, soils and land use, an arbitrarily chosen integer value or range is linked to specific parameter value through the appropriate LUT. The creation of images and use of LUTs are described in more detail below.

4.4 Production of a Rainfall Image

For the calculation of source soil erosion an estimate of rainfall erosivity is required. Rainfall erosivity in the USLE is based upon total annual rainfall energy times the maximum 30 minute rainfall intensity, (EI_{30}). As insufficient detailed rainfall event data are available for the Magat catchment, rainfall erosivity was based upon annual rainfall totals, as described in Section 5.2.

Even standard rain gauges have a poor spatial distribution within the Magat catchment so in order to interpolate annual rainfall values, for each pixel a rainfall-elevation model was used as described below. The interpolation of rainfall data using Theissen polygons or Kriging was found to be unsuitable because the terrain is very mountainous and because rainfall is closely correlated with elevation. The use of a regression equation for elevation and rainfall for each year under study is preferred, however for many years rainfall data are restricted to only a small number of stations, and therefore a single regression equation was used.

An analysis of rainfall and elevation within the Magat catchment by Blyth and White (1990) showed that a linear relationship exists of the form:

$$\text{Rainfall} = A + (B \times \text{Elevation}) \qquad \text{Equation 4.1}$$

where Rainfall = annual rainfall in mm.
Elevation = elevation above sea level in m.

The values A and B vary from year to year but can be obtained by regression of the measured rainfall at Consuelo in the south west of the catchment by the following formulae, based upon rainfall data from 1959 to 1987.

$$A = 312 + 0.515\ R_c \quad (r^2 = 0.39) \qquad \text{Equation 4.2}$$

and

$$B = (2400 - A) / 707 \qquad \text{Equation 4.3}$$

where R = annual rainfall at Consuelo in mm.

Figure 4.1 shows the rainfall image produced for the Magat catchment. The values for annual rainfall, shown in brackets, are for the year 1986. The

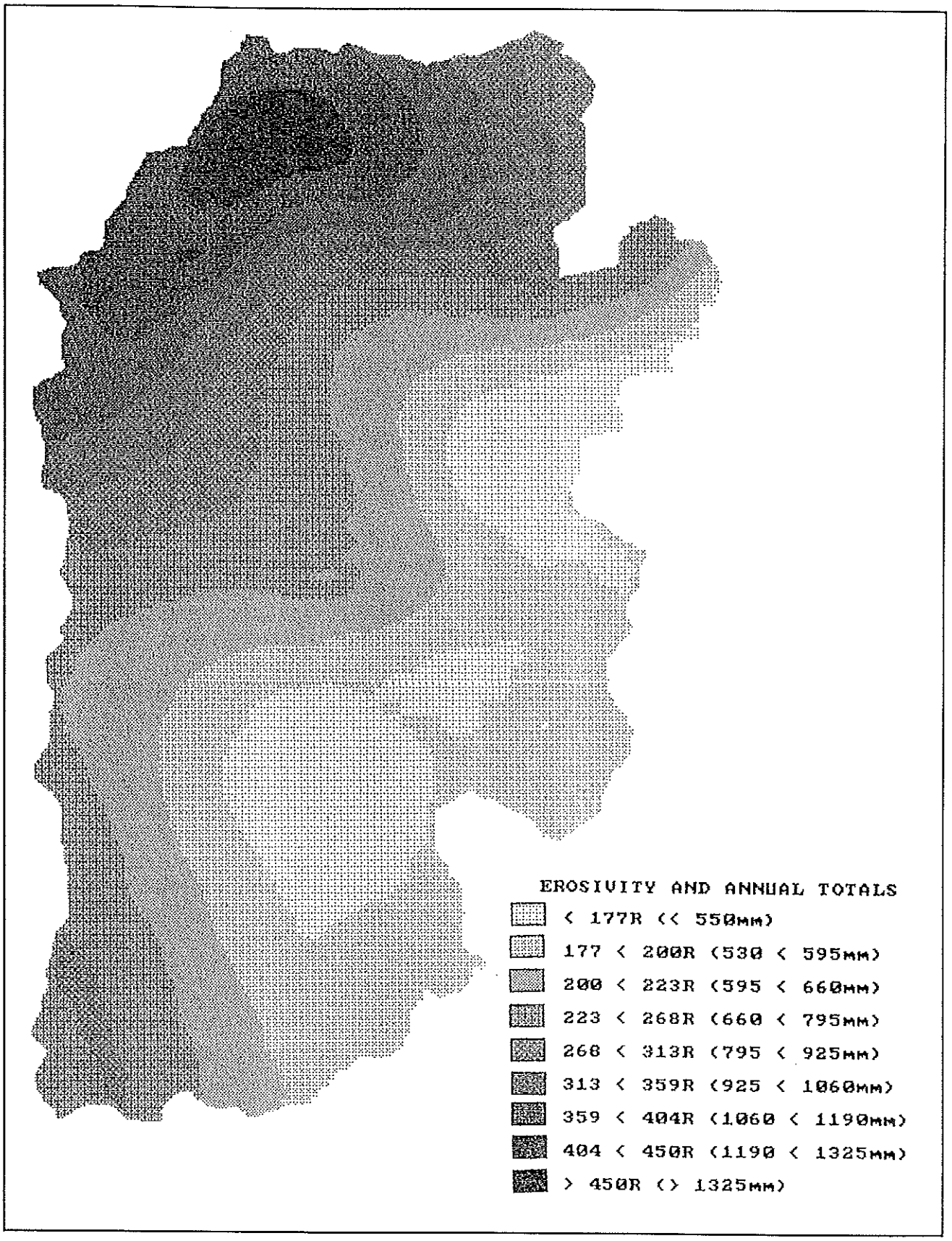

Figure 4.1 Rainfall image (1986)

rainfall erosivity values referred to in the key to this image are discussed in Section 5.2.

4.5 Production of a Land Cover Image

Although a land use map was available for the Magat catchment it was considered to be too inaccurate for use for soil erosion prediction. A classification of land use and vegetation cover was therefore undertaken using a satellite image.

The Landsat 4 Multi Spectral Scanner (MSS) image dated 17 March 1987 was considered to provide adequate information on land cover for the purposes of this study. Such imagery has a ground resolution of approximately 80 metres and four wavebands covering the green (0.5 - 0.6 microns), red (0.6 - 0.7 microns) and two near infrared (0.7 - 0.8 and 0.8 - 1.1 microns) parts of the spectrum. It enables the major land cover types such as forest, scrubland, grassland, arable land, settlement and water bodies to be distinguished based upon their spectral differences. The use of Landsat Thematic Mapper (TM) imagery, which has a higher spatial resolution and a greater number of infra-red wavebands, would have been preferable for land cover classification, however a clear image of the study area was not available.

There are two main types of digital classification, 'supervised' and 'unsupervised'. A supervised technique uses 'training data' located in areas of known land cover to define the spectral characteristics or 'signature' of particular land cover types, which are then used to classify an image into several cover types. An unsupervised technique involves the classification of an image into areas of similar spectral properties, which are subsequently related to land cover classes. For the Magat catchment area a supervised technique was used as this was considered most suitable for identifying specific cover types.

The Landsat digital data were read from a magnetic tape into the image processing system, then geometrically rectified, as described in Section 4.2. Field data and aerial photographs taken during March 1987 were used to provide training data for the generation of spectral signatures for a supervised digital classification. This involved the identification of areas of known land cover on a false colour Landsat image displayed on the computer screen, and the generation of spectral statistics. A 'maximum likelihood' algorithm was used to assign a classification to each pixel according to 8 main cover types. The resulting image is shown in Figure 4.2.

4.6 Production of an Elevation and Slope Image

In order to produce an elevation image for the production of both the rainfall and slope images contour lines from a topographic map were digitised then an elevation image created using the ICONOCLAST GIS software.

In the case of the Magat catchment the 1:500 000 Tactical Pilotage Map was digitised using a drum-scanner, which produces a more accurate result than by video digitising. Larger scale topographic maps were available but would have made scanning and data extraction extremely expensive. Once the topographic map had been digitised it was displayed on a computer screen and used in conjunction with a mouse to record spot heights throughout the catchment. A digital elevation model (DEM) within ICONOCLAST was then used to interpolate the series of spot heights to create an elevation image.

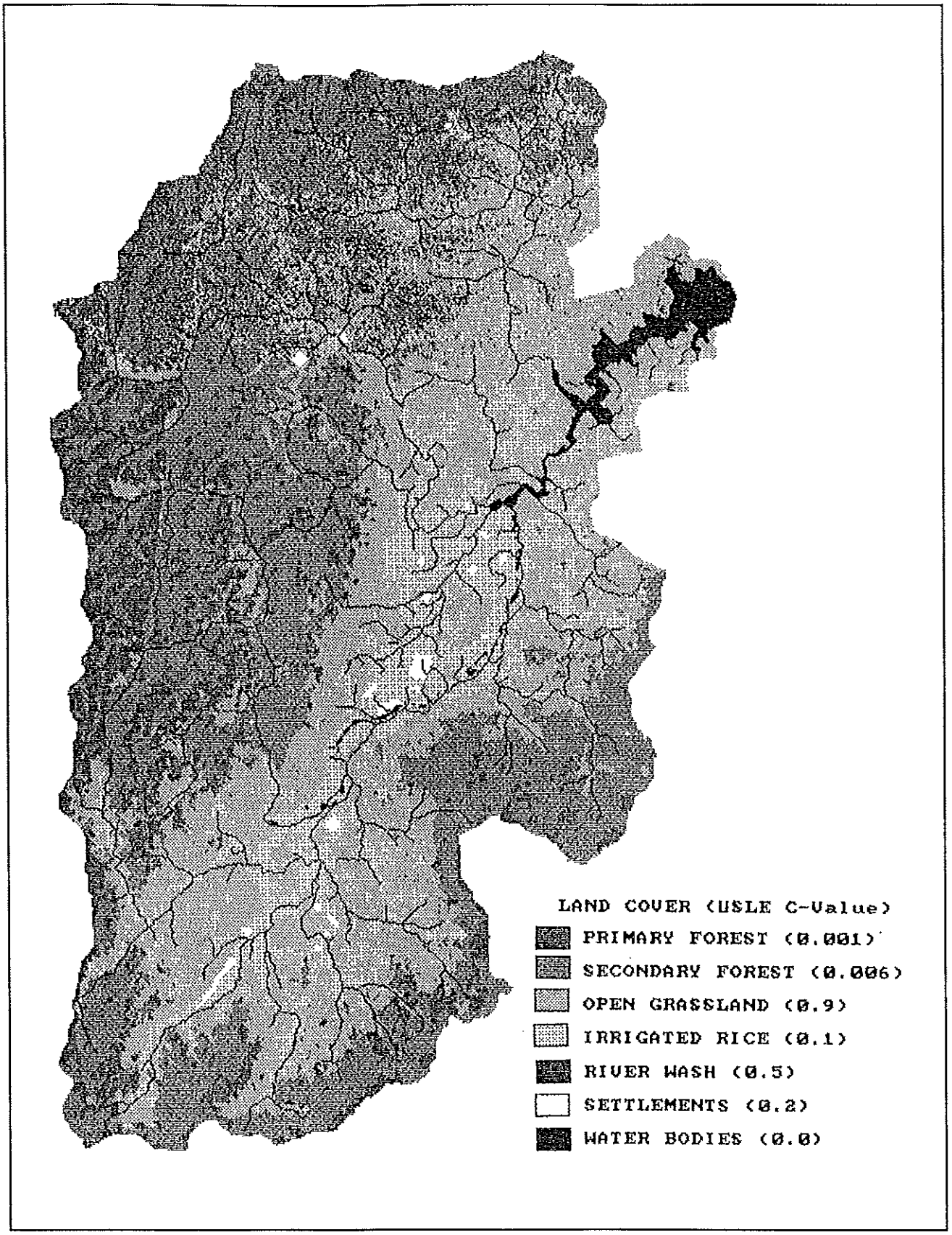

Figure 4.2 Land cover image

Three methods of interpolation were investigated: bi-linear; multi-quadrilateral and least squares. The least squares technique was found to be the most accurate and was therefore used to produce the elevation image. Appendix 2 provides further details of the data extraction and interpolation techniques used.

A slope image is produced from the elevation image. The simplest algorithm for this is to consider for each pixel the difference in elevation of its four adjacent pixels and from this to calculate slope. However, Lea (1991), in an attempt to produce unambiguous flow paths produced a more sophisticated algorithm for calculating a pixel's aspect vector. In the course of this calculation, improved estimates of slope are also produced. The algebra is reproduced in Appendix 3. A slope image produced, as shown in Figure 4.3. The LS factor values shown on the key to this image are discussed in Section 5.5.

4.7 Production of a Soils Image

The reconnaissance soil survey conducted by the Bureau of Soils during 1977 and 1988 identified 16 soil types in the Magat catchment. Soil maps at 1:50 000 scale from this survey were used to produce a soils image by transferring the information onto a smaller scale map which was digitised using a drum scanner. Although some of the map detail was generalised in this manner this was not important as soil erodibility values are uniform over much of the catchment.

Figure 4.4 shows a digital map of soil erodibility in the Magat catchment based upon a map of the 16 soil types. As can be seen from the map most of the soils are clay loam in texture which have been given the soil erodibility K value of 0.26. Soil erodibility is discussed in more detail in Section 5.4.

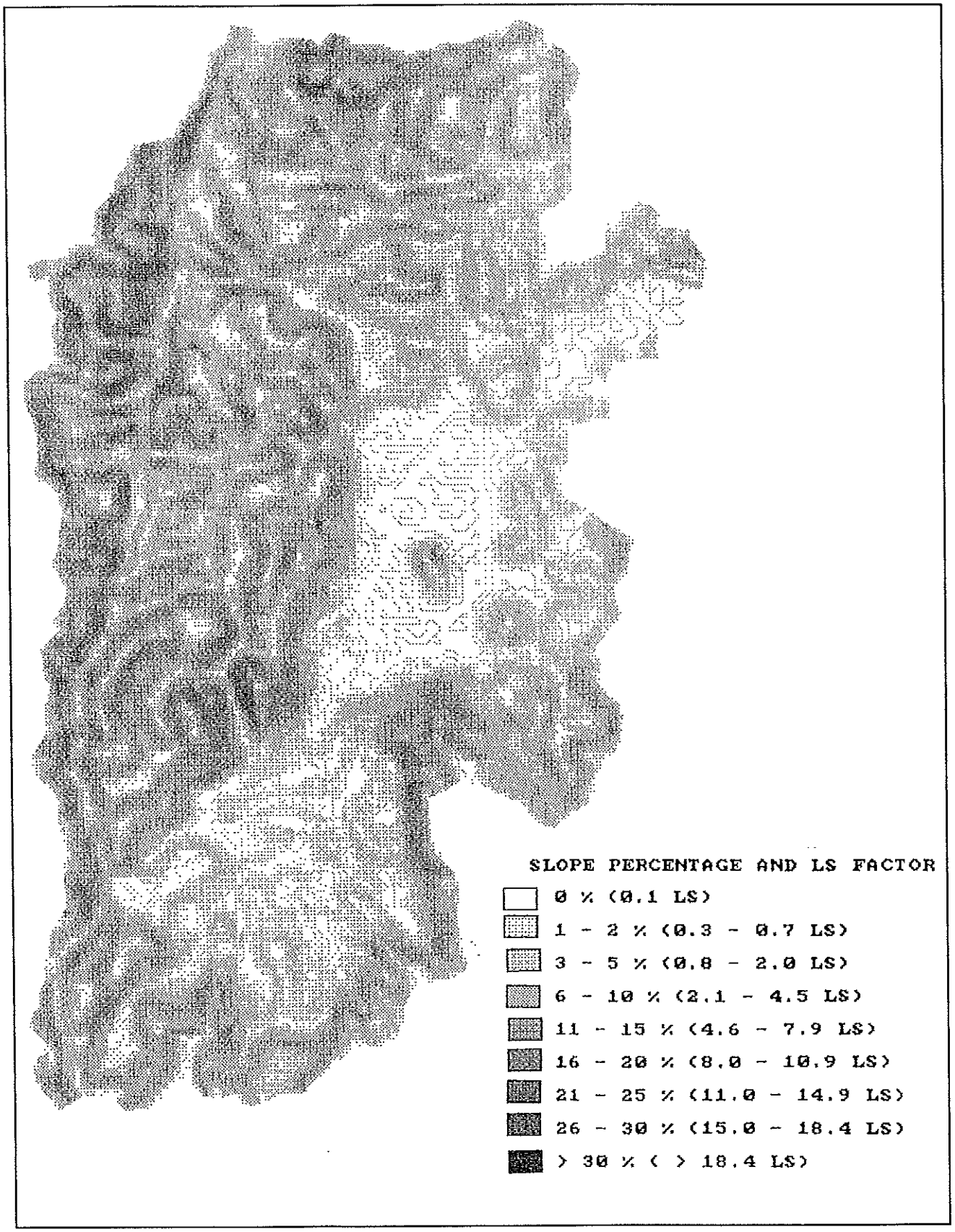

Figure 4.3 Slope image

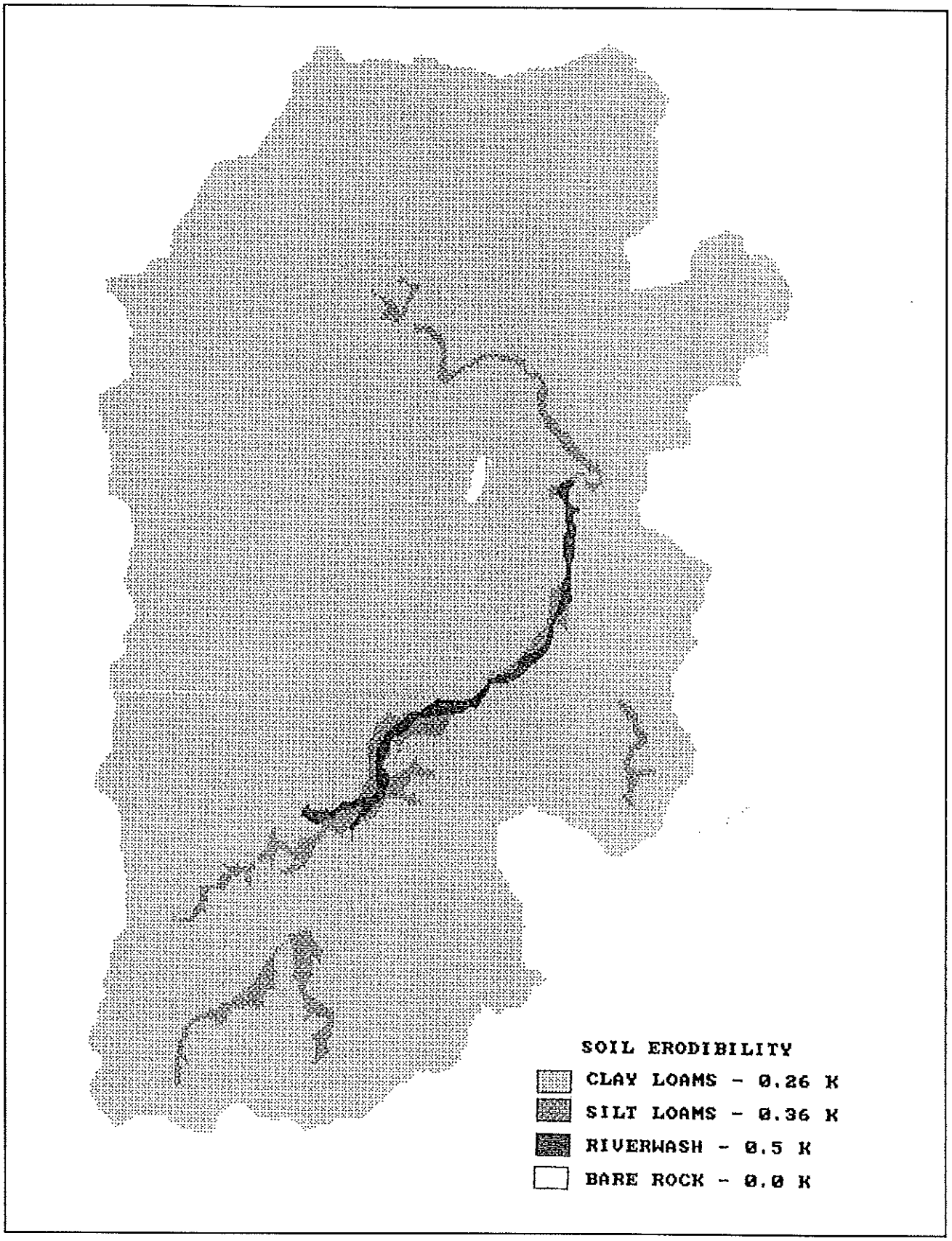

Figure 4.4 Soils image

5 Calculation of source soil erosion

5.1 Selection of Technique

CALSITE could be adapted to use whatever predictor the user specifies. Trial software using both USLE and SLEMSA were tested initially (White, 1989). As SLEMSA was developed for use in semi-arid southern Africa it was found not to take sufficient account of the effects of high rainfall erosivity. The USLE had already been used in the Philippines and in similar environments such as Indonesia, where it was considered to provide reasonable estimates given some modifications to the parameter values used in the equation (Lenvain, 1975; David, 1982). David (1982) used the USLE within the Magat catchment and suggested suitable parameters for soils and land cover and techniques for the estimation of rainfall erosivity and the effects of slope. Much of this information has been incorporated into the USLE calculations discussed here.

The four image files containing information on rainfall, land cover, soil type and slope are used to determine the R, C, K and LS factor values respectively, for the USLE. This was achieved within the GIS by the use of 'look up tables' (LUTs) which convert the 8-bit binary numbers within the image file into meaningful factor values. The following sub-sections describe how this is achieved for the four images.

5.2 Determination of Rainfall Erosivity (R-Value)

Section 4.3 described how annual rainfall was estimated from altitude. This section describes how annual rainfall values were used to determine rainfall erosivity.

The USLE measures rainfall erosivity as the product of the annual kinetic energy of rainfall (E) and the greatest intensity of a 30 minute storm (I_{30}). When measuring energy in J m^{-2} mm^{-1} and intensity in cm hr^{-1}, the R value of USLE is $EI_{30}/100$ where, EI_{30} is in J hr^{-1}.

The determination of R by the above technique is impractical whenever detailed rainfall event information is not available. An analysis of rainfall measurements from a small area near Dallao, near to Magat Dam, between 1984 and 1987 indicated that the annual kinetic energy of rainfall (E) was correlated with annual rainfall (P_a) and could be represented by the following equation:

$$E = 29.83\ P_a^{1.067} \qquad (r^2 = 0.85) \qquad \text{Equation 5.1}$$

(Amphlett and Dickinson, 1989).

This indicates that the annual rainfall total may be suitable for use as a measure of rainfall erosivity.

David (1989) recommended that the R factor can be calculated in the Philippines based upon annual rainfall (P_a) in mm using the following formula:

$$R = \frac{2.5\ P_a^2}{100 \times (0.073\ P_a + 0.73)} \qquad (r^2 = \text{unknown}) \qquad \text{Equation 5.2}$$

This equation was therefore used to convert the rainfall image into a rainfall erosivity image. This involved the use of a LUT which converts the rainfall image pixel values with a range of 0 to 255 to rainfall erosivity values. As the pixel values represent 1/20th of the annual rainfall in mm the LUT equation used was:

$$R = \frac{2.5\ (20\ X\ pixel)^2}{100\ x\ ((0.073\ x\ (20\ X\ pixel)\ +\ 0.73)} \qquad \text{Equation 5.3}$$

Figure 5.1 shows the LUT which was used to convert 1986 rainfall to rainfall erosivity, based upon the image shown in Figure 4.1.

5.3 Determination of Crop Management Factor (C-Value)

The crop management factor C is a ratio which compares the soil loss from a particular crop type or vegetation cover with that from a field of cultivated bare soil. It is therefore a ratio from a value of zero, when the soil is completely protected, to a value of one for cultivated bare soil.

The land cover image stores land cover classes as integer codes. A LUT is used to convert each integer code to a C value for the USLE. Table 5.1 shows the C values used for the 8 land cover classes, and is based upon work by David (1982) and discussions with NIA. It can be seen that the C value is highest for open grassland, where overgrazing and burning has resulted in the vegetation providing little protection against soil erosion. In contrast the C values for forest are very low, and zero in the case of water bodies where there is no soil surface.

Table 5.1 USLE C-Factors used for Magat land cover classes

Land Cover Class	C - Value
Primary Forest	0.001
Secondary Forest	0.006
Open Grassland	0.9
Irrigated Rice	0.1
Dryland Rice	0.1
River Wash	0.5
Settlements	0.2
Water Bodies	0.0

5.4 Determination of Soil Erodibility Factor (K-Value)

The soil erodibility K-value is the soil loss per unit of rainfall erosivity index, from bare fallow ground on a 9% slope of length 22.1 m. Values of K range from 0 to about 0.7. The soil erodibility nomograph of Wischmeier et al (1971) relates soil erodibility to the texture, organic matter content, structure and permeability of soils.

Table 5.2 provides the K-values for the 12 major soil types of the Magat catchment, based upon studies by the Bureau of Soils. No information is

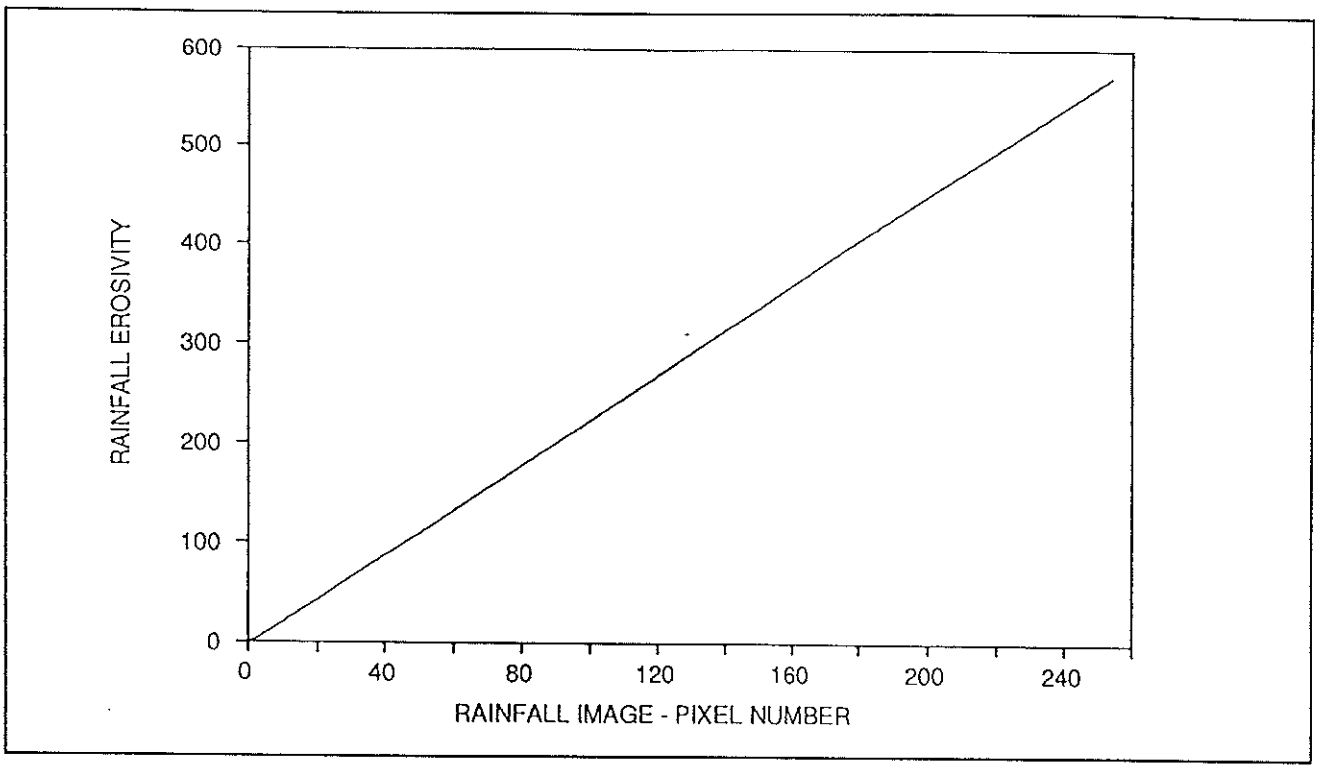

Figure 5.1 Rainfall erosivity LUT for 1986

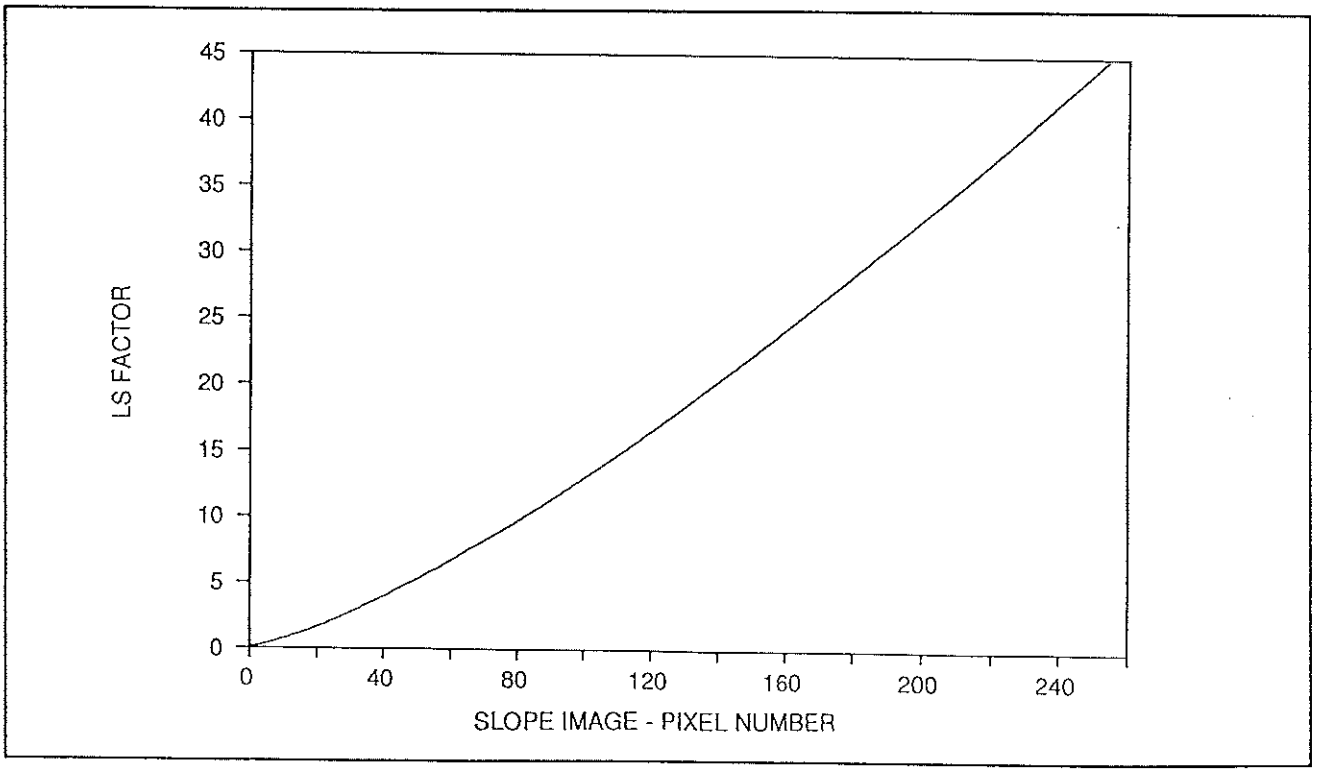

Figure 5.2 LS factor LUT

available on aggregate stability and infiltration capacities of soils in the catchment and therefore erodibility values are based upon soil texture alone. As most of the soils in the area are clay loam in texture there is little variation in soil erodibility values. In fact there are only three classes which have a soil erodibility value other than 0.26.

Table 5.2 Soil erodibility factors

Soil Series	USLE K-value
Annam clay loam	0.26
Bago clay loam	0.26
Bantog clay loam	0.26
Balog clay loam	0.26
Faraon clay loam	0.26
Guimbalaon clay loam	0.26
Guimbalaon-Annam clay loam	0.26
Longa clay loam	0.26
Luisiana clay loam	0.26
Maligaya clay loam	0.26
Nayon clay loam	0.26
Penaranda silt loam	0.36
Prensa clay loam	0.26
Quinga clay loam	0.26
Riverwash	0.50
Rugao clay loam	0.26
Rock	0.00
San Manuel clay loam	0.26
Sevilla clay loam	0.26

5.5 Determination of Slope (LS) Factor

The USLE takes into account both the slope and the slope length when determining erosion. Although the average land slope(s) may be determined with reasonable accuracy from elevation data, slope length cannot easily be determined. The CALSITE model therefore assumes that slope length is constant and uses the empirical equation for the determination of LS used by David (1982) and based on work by Smith and Whitt (1948):

$$LS = 0.2\ S^{1.33} + 0.10 \qquad \text{Equation 5.4}$$

where S = slope in %.

The pixel values in the slope image were first converted to slope using the equation:

$$S = 0.23 \times \text{pixel value in the slope image.} \qquad \text{Equation 5.5}$$

Then S values are converted to the LS factor using a LUT based on Equation 5.4

Figure 5.2 shows the LUT used for the slope image shown in Figure 4.3 derived from the product of Eq. 5.4 and Eq. 5.5.

5.6 Production of Source Erosion Image

Figure 5.3 shows the source erosion image for the year 1986 produced by multiplying the R, C, K and LS factor values. It may be noted that soil erosion is low both on the forested uplands and the flat areas of paddy cultivation but high for areas of grassland, particularly on the steeply sloping foothills.

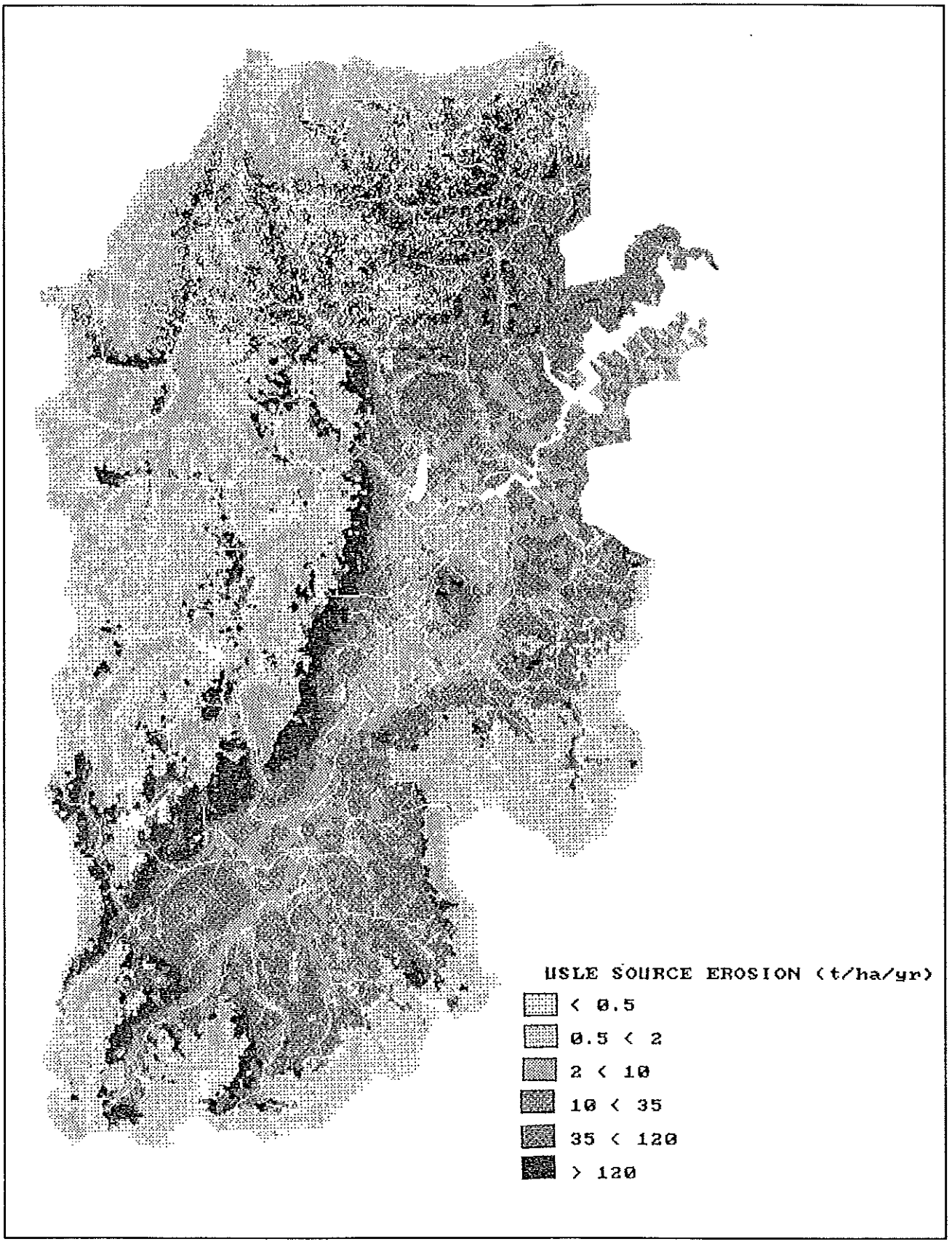

Figure 5.3 1986 Source erosion image

6 Determination of sediment delivery

6.1 Conceptual Considerations

A model of sediment yield needs to consider the quantity of soil eroded from the soil surface and the ability of overland flow and the drainage system to transport the eroded soil down the catchment. This model uses a modified USLE to determine soil erosion and a physically-based sediment delivery algorithm to predict sediment transport.

Sediment delivery values are determined by the transporting capacity of both overland flow and river channel flow. Studies in the Magat catchment by Atkinson (1992) have shown that once sediment reaches the river system a very high proportion is transported downstream. The delivery ratio used in this model is therefore based solely upon the physical factors affecting the transporting capacity of overland flow, in a similar manner to the physically-based model of Morgan et al (1986).

In Chapter 2 a number of delivery ratio formulae were reviewed that are based upon catchment characteristics such as slope and slope length. These empirical relationships were developed for application over whole catchments to take into account sediment transport and redeposition in both the upper and lower reaches. Hession and Shanholz (1988) used this type of delivery ratio in a GIS based sediment yield model. Their simple equation for delivery ratio (DR) is:

$$DR = 10\ (r/L) \qquad \text{Equation 6.1}$$

where r is the 'relief', the difference in elevation between a given pixel and the stream outlet, and L is the slope length (both in m.). Equation 6.1 was used in the initial developments of CALSITE but was not considered to be a very good measure of the transporting capacity of overland flow. The expression takes account of the slope of the land and the distance of a pixel from a stream but does not take account of the volume of overland flow which is influenced by the concavity or convexity of the land surface.

The software package HR_CASCADE was developed to determine overland flow paths from a digital elevation model (DEM) within a GIS. Knowledge of overland flow paths was considered to provide an improved basis for the calculation of sediment delivery values for each pixel within the catchment. The method is described in Section 6.2.

There have been many studies to determine the physical characteristics of the land surface which influence the transporting capacity of overland flow. The velocity of flow is one of the main determinants of its sediment transporting capacity, but is difficult to determine without detailed flow measurements. Meyer and Wischmeier (1969) have shown that the transporting capacity of flow is proportional to water discharge and slope. This fundamental relationship has been used by several erosion modellers to determine a sediment delivery function. Julian and Simons (1984) found that sediment transport in rills was highly correlated (R^2 = 0.96) with slope, using the exponent 1.31; and with discharge, using the exponent 1.93. Some other workers have included a factor to take into account the resistance of the land surface to overland flow, that will reduce the flow velocity and transporting capacity. Morgan et al (1986)

included the USLE C-factor in the following equation for transport capacity of overland flow (T), which is based upon a hydrological model of Kirkby (1974):

$$T \text{ (in kg m}^{-2} \text{ yr}^{-1}) = C\, V_a^2 \sin S \times 10^{-3} \qquad \text{Equation 6.2}$$

where C = Crop and Management factor of USLE;
V_a = Annual volume of overland flow measured as depth in mm;
S = Slope angle (degrees).

Dickinson and Rudra (1990) in their GAMES model take into account Manning's surface roughness coefficient as well as discharge and slope when calculating the delivery function. Foster and Meyer (1975) consider that raindrop impact also increases the transporting capacity of interrill (or sheet) overland flow. Other workers have taken into account the effects of soil type on infiltration and the effects of sediment particle size on deposition (Walling, 1983)

6.2 Delivery Index used by CALSITE

A GIS model of sediment yield requires a sediment delivery function that is theoretically or empirically valid and at the same time easy to derive for each pixel within the catchment from readily accessible data sets. A fairly simple physically based function was therefore chosen for the current version of CALSITE which could be derived solely from the elevation image without requiring any runoff data. The delivery index values are derived from an understanding of the relationship between sediment transport capacity (T) liquid discharge (Q) and channel slope (S).

$$T = k\, Q^a\, S^b \qquad \text{Equation 6.3}$$

where k, a and b are constants.

Alternatively, it is more useful, as shown below, to present the relationship in terms of the concentration f the transported sediment (X):

$$X = T/Q = k_1 Q^{a-1} S^b \qquad \text{Equation 6.4}$$

The choice of appropriate coefficients for Equation 6.3 is a matter of debate. The application of empirical relationships derived for sediment transport and channel regime in alluvial rivers and channels (see Appendix 4) suggests that appropriate values for the coefficients might be: a = 1.35; b = 1.66. However, overland flow conditions are unlikely to be equivalent to those in an alluvial channel.

Govers (1990) undertook extensive experimental studies of sediment transport under conditions of sheet flow in a sloping laboratory channel containing sediment of different sizes. He summarised this results as shown in the following table according to the grain size of the material and whether the flow was laminar or turbulent:

Table 6.1 Sediment transport Results of Govers (1990)

D_{50} sediment size (μm)	Laminar flow			Turbulent flow		
	a	b	correlation coeff (r^2)	a	b	correlation coeff (r^2)
58	1.65	2.62	0.98	1.66	1.44	0.87
127	1.55	2.76	0.98	1.80	1.69	0.95
218	1.70	2.50	0.98	1.50	1.96	0.98
414	1.53	1.97	0.96	1.24	1.71	0.99
1098	1.73	1.76	0.98	1.04	1.47	0.97

For the purposes of CALSITE it may be assumed that, for long flow paths crossing several pixels in relatively steep terrain, the main sediment transporting flow is more likely to be turbulent than laminar. Govers' results suggest, therefore, that the coefficient 'a' should take a value between 1.80 and 1.04 (the larger particle sizes giving lower values of 'a') and the coefficient 'b' should take a value between 1.44 and 1.96. Atkinson (1991) reviewed data on the soils of the Magat basin and concluded that the eroding material has a D_{50} grain size of approximately 200 μm and a broad size distribution. On the basis of these data, and considering Govers' results in the light of the behaviour of alluvial channels, it was decided to adopt the following coefficient values in applying CALSITE to the Magat basin

a = 1.5
b = 1.67

Hence the equation for the limiting concentration of overland flow becomes

$$X = kQ^{0.5}S^{1.67}$$

Along a particular flow path the sediment delivery from a source pixel to a stream will be limited the pixel having the capacity to transport the minimum sediment concentration. If, for example, the overland flow path from a pixel crosses a gently sloping and convex surface, before reaching a stream, some deposition may occur. The delivery index value of a pixel should therefore be related to the minimum transporting capacity along the flow path from that pixel to the stream network. The determination of flow paths is described in Section 6.3.

In introducing the principles of sediment delivery to the CALSITE model it is appropriate to use sediment concentration (X) rather than sediment transporting capacity (T) as the controlling variable since it is independent of the position along the flow path. This can best be illustrated by the simple example of two planar uniform slopes meeting along a common downward sloping valley (like an open book). It is assumed that the runoff and sediment loss is identical for each pixel on this surface and hence the sediment concentration in overland flow is identical. If we combine the flow from the

different pixels in the 'valley bottom' the sediment concentration remains the same across the whole surface but the total discharge (Q) and the total sediment load increase as the contribution from each pixel is added. Thus, if we wish to study the conditions limiting the onward transport of sediment by a simple index giving a direct comparison between neighbouring pixels the variable X rather than T must be used.

It should be noted that applying Equation 6.4 to CALSITE also assumes that delivery functions based on consideration of instantaneous flow conditions are equally valid when applied to annual totals and hence the variable Q can be replaced by V_a, the total annual volume of overland flow.

A delivery index (DI_p) value ranging from 0 to 100 was produced for each pixel based on the equation.

$$DI_p = \min X_f \qquad \text{Equation 6.5}$$

where $\min X_f$ = minimum sediment concentration transporting capacity along the flow path from each source pixel within the catchment to a defined stream channel.

The DI_p values calculated in this way are ascribed to the source pixel and together form the Delivery Index Image (see Section 6.5).

In order to determine values of DI_p using Equation 6.5 a value of S may be obtained from the Slope Image (see Section 4.6) for each pixel over which the flow path passes. However, the CALSITE model does not contain explicit data for, or a method for estimating, the annual volume of overland flow (V_a); so a surrogate variable is required for this.

In calculating the overland flow paths (section 6.3), an image is created in which, for each pixel, a score (F) is kept of the number of flow paths from upstream which cross it. The F image is later used in locating the major stream network: the higher the value of F, the more likely that it contains a definite stream channel. The likely scale of the annual discharge, V_a, crossing a pixel is indicated by relating it to the flow path score (F) giving the size of the 'catchment' (number of pixels) contributing runoff from upstream. However, another factor also affects V_a: the amount of rain falling on this 'catchment'. The relationship between rainfall and runoff is not linear. For the Dallao sub-catchments studied by NIA and HR (Amphlett and Dickinson, 1989) the relationship as seen in Figure 6.1 can be represented as

$$V_a = k_2 P_a^{1.66}$$

where P_a = total annual rainfall
k_2 = a constant.

This seems a fairly representative formula for annual runoff but may not hold good for exceptionally wet years or for steeper catchments when the upper part of the curve is expected to rise less steeply than the formula suggests. For use in CALSITE, therefore, the exponent has been reduced to 1.4. Hence in the Equation 6.4 the variable Q (which for annual totals we have taken as V_a) is substituted by the surrogate variable

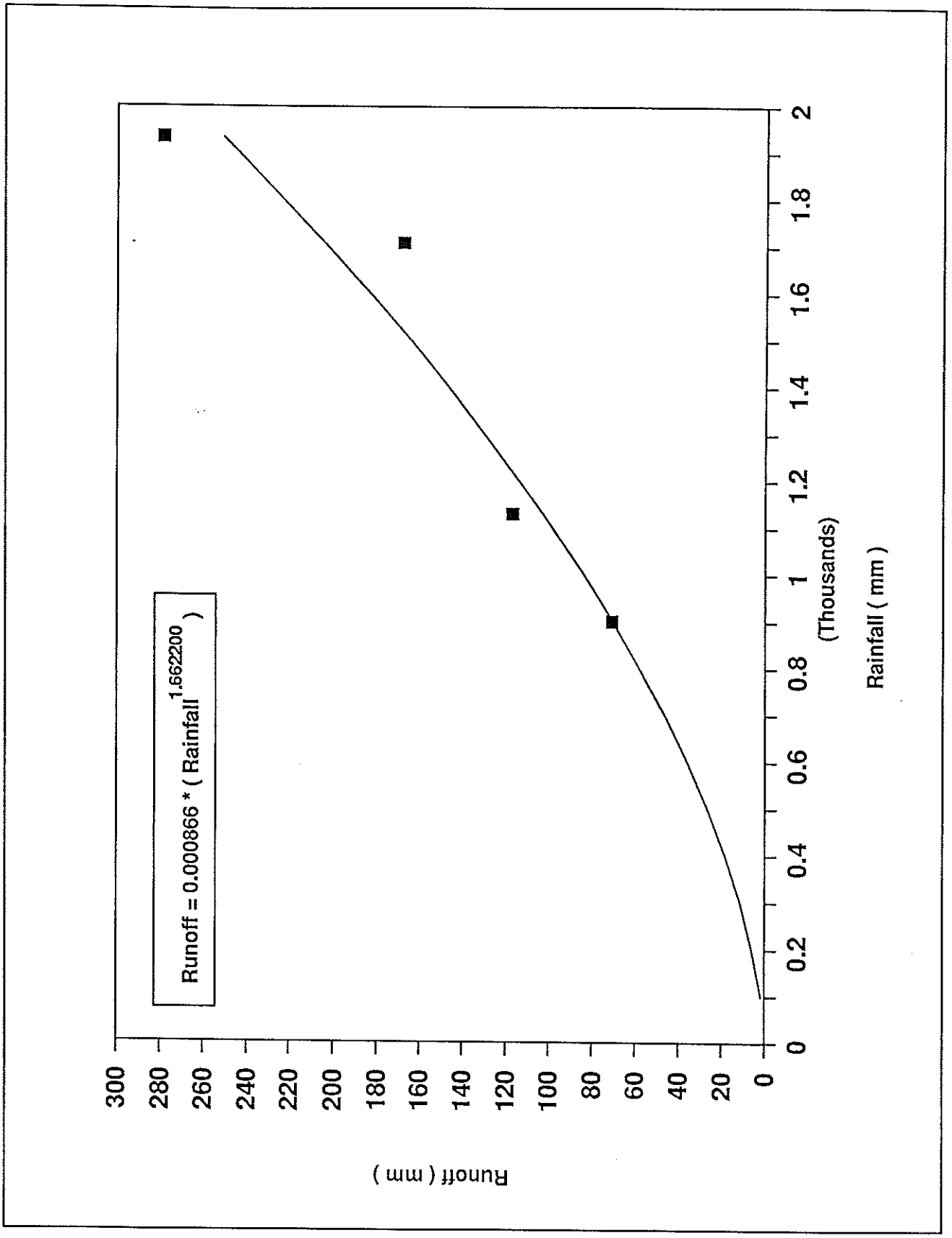

Figure 6.1 **Annual rainfall against runoff for Dallao, Magat Catchment, The Philippines**

$V_a' = FP_a^{1.4}$

combining the two component contributions discussed above.

Equation 6.5 then becomes:

$$DI_p = \min[F^{0.5} P_a^{0.7} S^{1.67}] \qquad \text{Equation 6.6}$$

In calculating the Delivery Index values for each source pixel the constant k_1, from Equation 6.3, is omitted. It is reinserted later, during the calibration process as part of the calibration coefficient k (see Section 7.2). Also the value of P_a is taken as constant for all pixels contributing flow to a given flow path and its value is taken to be that of the annual rainfall at the source pixel. In the current version of the software the coefficients in Equation 6.6 are fixed but in future, variation of these coefficients by the user will be possible to suit different types of catchment.

6.3 The Delivery Look Up Table

The values recorded on the Delivery Index Image are scaled by an appropriate factor and rounded to the nearest integer so that they can be recorded as an 8-bit number (an integer from 0 to 255). These are converted to values of Delivery Ratio (DR_p) in the range 0 to 1 by use of the Delivery LUT.

The Delivery LUT is the means by which physical meaning is given to the Delivery Index values calculated as explained in Section 6.2. If individual storms are considered rather than annual totals it might be expected that the Delivery LUT would approximate to a step function such that flow paths having a value of DI_p below a specified threshold value will have a delivery ratio (DR_p) of zero whilst those above this threshold, will have a DR_p of one. The initial value of zero arises because, for a given rainfall, the slope/overland flow conditions in some pixels will result in little or no onward flow and the deposition of all incoming sediment.

As rainfall and, therefore, runoff increases two things happen. First, there will be a decrease in the concentration of the eroded sediment. This rather surprising result arises from the fact that soil loss is related more-or-less linearly to rainfall (see Section 5.2) but runoff is related to rainfall to a power greater than one (see Section 6.2). Thus, concentration is inversely related to rainfall. This result is borne out by measurements undertaken by HR at small catchment scale both in the Magat basin at Dallao (Amphlett and Dickinson, 1989) and in Malawi (Amphlett, 1989). Secondly, the transporting capacity of a pixel increases as rainfall, and therefore runoff, increases (see Equation 6.6). In all cases beyond the point where the rising graph of transporting capacity cuts the falling graph of supplied sediment concentration, there will be more than adequate capacity to transport incoming sediment and DR_p will have a value of one.

The assumption that there is a fairly abrupt change from the condition of zero sediment delivery to 100% sediment delivery applies only to the analysis of individual storms. On an annual basis, the value of DR_p shows the combined influence of the sediment delivery values for individual storms so, using the step function for individual storms discussed above, at low values of DI_p the annual value of DR_p will be zero; at higher values it will be a weighted mean

of some storm events with a value of zero and some with a value of one; and at even higher values the annual DR_p will approach one. Hence a suitable form for the Delivery LUT, as shown in Figure 6.2, has a lower threshold (t) below which $DR_p = 0$; and an upper saturation value (s) above which $DR_p = 1$. For values between the two thresholds the following function is used.

$$DR_p = \frac{1 - \cos(\pi \times (DI_p - t)/(s - t))}{2} \qquad \text{Equation 6.7}$$

This results in the S-shaped LUT shown in Figure 6.2.

6.4 Determination of Overland Flow Paths

Most flow routing models that have been developed for application to digital elevation data stored in raster files are based upon 'lowest neighbour' algorithms which decide the flow path from a pixel by the lowest altitude of the eight neighbouring pixels. A more accurate 'aspect driven' routing algorithm was proposed by Lea (1991) based upon the calculation of the aspect of each pixel and is described in detail in Appendix 3. The algorithm routes flow over a grid of planes each with a known aspect derived from the estimated altitude of the corner points of each pixel and, if required, pixels further afield. The direction of flow across each pixel is derived from the direction of the pixel's aspect vector. At the perimeter of a pixel, flow is transferred to the coincident point on the neighbouring pixel. The algorithms proposed by Lea (1991) ensure that a flow direction is ascribed to each pixel thereby avoiding situations where flow paths terminate when they reach pixels which are horizontal.

By determining the flow paths from each pixel within the catchment it is possible to identify areas where overland flow converges, indicating either areas of high overland flow or channel flow. A flow path index (F) is kept to show the number of flow paths from individual pixels which cross a given pixel further down the catchment and the image of these flow path scores is used to derive the principal stream network as described in Section 6.5 below.

A series of routines based upon the aspect driven routing algorithm have been developed as a part of the HR_CASCADE software package.

6.5 Estimation of the principal stream network

A comprehensive prediction of river locations within a river basin would require a distributed hydrological model (Abbot et al. 1986). Among other things, this would need to take into account varying infiltration rates, hydraulic roughness of vegetation, the effect of slope, groundwater recharge, and backwater effects on shallow slopes before such a prediction could be reached. Without such sophistication, however, acceptable predictions of river locations are possible using the routing algorithm described in Appendix 3.

Instead of using hydrological modelling, drainage paths may be constructed from each pixel and their convergence used to identify streams. The number of paths converging on a particular pixel can be used as an index (F) of the overland discharge at that point. The resultant array of F values provides sharp distinction between river locations and their drainage areas. An arbitrary threshold dictates the number of flow paths needed to converge on a pixel

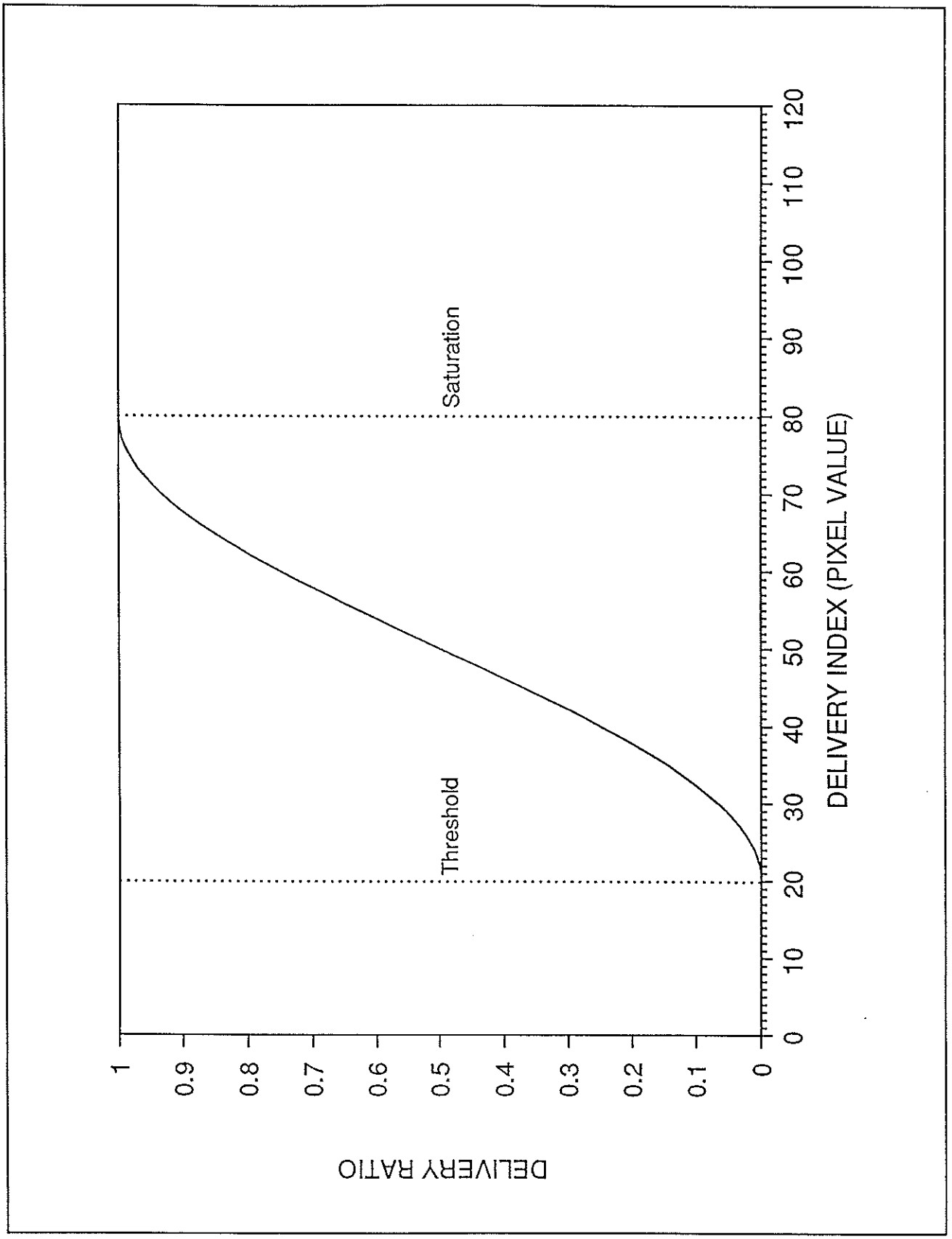

Figure 6.2 Delivery Index Look Up Table (LUT)

before it is classified as a stream. It is useful therefore to refer to published maps of stream locations with which to calibrate these predictions.

Figure 6.3 shows a convergent flow-paths map of the Magat river basin. The map is shaded such that the dark areas represent the highest convergence of flow paths (i.e. the river system) and the lighter areas represent the lowest (uplands and watershed boundaries). By further calibration against cartographic maps, a reliable estimate of stream network location may be obtained.

6.6 Derivation of sub-catchment boundaries

A sub-catchment may be defined as the drainage area of a stream segment. As in the discussion of the previous section, by constructing flow paths from each pixel in the basin, it is possible to derive the drainage area of every pixel that lies on the stream network. By use of the routing algorithm, the problem of deriving sub-catchment boundaries is thus reduced to the problem of identifying segments of the stream network that generate distinct sub-catchments.

River-links are spanning confluences, junctions or source nodes used to generate sub-catchments. The stream network derived in the previous section by reference to convergent flow paths needs to be refined before it is suitable for this calculation. To provide accurate distinction between stream links, it is necessary for streams to be represented as sparsely as possible. An algorithm is used that constructs the sparsest possible representation that maintains an eight-connected stream network (i.e. pixels are connected if they are N, NE, E, SE, S, SW, W or NW neighbours).

The algorithm chooses an eight-connected path that follows the centre pixels of the stream network. A system of weighting is used assigning each stream pixel with the value of the number of neighbouring stream pixels and an eight-connected path is then traced, following the pixels with greatest weighting. When problems are encountered, the user directly specifies the drainage path, and the final sparsely eight-connected network is corrected to ensure that it drains the whole basin.

A recursive routine is used to 'tree-walk' this stream network and assign a different value to each river-link. The routing path from each pixel in the basin is calculated and the source pixel assigned the same value as the first stream pixel reached. By this method, all pixels in the basin are assigned the value of their drainage river-link and sub-watershed boundaries are thus derived.

Figure 6.4 shows the results of the calculation for the Magat Basin with the eight-connected stream network superimposed. The map is shaded to differentiate neighbouring sub-catchments.

6.7 The HR_CASCADE software package

The HR_CASCADE software package was developed by HR Wallingford for use with the ICONOCLAST GIS. It makes heavy use of the PC4000 graphics framestore to store and manipulate image files. A future version of HR_CASCADE will be developed which only requires standard PC hardware, such as a VGA framestore and a 2 Mbyte RAM chip.

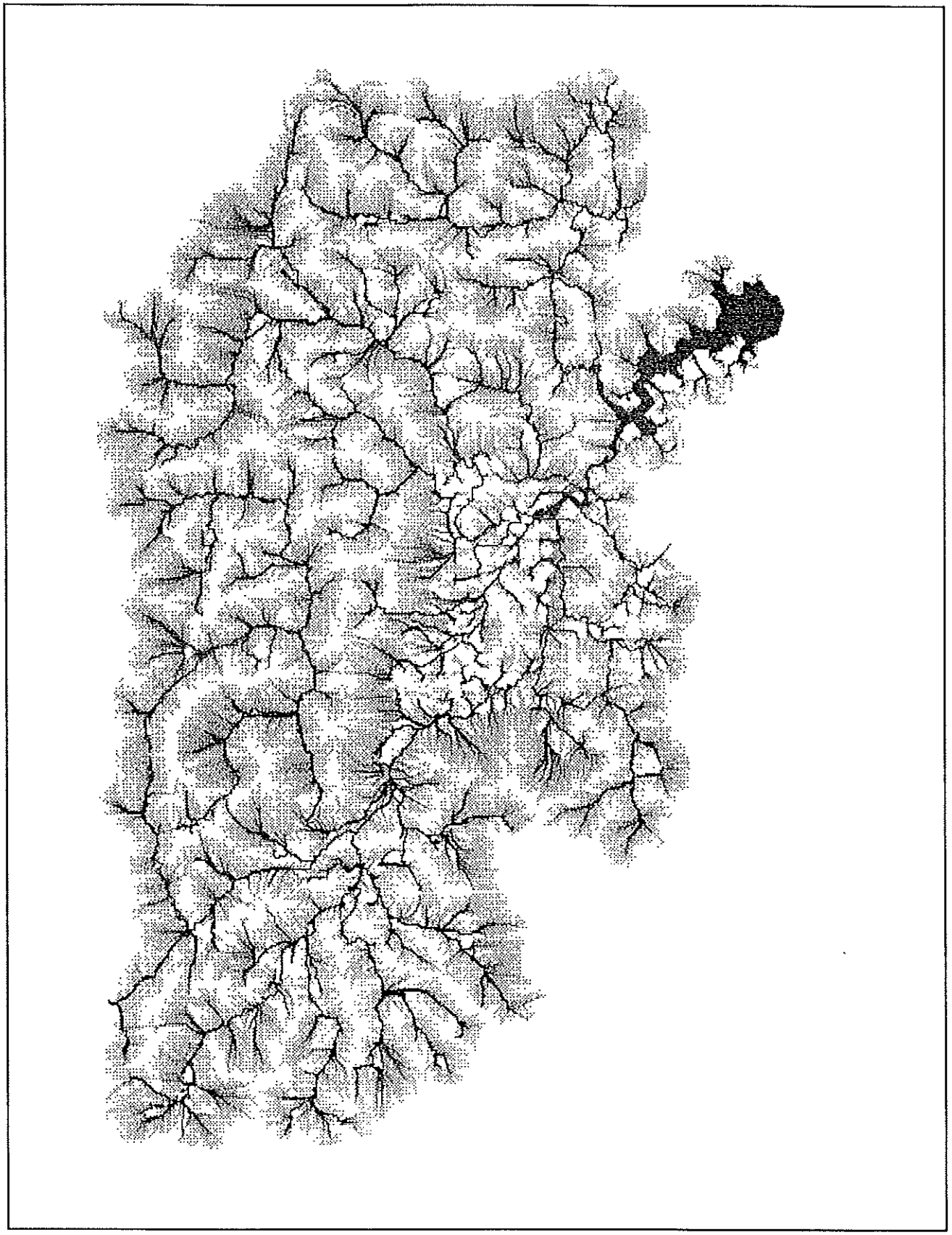

Figure 6.3 Convergent flow paths image

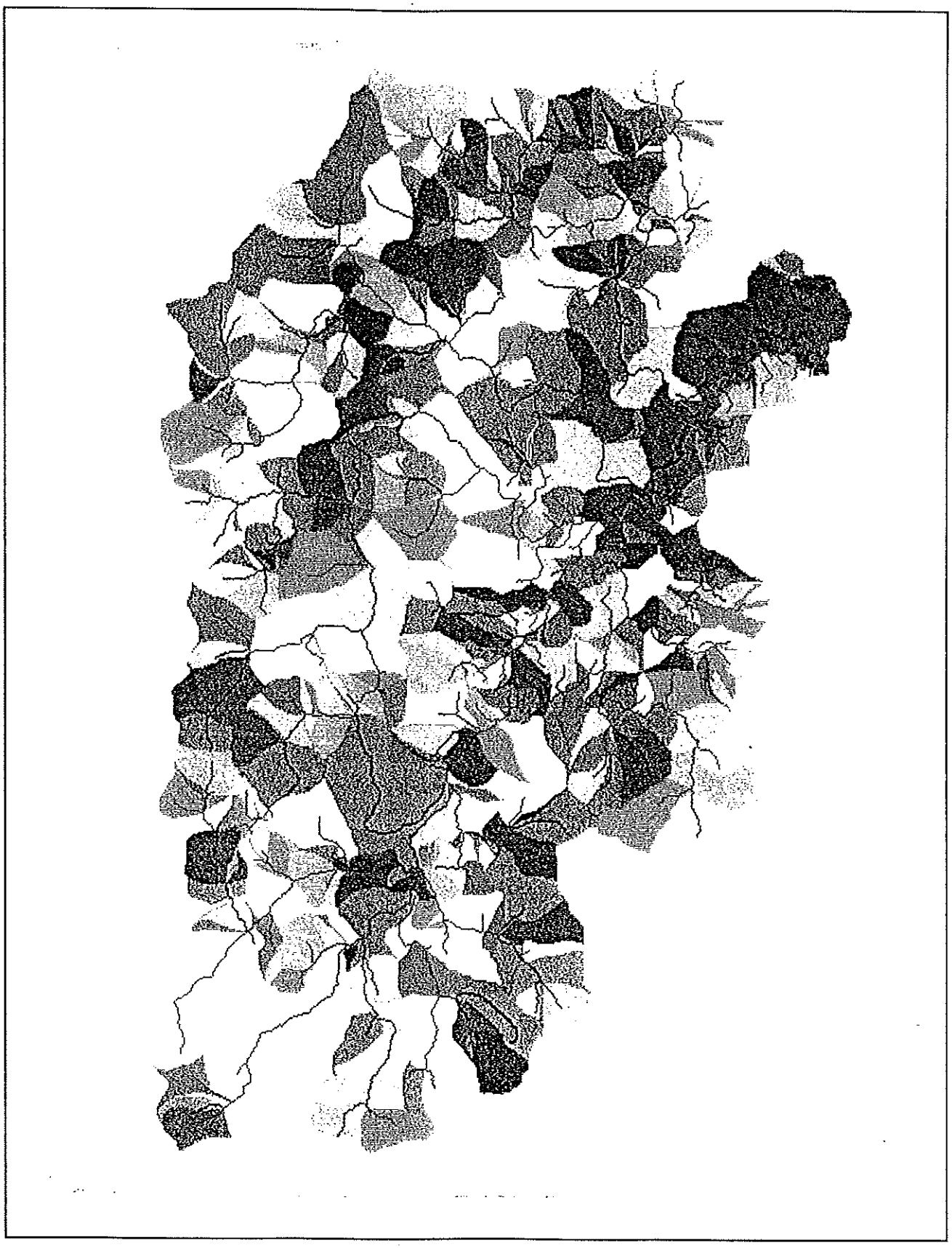

Figure 6.4 Sub-catchments image

HR_CASCADE performs a variety of transformations which are based initially on the digital elevation image. The following images may be produced:

i) Aspect image from the elevation image;
ii) Slope image (S) from the elevation image;
iii) Overland flow path index (F) based upon the aspect image;
iv) Transport function image based upon the overland flow path and slope images currently set at $F^{0.5}$ $S^{1.65}$;
v) Delivery image based upon the minimum of rainfall at the source pixel times the transport function value from a pixel source to a stream channel based on the rainfall and transport function images;
vi) Drainage area image based upon catchment boundary, aspect image and stream network;
vii) An image showing the location of hollows within the aspect image which do not drain into the stream network;
viii) Distance to stream images from the aspect image and the stream network;
ix) Height above stream pixel based upon stream and elevation images.

In addition to these image transformation routines there are two editing routines in HR_CASCADE, one to remove any hollows within the aspect image which prevent overland flow from reaching the stream network, and the other to thin out a complex stream network.

6.8 Production of a Delivery Index Image

As described in Section 6.3 the delivery index image is based upon the minimum value of $F^{0.5}$ $P_a^{0.7}$ $S^{1.65}$ that occurs along the flow path from each pixel to the stream. The image was created using HR_CASCADE and the following procedure, as illustrated in Figure 6.5:

i) An aspect image was produced from the elevation image;
ii) Areas of hollows were identified and edited;
ii) A flow path index image was produced from the aspect image showing the number of flowpaths which cross each pixel;
iii) The square root of the flow path index was calculated and rescaled to store as an 8-bit image;
iv) A slope image was produced from the elevation image;
v) The square root of discharge index image was multiplied by the slope image to the power 1.65 to produce a transport function image;
vii) An image showing stream networks was created based from the flow path index image;
viii) This image is compared with map information and edited to thin out a detailed network and to ensure that the aspect of each stream pixel results in downhill flow;
vi) For each pixel, the rainfall value is taken from the rainfall image and raised to the power 0.7 then the flow path is traced from each pixel to the stream network and the minimum value of $P_a^{0.7}$ times the transport function value along the flow path is found. This value is recorded as the DI_p value for the source pixel to form the delivery index image.

Figure 6.6 shows a colour plot of the final delivery index image.

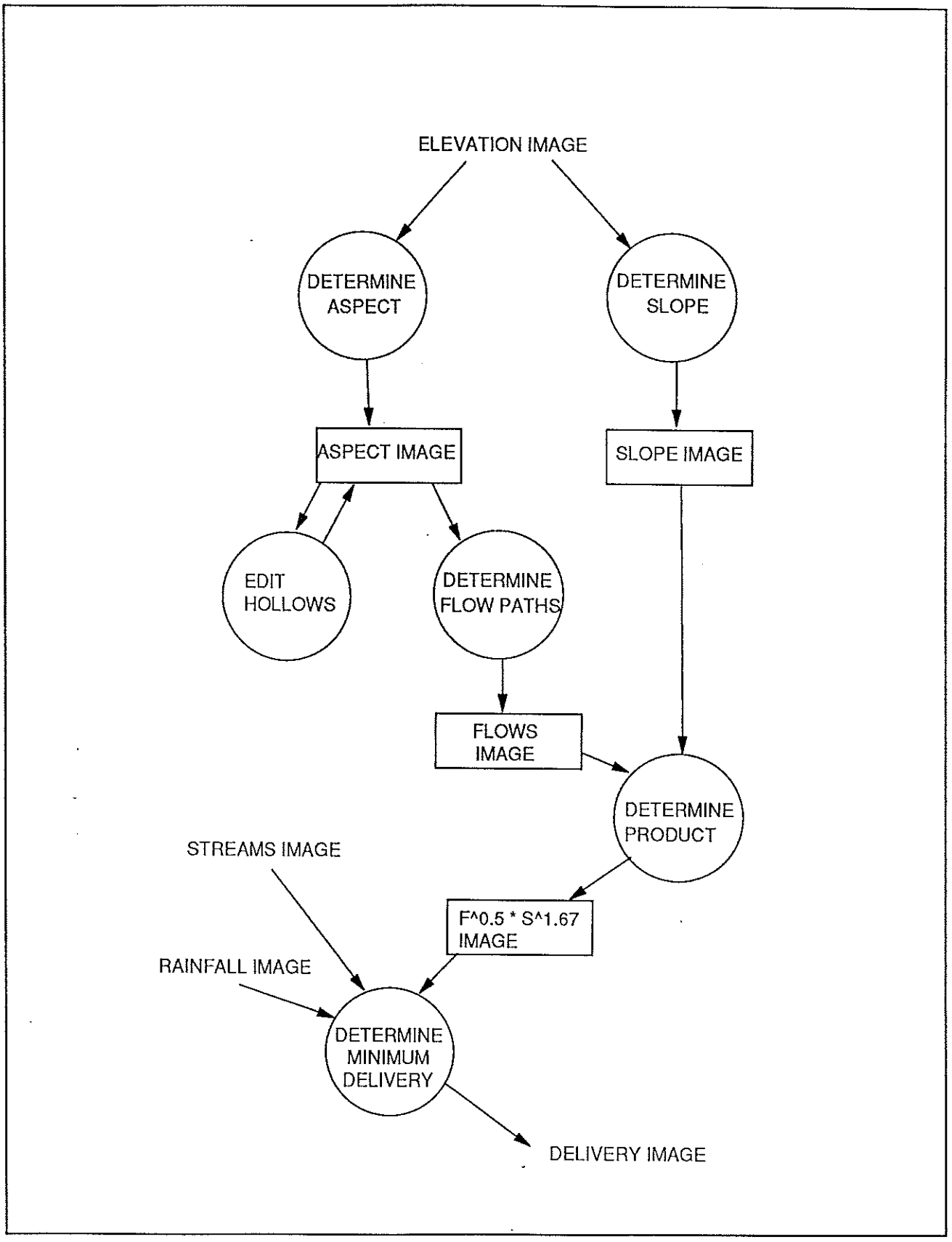

Figure 6.5 HR_CASCADE data flow diagram

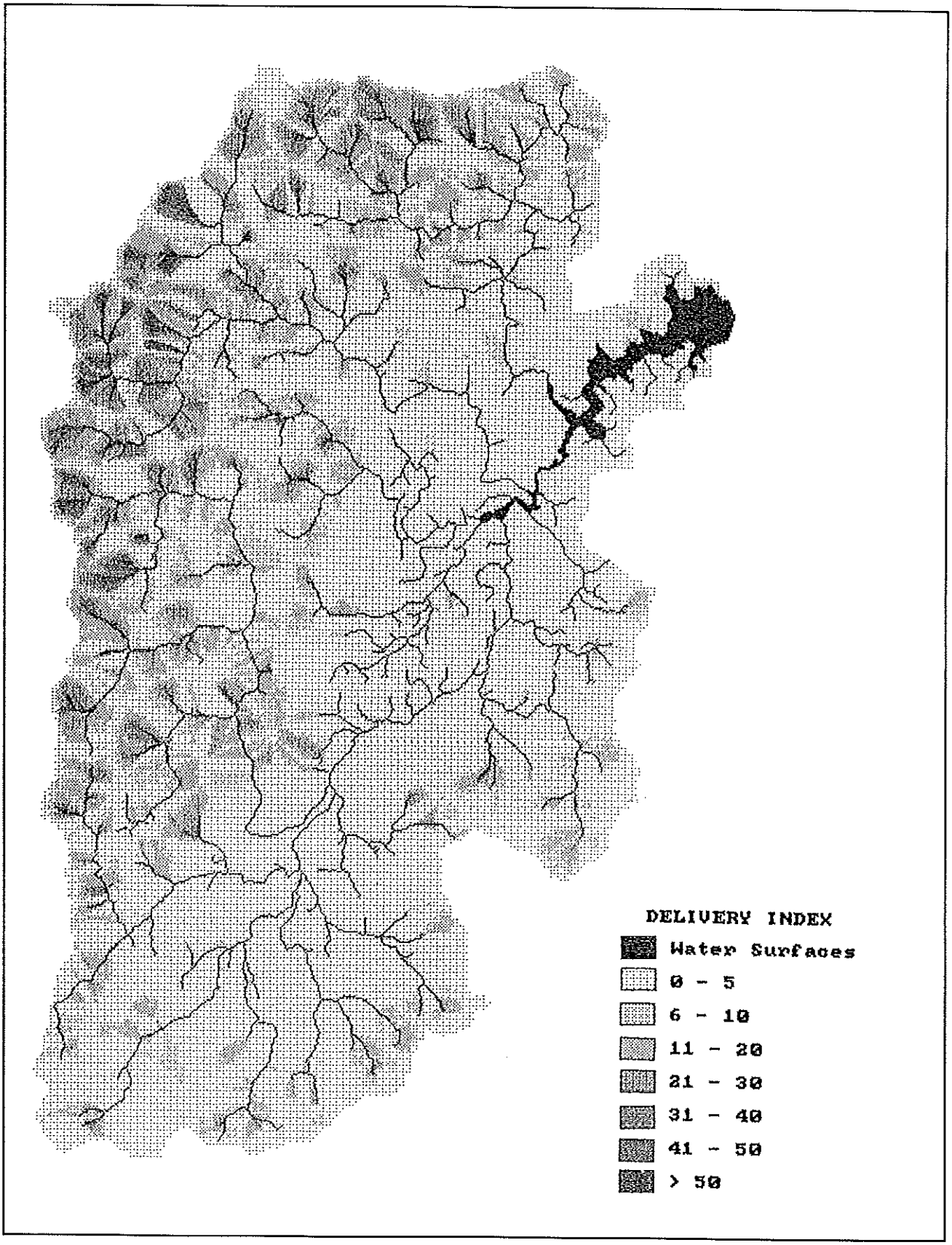

Figure 6.6 Delivery index image

7 Model calibration and prediction of transported erosion

7.1 Introduction

Version 1.0 of CALSITE uses observed sediment rates in t $ha^{-1}yr^{-1}$ for up to 7 sub-catchments in order to calibrate the predicted transported erosion values. The current version of the model is designed to enable the calibration of predictions using observed measurements for the year under study. Future versions of the model will enable the calibration of predictions for different rainfall regimes or land cover scenarios using observed sediment rates for a number of years.

The calibration procedure focuses on the coefficients of the delivery function and is performed by manipulating the delivery look up table (LUT) until the minimum variance between the observed and predicted sediment yields occurs for the sub-catchments under study. Transported erosion is then calculated by multiplying the source erosion image by the delivery image, involving the use of the 'calibrated' delivery LUT.

The sedimentation data used in the Magat study are shown in Table 1.1. An estimate of total erosion for the whole catchment must be supplied. Reservoir surveys during the 1980s have indicated that mean annual sediment yields are of the order of 24 t ha^{-1} (see Appendix 1). As this figure will vary from year to year total catchment sedimentation values were based upon the mean erosion per unit area, using the observed sediment measurements for each year.

7.2 Determination of Delivery LUT Parameters

The predicted transported erosion measurements for each pixel are based upon the source erosion (SE) for that pixel multiplied by the delivery ratio (DR_p) value for that pixel, multiplied by a scaling factor (k) which is a constant that matches the observed and predicted total erosion for the whole catchment. Equation 3.3 summarises this calculation, and is repeated below:

$$TE = SE \times f(DI_p) \times k \qquad \text{Equation 7.1}$$

where:

SE	=	Source Erosion (from USLE);
DI_p	=	Delivery Index;
$f(DI_p)$	=	Calibrated Delivery Ratio;
k	=	Scaling Constant.

As both the source erosion and the delivery images are stored as a series of 8-bit (0-255) integers they have to be converted to meaningful values using the LUTs. Section 6.3 describes the function used to convert the delivery index values into delivery ratio values. CALSITE displays a two dimensional colour graph which shows the variation between observed and predicted sediment yields for all combinations of the threshold from 0 to 50 and saturation from 1 to 100.

The variance of the observed and expected values is based upon a sum of squares technique for each sub-catchment under study:

max
sum($((P_{r_i} / O_i) - 1)^2$) Equation 7.2
0

where P_{r_i} = predicted erosion for catchment i
O_i = observed erosion for catchment i
max = maximum number of sub-catchments.

The threshold and saturation levels for the delivery LUT function are set by default to those values which minimise the variance between observed and predicted. These values may also be input by the program user having studied the analysis of the plotted variance values for all combinations of threshold levels.

7.3 Production of a Transported Erosion Image

Once the threshold levels for the delivery LUT function have been selected a delivery LUT file is created and an image of transported erosion is created using Equation 7.1.

Figure 7.1 shows a map of transported erosion for the Magat area in 1986 based upon threshold and saturation values for the delivery LUT of 0 and 10 respectively. A file containing the estimates of transported soil erosion by 1km or 10km grid square or for predefined areas may also be produced, as shown in Table 7.1

The relatively high observed sediment yield values for 1986 result in a calibrated delivery ration based on low threshold and saturation values of 0 and 10 respectively. This results in some contribution to reservoir sedimentation from almost all locations within the catchment. Comparing the transported erosion image of Figure 7.1 with the source erosion image of Figure 5.3 it can be seen that although source erosion in the north-western area of forested uplands is low, some areas provide a significant contribution to reservoir sedimentation, indicated by high transported erosion rates, due to the high delivery ratios of these localities, which are associated with steep slopes and high rainfall. On the other hand low lying areas of grassland and cultivation in the central valley close to the Magat reservoir have moderate source erosion values (Figure 5.3) but low transported erosion due to very low delivery ratios.

The observed sediment yield measurements for 1987 were much lower than 1986 and as a result the calibrated delivery ratio is based upon higher threshold and saturation values of 15 and 30 respectively. Figure 7.2 shows the resulting transported erosion image for 1987 and includes large areas of the catchment where there is no transported erosion. This is because the delivery ratio value for these areas is less than the threshold of 15. Figure 7.2 suggests that years of low sediment yield may be associated with soil erosion from a few very small problem areas within the catchment.

The CALSITE model determined default values for t and s where t is less than 50 and s is less than 100. A graph showing variation values for different s and t values is displayed on the screen to enable the user to select appropriate values. For some situations there may be more than one combination of s and t values which provide a good correspondence of observed and predicted

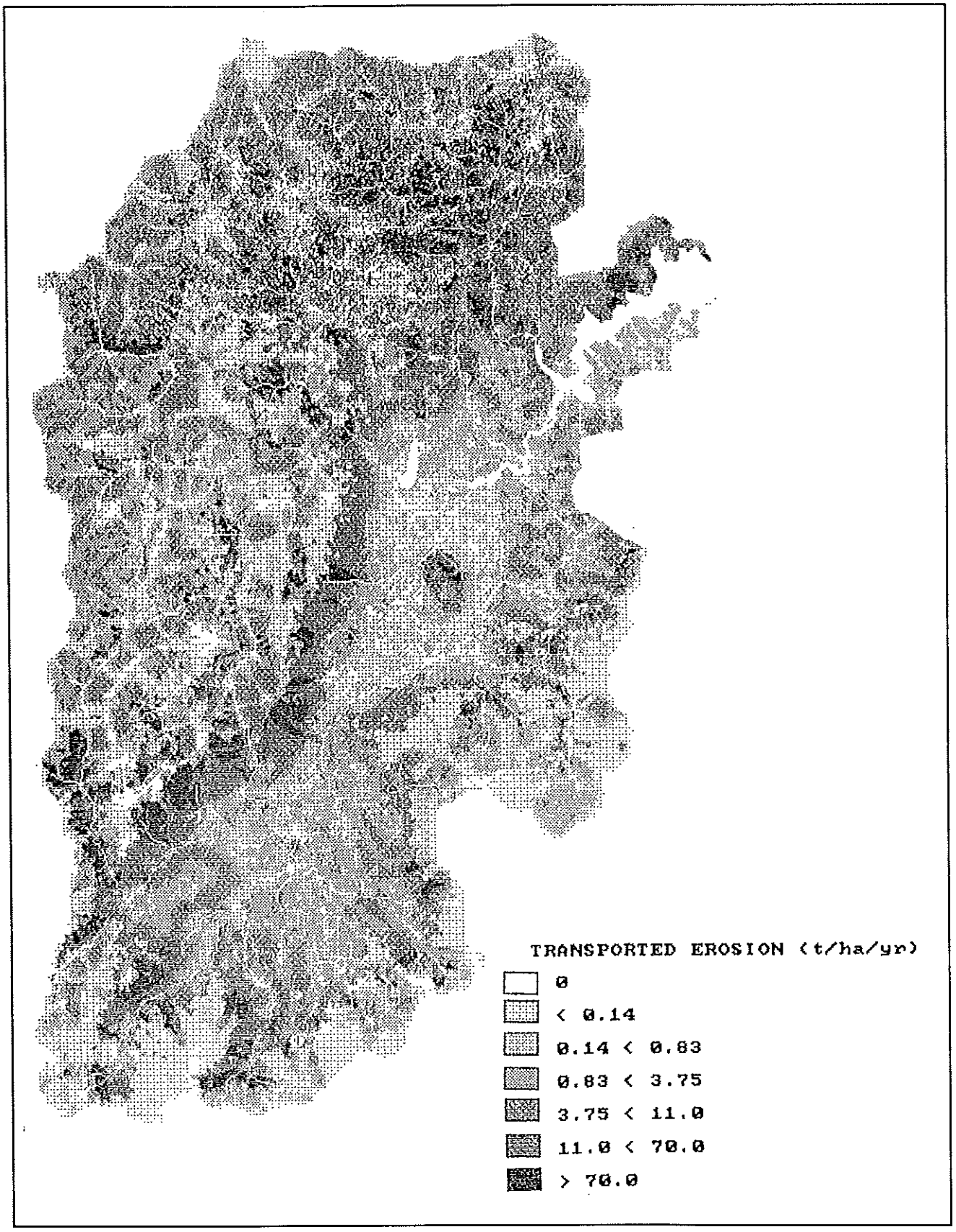

Figure 7.1 1986 transported erosion image

Table 7.1 CALSITE results file for 1986

Date 15/04/93

CALSITE RESULTS FILE	
Land-use file	landuse.rdb
Rainfall file	rainfall.rdb
Soil type file	soils.rdb
Slope file	slope.rdb
Delivery file	dv-pfs2.rdb
Calibration areas	calibrat.rdb
USLE calculation	14/04/93 source.rdb
Yield calculation	14/04/93 trans86.rdb
Calibration	14/04/93

Square	Km East								
Km North	260	270	280	290	300	310	320	330	340
1880				0	1	8	40		
1870			18	11	40	54	37		
1860		6	23	55	91	54	25	27	
1850		29	43	40	16	18	15	3	
1840		6	9	25	9	1	3		
1830		1	10	21	12	4	8		
1820		12	14	36	1	6	7		
1810		80	79	28	3	2	2		
1800		70	16	1	9	2	0		
1790		13	32	13	10	9			
1780		18	15	20	0				
1770									

NB. Grid reference gives the bottom left hand corner of a square.
Predicted values are in tonnes/hectare/year.

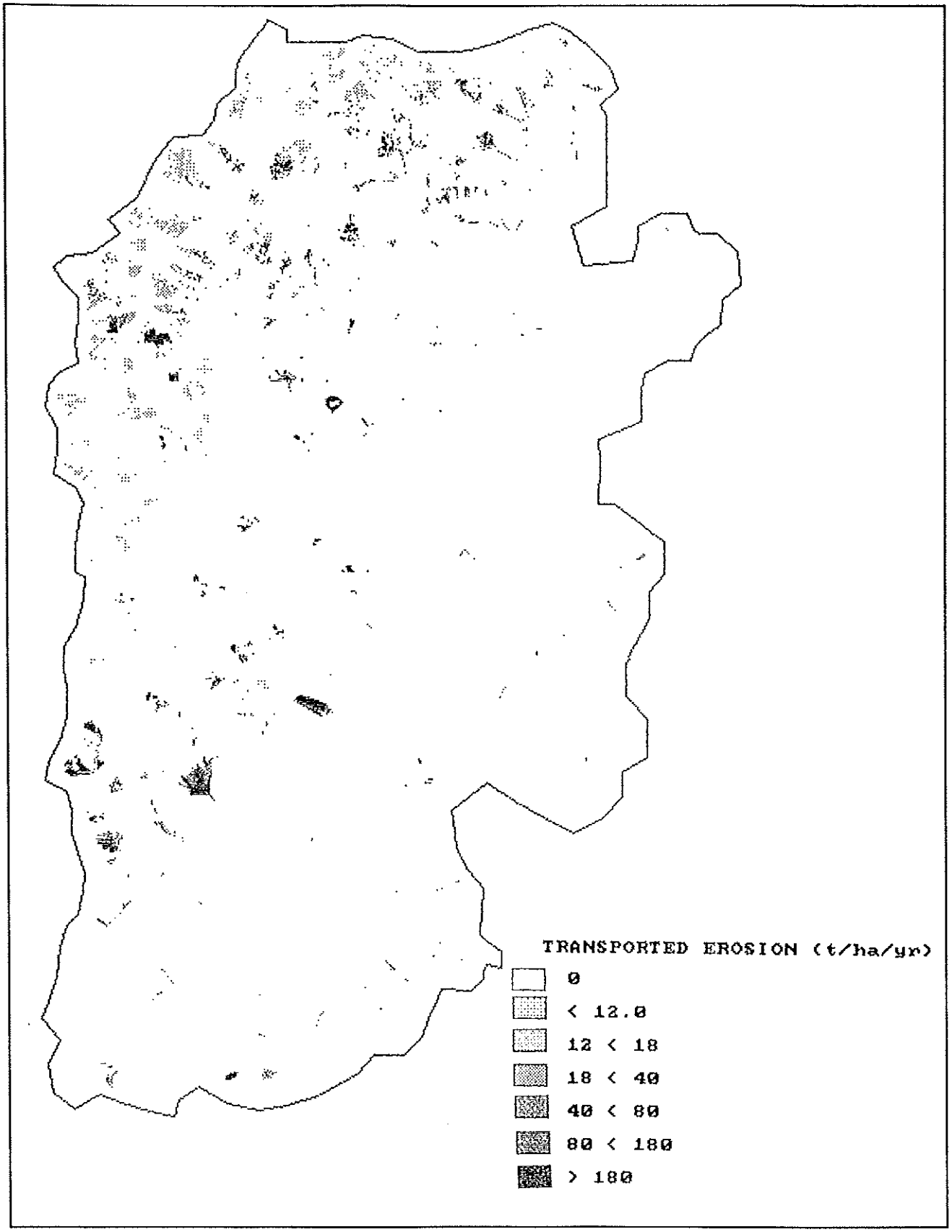

Figure 7.2 1987 transported erosion image

sediment yield. The user can try alternative s and t values then display the sedimentation predictions for each sub-catchment before the transported erosion values are calculated. Version 1.1 of CALSITE displays the k value on the screen for each iteration of this procedure. Where the k value and threshold values are both high this may result in a transported erosion image which suggests that reservoir sedimentation is from a small number of highly erosive locations which have specific delivery index values. Sometimes the result is unrealistic because the erosion is attributed to less than 1 per cent of the catchment. In such cases the user must use professional judgement to select appropriate s and t values which result in both a good correspondence between observed and predicted sediment values and a realistic transported erosion image.

8 Model validation

8.1 Introduction

This Chapter describes tests that were performed on CALSITE using rainfall and sediment measurements from the Magat catchment for the years 1986 to 1991. The rainfall, soils, slope and land cover images described in Chapter 4 were used for these analyses. The LUT for the rainfall image was modified for each year under study to take account of different rainfall regimes. This resulted in different values for soil erosion and sedimentation over the six years. No changes in land cover, soil or slope were assumed over the six years of the study.

The CALSITE model may be of value for two types of prediction: firstly for identifying the locations within a catchment where source or transported erosion is high, and secondly for predicting erosion and sedimentation for different years, under different rainfall or land cover conditions.

The predictions of transported erosion were calibrated for each year using the observed sediment measurements shown in Table 1.1, as described in Section 8.2. This enabled the accuracy of the predictions within the catchment to be assessed and any inaccuracies peculiar to certain sub-catchments to be identified. The use of CALSITE for modelling possible changes in land cover is discussed in Section 8.3.

8.2 Calibrated Results for Each Year

Tables 8.1 to 8.6 present the predicted and observed transported erosion values for the years 1986 to 1991. The area measurements of each sub-catchment differ slightly from those of Table 1.1 indicating slight discrepancies between the areas as calculated by the method of Section 6.6 and those previously calculated by planimetry from maps. The differences are not significant. The observed values are based upon Dickinson and Reid (1992); however, where a range of observed values was quoted the median value is used here. As sediment measurements were not taken for the Magat catchment as a whole the observed values for Magat represent weighted averages of the other three sub-catchments, taking into account the size of each catchment. The 'variation' column represents the percentage over- or under-estimate of the predicted values (i.e. $(P_r - O)/O \times 100$, where P_r is predicted and O is observed).

The annual rainfall totals for the Consuelo meteorological station are shown in Table 8.1. These values were used to determine rainfall erosivity for each year over the catchment, using the rainfall-elevation model described in Section 4.4, and the rainfall erosivity equations described in Section 5.2.

The lack of rainfall data for the years when sediment measurements were undertaken limits the accuracy of soil erosion and sedimentation estimates, particularly as rainfall data are used in the determination of both the source erosion image using USLE, and the delivery index image. The validity of using the Consuelo meteorological station data as being representative of rainfall over the whole catchment would appear to be questionable since there is little correspondence between observed sediment rates and rainfall at Consuelo, as shown by Figure 8.1. The possibility of interpolating between meteorological stations and using a separate rainfall-elevation model for each

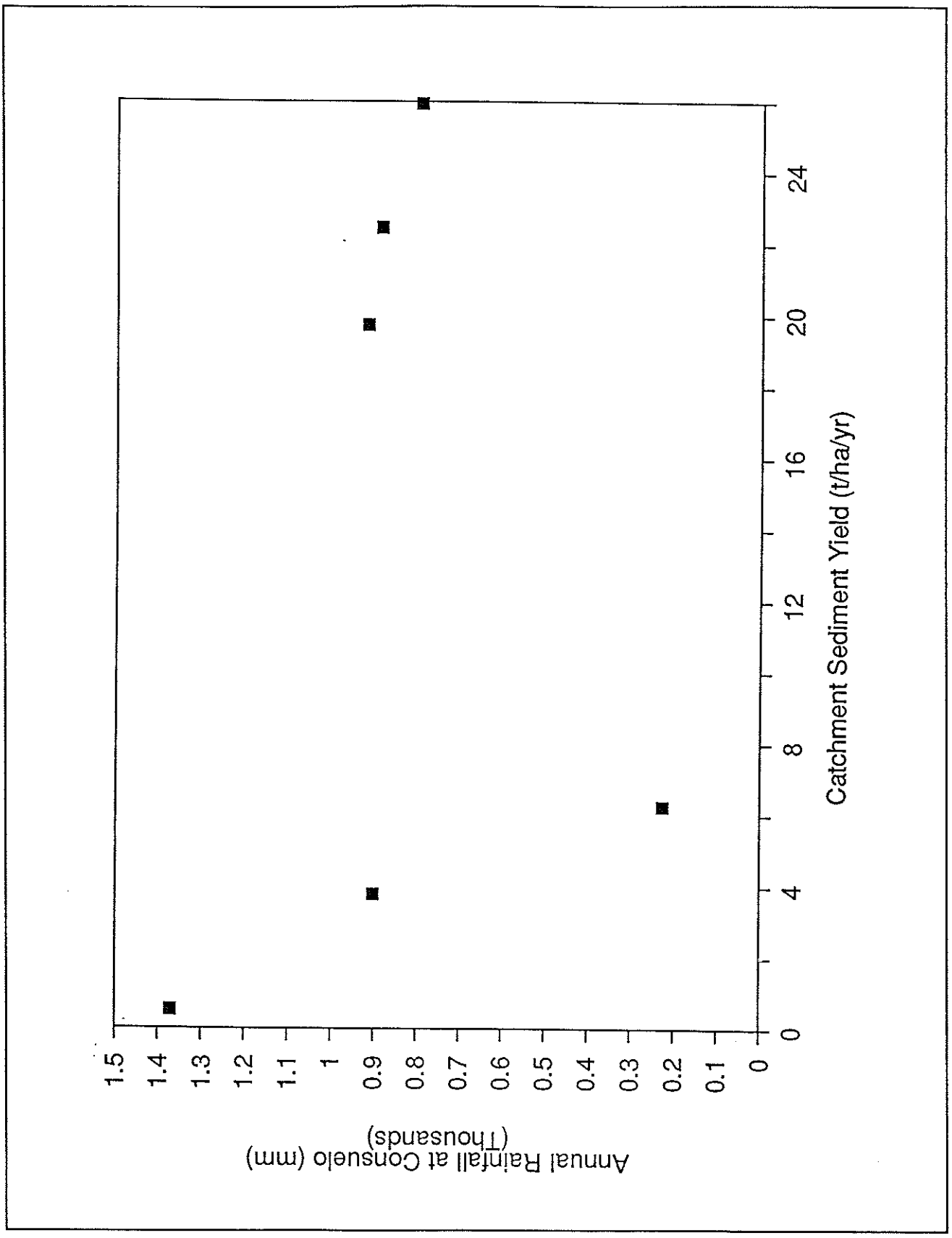

Figure 8.1 **Annual rainfall at Consuelo vs Mean Observed Sediment Yield**

year was investigated but rejected as unsuitable. The technique used was considered suitable given the paucity of rainfall data.

Tables 8.2 to 8.7 and Figures 8.2 to 8.5 show the predicted and observed rates of erosion for the years 1986 to 1991 for each sub-catchment where sediment observations were made. The five sub-catchments used for this study are shown in Figure 1.1. Table 8.8 provides details of the land cover of each sub-catchment.

The observed estimates of transported erosion for the Magat catchment as a whole are based upon average values of the observed measurements, taking into account the area of each sub-catchment. Predicted source erosion rates are given for each sub-catchment based upon uncalibrated USLE estimates. These values vary from year to year depending upon the variation in annual rainfall. The fact that the source erosion estimates are not calibrated by any observed measurement means that sometimes there are large differences between the predicted source and transported erosion values. In 1986 source erosion appears to be slightly less than transported erosion, which of course is physically impossible; and in other years, such as 1989, transported erosion over the catchment as a whole is only 1 per cent of the source erosion.

Figures 8.2 to 8.5 include estimates of possible future soil erosion fates for a rainfall regime for th year under study given the scenario that secondary forest is replaced by scrubland and primary forest is replaced by secondary forest. These results are discussed in Section 8.3.

The calibration technique, described in Chapter 7, minimises the variation between observed and predicted values of transported erosion by manipulating the LUT of the delivery index image. Ideally the calibration should be based on as least 4 or 5 sub-catchments spread over the catchment each representing 10 per cent or more of the catchment and covering a wide range of land uses, soil types and topographies. In practise the available sediment observations for a catchment can be very few, if any, and may be for small catchments which are not typical of the catchment as a whole. Furthermore technical and practical difficulties of sediment observations in an upland tropical environment can result in the sediment observations being restricted to a few short time periods, making it difficult to accurately assess annual sediment yields. The inclusion of observed sediment values in the calibration data for sub-catchments which are anomalous compared with the catchment as a whole, or are based on data which are likely to be inaccurate, may result in a poor calibration of the transported erosion estimates. If the observed sedimentation yield for one out of three of the sub-catchments used for calibration is much higher than expected then the calibrated transported erosion estimates for the whole catchment may be skewed by the anomalous calibration data.

Table 8.2 shows that there is a good correspondence between the observed and predicted transported erosion estimates for the year 1986. Santa Fe sub-catchment has the highest observed and predicted transported erosion values, of the three sub-catchments studied. The source erosion values for Santa Fe are not particularly high relative to the other areas, so the high transported erosion values must be due to relatively high delivery index values associated with steep slopes in this part of the catchment.

The rainfall in 1987 was slightly higher than in 1986, yet the observed sediment yield values were much lower. The observed values for the Aritao sub-catchment are much lower than Baretbet and Santa Fe. The calibration results in quite a good fit for the Baretbet and Aritao sub-catchments, but sedimentation in the smaller Santa Fe catchment is over-estimated by over 200 per cent.

In 1988 rainfall was similar to 1987, but the observed sediment yields were higher. Again low sediment yield values were measured for the Aritao sub-catchment. As with the 1987 calibration quite a good fit results for Baretbet and Aritao sub-catchments, but Santa Fe is overestimated by over 200 percent.

In 1989 no sediment observations were made in Aritao, however measurements were started in the Lamut sub-catchment immediately to the south of the Magat reservoir, as shown in Figure 1.1. The Lamut catchment has negligible forest cover, as shown in Table 8.8, but a high proportion of open grassland leading to the fairly high source erosion rates shown in Table 8.5. Slopes in the Lamut catchment are, however, fairly gentle so that delivery ratio values and the predicted transported erosion estimates are low.

Rainfall at Consuelo in 1989 was recorded to be the highest out of the six years under study, yet the average values for sediment yield were low over the catchment as a whole, with the exception of Santa Fe.

In 1990 sediment measurements were taken at a new sub-catchment called Burnay, situated towards the north of the catchment, as shown in Figure 1.1. The sub-catchment is a mixture of forest and grassland as shown in Table 8.8, and quite steeply sloping. The calibration of transported erosion for 1990 results in close correspondence of observed and predicted erosion for Baretbet and Burnay but underestimates the Lamut catchment.

In 1991 sediment observations were only made for Baretbet and Santa Fe, and at Santa Fe the measurements were influenced by the landslips associated with a major earthquake on 16 July 1990. Calibration of the transported erosion values is therefore difficult. Rainfall in 1991 was low at Consuelo and so too were the observed sediment measurements for the Baretbet sub-catchment.

Table 8.1 Annual Rainfall at Consuelo

Year	Rainfall (mm)
1986	794
1987	901
1988	917
1989	1372
1990	886
1991	226

Table 8.2 1986 Predicted and observed erosion rates ($t^{-1}ha^{1-}y^{-1}$)

Catchment	Area (km^2)	Predicted source erosion	Predicted transported erosion	Observed transported erosion	Variation
Magat	4176.3	22.07	25.94	25.94	0
Baretbet	2148.9	19.05	19.93	25.25	-21.07%
Aritao	143.8	26.66	23.17	22.00	+5.32%
Santa Fe	15.0	24.83	41.87	39.70	+5.47%
Lamut	17.9			N/A	
Burnay	28.6			N/A	

Calibration coefficients: k = 3.351; t = 0; s = 10
N/A = not available

Table 8.3 1987 Predicted and observed erosion rates ($t^{-1}ha^{1-}y^{-1}$)

Catchment	Area (km^2)	Predicted source erosion	Predicted transported erosion	Observed transported erosion	Variation
Magat	4176.3	25.08	3.77	3.77	0
Baretbet	2148.9	21.65	2.63	4.00	-34.25%
Aritao	143.8	30.30	0.61	0.60	-1.67%
Santa Fe	15.0	28.21	4.82	1.50	+221.3%
Lamut	17.9			N/A	
Burnay	28.6			N/A	

Calibration coefficients: k = 2.71; t = 15; s = 30
N/A = not available

Table 8.4 1988 Predicted and observed erosion rates ($t^{-1}ha^{1-}y^{-1}$)

Catchment	Area (km^2)	Predicted source erosion	Predicted transported erosion	Observed transported erosion	Variation
Magat	4176.3	25.57	19.73	19.73	0
Baretbet	2148.9	22.08	13.66	20.8	-13.33%
Aritao	143.8	30.89	2.47	5.18	-52.32%
Santa Fe	15.0	28.76	18.52	5.42	+241.7%
Lamut	17.9			N/A	
Burnay	28.6			N/A	

Calibration coefficients: k = 12.56; t = 20; s = 22
N/A = not available

Table 8.5 1989 Predicted and observed erosion rates ($t^{-1}ha^{1-}y^{-1}$)

Catchment	Area (km^2)	Predicted source erosion	Predicted transported erosion	Observed transported erosion	Variation
Magat	4176.3	38.40	0.52	0.52	0
Baretbet	2148.9	33.17	0.40	0.35	-14.28%
Aritao	143.8			N/A	
Santa Fe	15.0	40.84	0.81	21.15	-96.17%
Lamut	17.9	45.03	0.17	4.10	-96.85%
Burnay	28.6			N/A	

Calibration coefficients: k = 0.039; t = 0; s = 10
N/A = not available

Table 8.6 1990 Predicted and observed erosion rates ($t^{-1}ha^{1-}y^{-1}$)

Catchment	Area (km^2)	Predicted source erosion	Predicted transported erosion	Observed transported erosion	Variation
Magat	4176.3	24.68	22.47	22.47	0
Baretbet	2148.9	21.31	16.44	22.85	-28.05%
Aritao	143.8			N/A	
Santa Fe	15.0			N/A	
Lamut	17.9	28.91	1.53	13.10	-88.32%
Burnay	28.6	40.52	7.58	7.15	+6.01%

Calibration coefficients: k = 12.833; t = 9; s = 32
N/A = not available

Table 8.7 1991 Predicted and observed erosion rates ($t^{-1}ha^{1-}y^{-1}$)

Catchment	Area (km^2)	Predicted source erosion	Predicted transported erosion	Observed transported erosion	Variation
Magat	4176.3	6.08	6.25	6.25	0
Baretbet	2148.9	5.22	4.77	6.0	-20.50%
Aritao	143.8				
Santa Fe	15.0	6.50	10.10	41.3	-75.54%
Lamut	17.9				
Burnay	28.6				

Calibration coefficients: K = 7.62; t = 8; s = 18
N/A = not available

Table 8.8 Land cover by sub-catchment

(Figures in percent of sub-catchment)

Land cover	Magat	Baretbet	Aritao	Santa Fe	Lamut	Burnay
River wash	0.1	0.2	0.0	0.0	0.0	0.0
Rice	14.7	12.2	14.7	8.4	31.3	11.1
Primary forest	16.4	15.8	11.9	22.4	0.0	24.3
Secondary forest	30.9	35.7	41.2	41.6	0.0	25.6
Grassland	32.3	31.0	26.3	22.4	67.1	35.7
Urban	0.4	0.6	1.4	0.0	0.0	0.0
Water	5.3	4.9	3.6	4.7	1.5	3.3

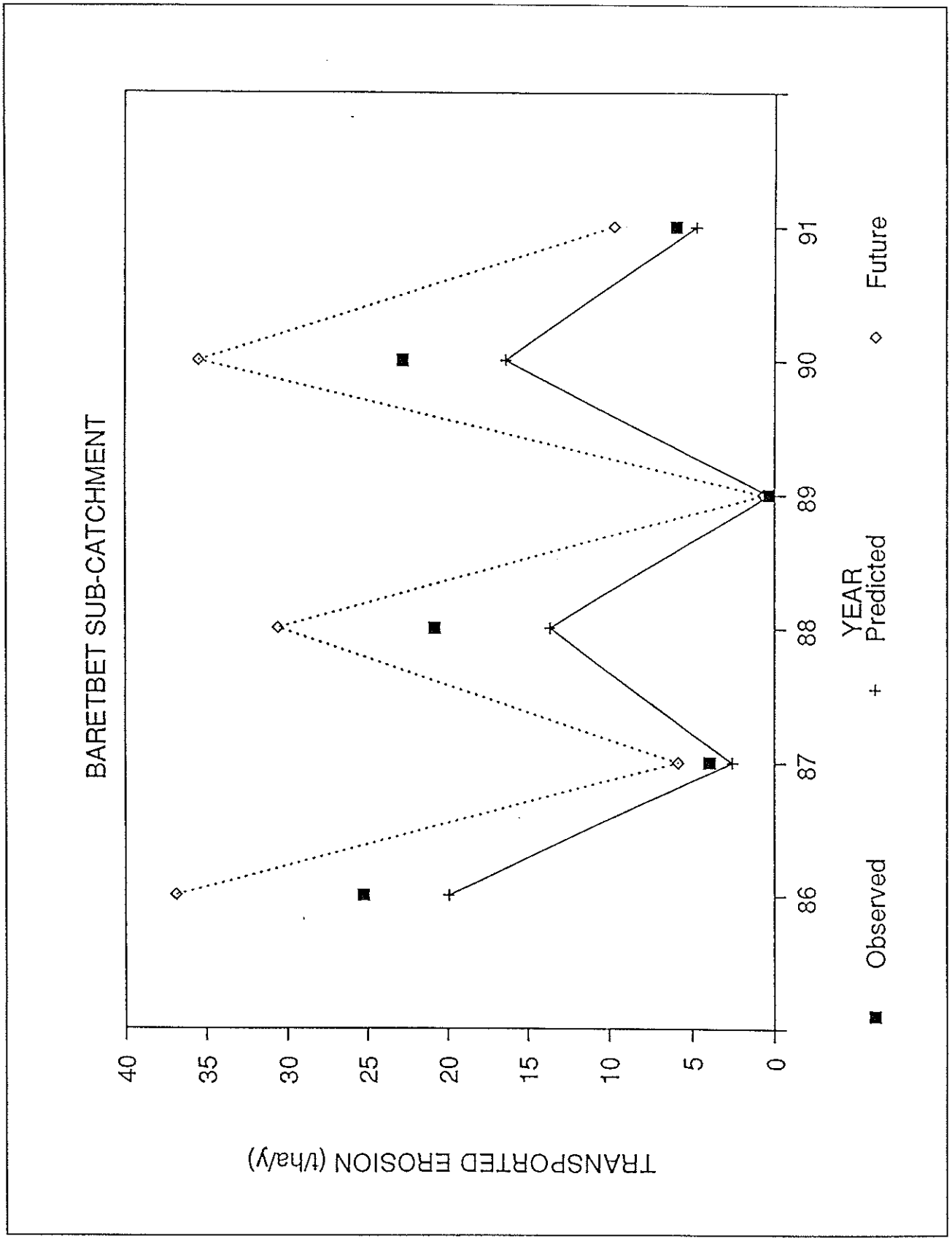

Figure 8.2 Baretbet sub-catchment transported erosion results

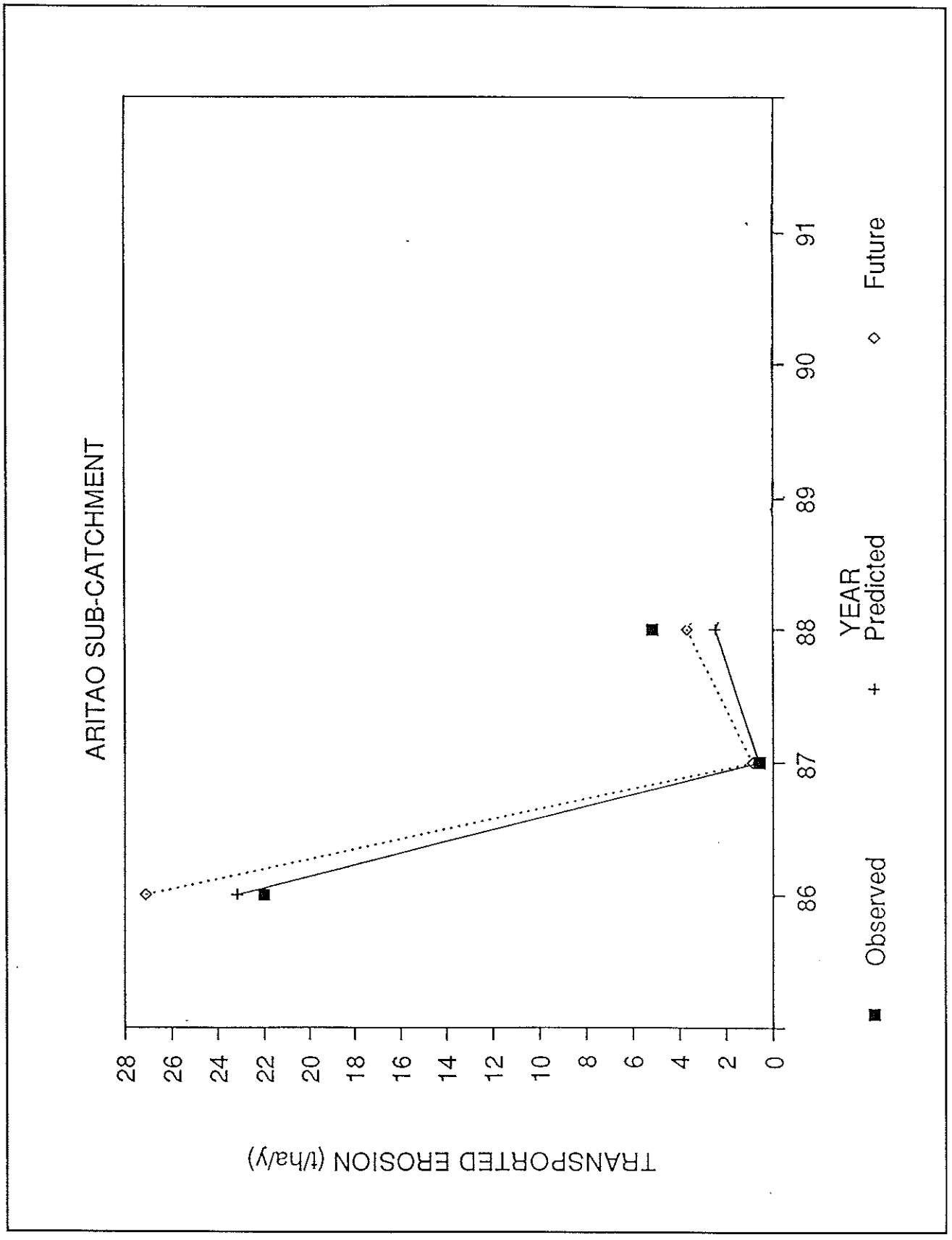

Figure 8.3 Aritao sub-catchment transported erosion results

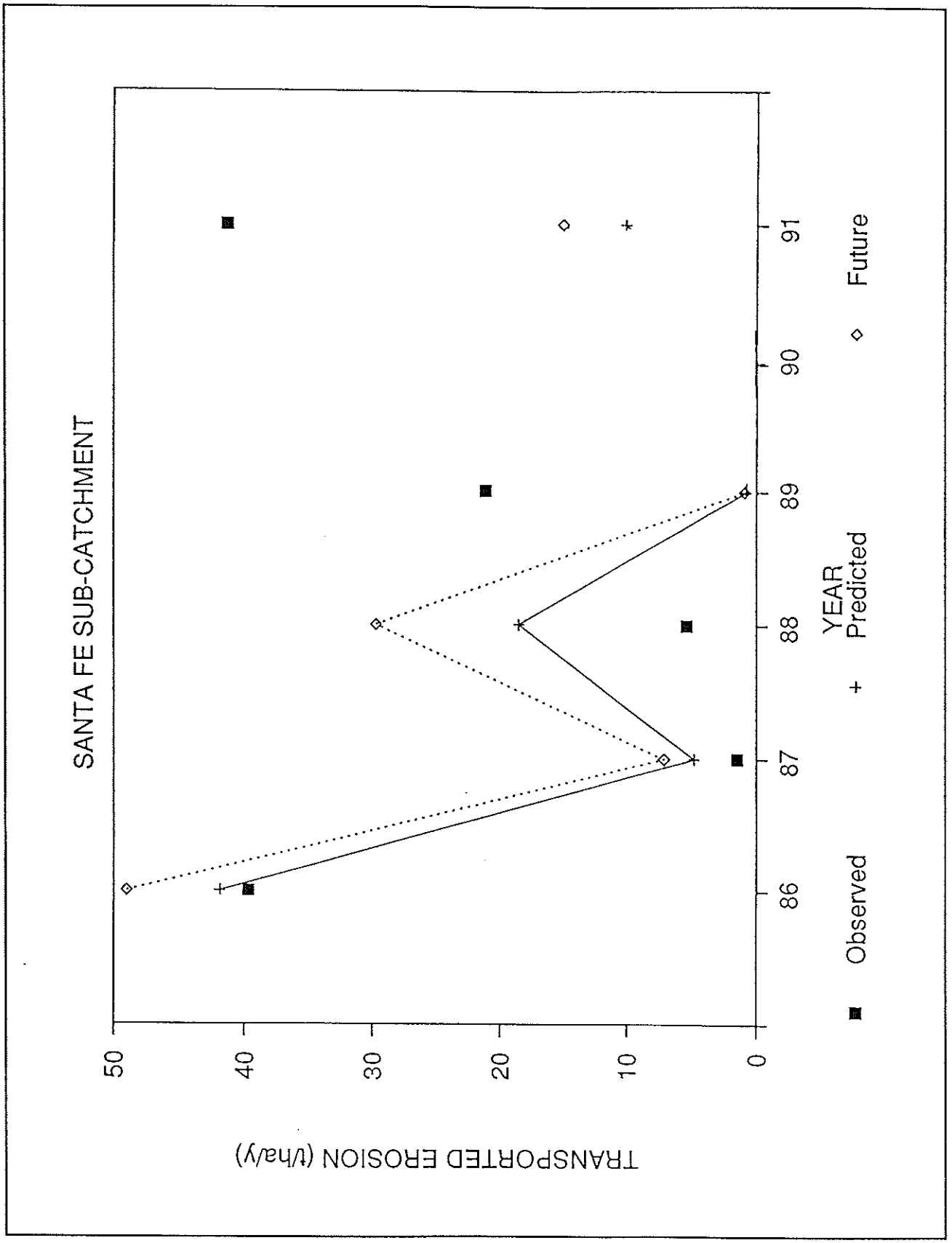

Figure 8.4 Santa Fe sub-catchment transported erosion results

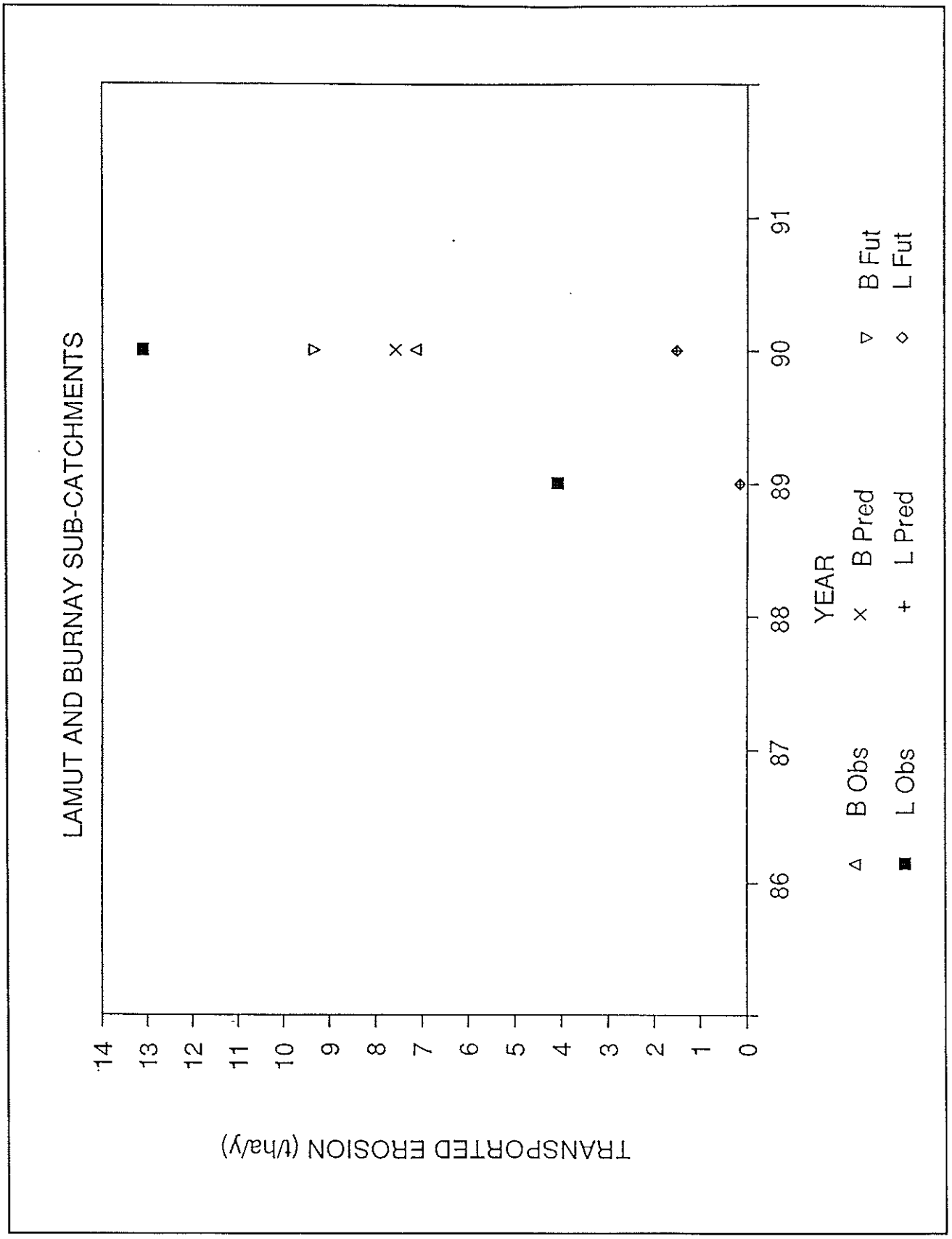

Figure 8.5 **Lamut and Burnay sub-catchment transported erosion results**

8.3 Modelling changing scenarios

One important use of CALSITE is in examining the impact of possible changes in land use and vegetation cover in terms of the effects of source erosion on the rate of reservoir sedimentation. In order to examine the effect of damage to the forest environment within the Magat catchment the assumption was made that the primary forest was part-felled to produce a secondary forest and the secondary forest was felled and left as scrubland. This was achieved within CALSITE simply by setting the crop coefficient value (C) for primary forest at 0.006 and the C-value for secondary forest at 0.25. The conversion of forest to grassland would result in a more drastic change.

Table 8.9 shows that for the rainfall regimes of the six years of this study the sedimentation would be increased by a factor of between 1.92 and 2.77 over the catchment as a whole, due to damage to the forest environment. The hypothetical land use change was modelled for several years to show the effect of different rainfall regimes. For each year under study the LUT for the land cover image was changed, yet all other factors, including the k, t and s calibration coefficients, were kept the same. Predictions based on current land use are labelled "current" in Table 8.9, whilst the future scenario of forest damage is labelled "future".

An examination of the transported erosion image for each of the years under study assuming damage to the forest environment shows that most of the increases in source and transported erosion are concentrated in the north-west of the catchment. The Baretbet catchment includes large areas of upland forest in the west of the catchment and, out of all the sub-catchments, results in the most pronounced increase in transported erosion is approximately doubled for the six years of the study. The catchments of Aritao, Santa Fe and Burnay have large proportions of forest, although as they are not affected by the high rainfall erosivity of the north-west of the catchment the effect of deforestation on sedimentation is less pronounced. Here transported erosion will be increased by between 5 and 60 per cent because of forest damage. The Lamut sub-catchment is unaffected by damage to the forest environment as the catchment contains little or no forest.

Table 8.9 The effect of damage to the forest environment on predicted transported erosion (t ha^{-1} yr^{-1})

Catchment	Year					
	1986	1987	1988	1989	1990	1991
Magat						
Current	25.94	3.77	19.73	0.521.	22.47	6.25
Future	49.72	10.44	53.86	01	59.10	14.81
Increase	1.92	2.77	2.73	1.95	2.63	2.37
Baretbet						
Current	19.93	2.63	13.66	0.40		4.77
Future	36.86	5.87	30.56	0.76		9.76
Increase	1.85	2.23	2.23	1.90		2.04
Aritao				N/A	N/A	
Current	23.17	0.61	2.47			
Future	27.13	0.85	3.67			
Increase	1.17	1.41	1.49			
Santa Fe						
Current	41.87	4.82	18.52	0.81		10.10
Future	48.98	7.17	29.67	0.96		15.10
Increase	1.16	1.48	1.60	1.17		1.49
Lamut	N/A	N/A	N/A			
Current				0.170	1.53	
Future				0.176	1.53	
Increase				1.030	1.0	
Burnay	N/A	N/A	N/A	N/A		
Current					7.58	
Future					9.32	
Increase					1.23	

9 Summary and conclusions

9.1 Summary of the CALSITE model

The CALSITE model combines a soil erosion model, based on the USLE, with sediment routing techniques in order to determine sediment delivery. The use of GIS technology enables the spatial variation in both source erosion and transported erosion to be visualised and mapped, so that areas of high erosion which greatly contribute to reservoir sedimentation can be identified for the implementation of conservation measures. Likewise the model may be used to assess the impact of proposed conservation measures or possible land use changes.

The model differs from most other soil erosion and sediment models in that a calibration routine is built-in to calibrate the estimates using observed annual sediment load values for sub-catchments, each time the model is run.

9.2 Summary of the results for the Magat catchment

The testing of the CALSITE model over 6 years for the Magat catchment has shown that even where information on rainfall, land cover and soils is limited quite a close correspondence can be made between the observed and predicted values of sediment yield. The year 1986 was the most successful, when for the three sub-catchments under study the differences between observed and predicted sediment measurements were between 5 and 21 per cent.

The model was found to be sensitive to anomalous calibration values, when a sub-catchment provided unexpectedly high or low observed sediment values which did not correspond to its environmental conditions. There are several possible explanations for such anomalous observed results. Firstly the method of sediment observation may be inaccurate, due to insufficient or erroneous samples over the year. High erosion rates may be associated with certain land management practices, such as clear felling, ploughing of grasslands, which are not identified on the land cover image used for source erosion estimation. Natural events such as earthquakes, landslips and intense localised storms may too result in unexpectedly high rates of sedimentation. Where one anomalous observed sediment value is used in the calibration this often reduces the accuracy of sediment yield predictions for the whole catchment.

The fact that sediment observations for the years 1986 and 1987 are so different, despite very similar annual rainfall totals, suggests that annual rainfall does not provide a good estimate of rainfall erosivity. An alternative method of estimating erosivity may be more appropriate which takes into account the frequency and duration of high intensity storms.

A major impedance to the production of accurate erosion and sediment predictions for the Magat catchment is the paucity of rainfall measurements over the catchment and the fact that the meteorological stations within the catchment, which have provided data over the six years of the study, are all below 700m elevation above sea level, yet the mountains in the catchment rise to about 2 900m elevation. Furthermore information on rainfall intensity is lacking.

The analysis of the Magat data has shown how possible land use changes can be modelled and their effects on sedimentation predicted. Further applications of CALSITE for modelling possible land use or rainfall regime changes will undoubtedly become apparent as the model is applied as a land management tool.

One aspect of the model which requires further development is how to use it to predict sediment yields for years when no sediment observations are available for calibration. The CALSITE version 1.0 has been adapted so that uncalibrated estimates of transported erosion can be made, based on standard delivery function, involving a standard LUT for a delivery image. The resulting uncalibrated transported erosion estimates could then be calibrated using calibrated data for one year for which reliable observed data are available. Such techniques were applied to the Magat data and have shown that such a technique is practical.

9.3 Possible improvements in the physical concept of the model

The estimation of source erosion is based on the USLE, which has been tried and tested in many countries over more than thirty years. One limitation of this equation is that it was derived in mid-west of the USA and may not be the best technique for erosion prediction in tropical environments. There may be scope for making use of empirical relationships which are based upon tropical catchments in a future version of CALSITE. Similarly if a physically-based model, such as WEPP, can be developed to provide reliable estimates of erosion, using data which are easily obtainable, then CALSITE could be adapted to use such a technique.

Whatever method of calculating source erosion is used it is important to use or collect data on source soil erosion from within or near to the catchment under study to ensure that these predictions are accurate. In the case of Magat the coefficients used for the USLE were based upon experimental work undertaken in the Philippines. Ideally soil erosion measurements should be made within a catchment under study, under a range of land cover, soil and topographic conditions to enable the accurate prediction of source erosion estimates.

As mentioned above the use of annual rainfall totals for predicting rainfall erosivity does not seem to provide accurate predictions of source erosion. The use of alternative techniques which take account of storm intensity are being considered.

The physical concepts used to determine the delivery index image and the method of converting this image to absolute delivery ratio values are based upon hydraulic principles. The delivery index is a function of annual rainfall, and the transporting capacity of overland flow, as defined by Equation 6.6. It may be the case that by modifying the exponents of Equation 6.6 a more accurate result may be achieved. The setting up of a field laboratory experiment to test this equation is beyond the scope of this research project. The alternative is to incorporate the ability for the user to change these exponents in future versions of the model, then to examine the effects of changes on the accuracy of predictions.

The calibration of the model is currently based on the modification of the delivery ratio values. This is because no calibration data are available to test the accuracy of the source erosion predictions. Ideally the accuracy of source erosion predictions should be improved by using more accurate predictive techniques and making use of source erosion calibration data from field plots.

Further investigations into how different rainfall regimes affect the threshold and saturation values for the delivery index from year to year would provide guidance on the selection of t and s values for model calibration. If experimental or theoretical research showed that these values were always within a certain range, then this could be taken into account when setting values within the model. The use of standard t and s values will be requried when using the model as a predictive tool.

Infiltration is assumed to be uniform over the catchment when determining overland flow, and in the case of the Magat catchment this is likely to be true as 99% of the soils are clay loam. However in some catchments sediment delivery will be influenced by variations in soil texture and permeability, which may have to be taken into account when calculating delivery ratios in future versions of the model.

The lack of sufficient rainfall data was found to be a major limitation for accurate erosion and sediment predictions. A similar situation is likely to arise when the model is applied to other tropical catchments. It may be feasible to obtain estimates of rainfall from satellite data, eg. from thermal measurements of cloud cover and temperature from meteorological satellites, or by the use of ground-based weather radar. If adequate runoff measurements are available throughout a catchment is may be possible to adapt the model to use runoff in place of rainfall in a similar manner to the adaption of USLE into its modified form 'MUSLE' (Williams, 1975).

9.4 Improvements in the computer implementation of the model

Version 1 of CALSITE and HR_CASCADE cannot be used as a general purpose catchment erosion prediction tool for several reasons. Firstly, HR_CASCADE is designed for use with a specific graphics card, the PC4000, which is not widely used and no longer in production. Secondly CALSITE Version 1 requires the use of files created on a GIS in a specific format and does not enable the creation of files within the package. Thirdly, CALSITE Version 1 can only be used for image sizes that are 500 by 700 in size. For larger areas the software would have to be modified.

One aim for the future development of the CALSITE software is to combine the existing functions of HR_CASCADE within the CALSITE package. A further aim is to make the package less dependent on the use of specific hardware and software. However, rather than including all pre-processing tasks such as satellite image classification and map digitization within CALSITE, it was considered more practical to assume that these are created using a GIS then converted, if necessary, into a standard image fill format for use with CALSITE.

In development of Version 2.0 of CALSITE trials have been made using image files created on the low-cost "IDRISI" Version 4.0 GIS software, produced by Clark University, Massachusetts, USA. Files may be converted to this format from ARC/INFO, ERDAS, MAP, AUTOCAD and several other computer software package formats.

Whereas some GIS software requires the use of an expensive graphics framestore card to display and manipulate image files, it is the intention for future version of CALSITE to display image files on a standard VGA or SVGA colour monitor and to perform any image file calculations either on disc files or by using large arrays in extended memory of the computer. Thus a computer with 2 or 3 MBytes of extended memory will be required, but there will not be the requirement for a specific graphics card with on-board memory, or a very high resolution colour monitor.

10 Acknowledgements

This research project was undertaken within the Overseas Development Unit of HR Wallingford in collaboration with the National Irrigation Administration, Government of the Philippines. The work formed part of the Units' research programme into erosion control, under the direction of Dr P Bolton, and is funded by the Overseas Development Administration of the British Government's Foreign and Commonwealth Office.

The participation in this project by the NIA is gratefully acknowledged. In particular, special thanks are due to Mr R L Baloloy, who enabled the successful installation of CALSITE in NIA's offices in Manilla.

The authors are indebted to Dr S M White and Mr H D Flach who were responsible for the initial developments of the model and to Mr A Dickinson of HR Wallingford who provided the data for calibration, ground data for satellite image classification and advice on the practical application of the model.

11 References

Abbot M B, Bathurst J C, Cunge J A, O'Connel P E and Rasmussen J (1986). An introduction to the European Hydrological System - System Hydrologique Europeen "SHE". 1: History and philosophy of physically based distributed modelling system. Journal of Hydrology. 87 pp 45-59.

Addiscott T M (1993). Simulation modelling and soil behaviour. Geoderma (in press).

Al Kadhami A M H (1982). Land use, water yield and soil erosion: simulation of cause and effect. PhD thesis of University of Strathclyde.

Amphlett M B and Dickinson A (1989). Dallao Soil Erosion Study, Magat, Philippines. Summary Report (1984 - 1987). Report No OD111, HR Wallingford, in collaboration with the National Irrigation Administration, Government of the Philippines.

Atkinson E (1992). Sediment Delivery in River Systems. OD/TN 48. Overseas Development Unit, HR Wallingford, UK.

Bathurst J (1992). Modelling sediment and contaminant transport at the catchment scale. Meeting of the British Hydrological Society. 21st Sept. 1992. University of Leeds.

Beasley D B, Mark E J and Huggins L F (1980). ANSWERS: a model for watershed planning. Trans ASAE, 23(4) pp839-944.

Beasley D B (1977). ANSWERS: a mathematical model for simulating the effects of land use and management on water quality. PhD thesis, Purdue Univ, Indiana, USA pp 266.

Becker A and Serban P (1990). Hydrological models for water-resources systems design and operation. Operational Hydrology Report No. 34. World Meteorological Organisation. Geneva, Switzerland.

Beven K (1989). Changing ideas in hydrology - the case of physically-based models. J Hydrol, 105, pp 157-172.

Biot Y (1990). THEPROM - An Erosion Productivity Model. In Soil Erosion on Agricultural Land. Ed. Boardman J, Foster I D L and Dearing J A. John Wiley and Sons Ltd.

Blyth E M and White S M (1990). Statistical analysis of rainfall in the Magat catchment, Luzon, The Philippines. Overseas Development Unit, OD/TN, November 1990, HR Wallingford, UK.

Borah D K (1989). Sediment discharge model for small watersheds. Trans ASAE 32(3), pp 874-880.

Brabben T E, Dickinson A and Amphlett M B (1991). Drainage basin monitoring for sediment yield prediction, in Wooldridge G (ed) Techniques for Environmentally Sound Water Resources Development, African Regional Symposium, Alexandria, Egypt, February 1991.

Bruce R R, Harper L A, Leonard R A, Snyder W M and Thomas A W (1975). A model for runoff of pesticides from small upland watersheds.

Cook D J, Dickinson W T and Rudra R P (1985). GAMES: Guelph Model for Evaluating the effects of Agricultural Management Systems on erosion and sedimentation. User's Manual. School of Engineering, University of Guelph, Guelph, Ontario.

Crawford D M and Linsley R K (1966). Digital simulation in hydrology: Stanford Watershed Model IV. Dept of Civil Eng, Stanford University. Tech Report 39, Palo Alto, CA, USA.

David W P (1989). Personal communication.

David W P (1982). Erosion and Sediment Transport. Seminar Paper presented to the MWFS staff and consultants, July 1982.

David W P and Beer C E (1975a). Simulation of soil erosion: Part 1, development of a mathematical erosion model. Trans ASAE 18(1), pp 126-129.

David W P and Beer C E (1975b). Simulation of soil erosion: Part 2, streamflow and suspended sediment simulation results. Trans ASAE 18(1). pp 130-33.

De Meijere J C, Mardarus, B and Van de Kasteele A M (1988). Land use modelling of the upper Komering Watershed. ITC Journal Vol 1. Int. Inst for Aerospace Survey and Earth Sciences, Netherlands.

De Roo A P S, Hazelhoft L and Burrough P A (1989). Soil erosion modelling using 'ANSWERS' and Geographic Information Systems. Earth surface processes and cardforms. Vol 14, pp517-532.

Dickinson A and Reid C M (1993). Sediment measurements (1986-1991) in the Magat catchment, Luzon, The Philippines. Overseas Development Unit, OD/TN 63. In press.

Dickinson A, Amphlett M B and Bolton P (1990). Sediment Discharge Measurements Magat Catchment. Summary Report: 1986-1988. Report No OD22, HR Wallingford, in collaboration with the National Irrigation Administration, Government of the Philippines.

Dickinson W T and Rudra R P (1990). GAMES. The Guelph model for evaluating effects of agricultural management systems on erosion and sedimentation. User's Manual, Version 3.01. School of Engineering, Tech Report 126-86, University of Guelph.

Dickinson W T, Rudra R P and Wall G J (1986). Identification of soil erosion and fluvial sediment problems. Hydrological Processes, Vol 1, pp111-124.

Douglas I (1967). Man, vegetation and the sediment yield of rivers. Nature, Vol 215, 26 August 1967.

Douglas I C (1968). Sediment sources and causes in the humid tropics of North Queensland. In: Harvey A M (Ed) "Geomorphology in tropical

environment", British Geomorphological Research Group, Occ Paper No 5, pp 27-39.

Elwell H A (1980). A soil loss estimation technique for Southern Africa. Proc. "Conservation 80". Silsoe College, Silsoe, UK.

Engelund F and Hansen E (1967). A monograph on sediment transport. Technisk Forlag, Copenhagen.

Fleming G (1969). Design curves for suspended load estimation. Proc Inst Civil Eng 43, pp 1-9.

Fleming G and Walker R (1976). A runoff erosion model for land use assessment and management. Tech. Report, Dept of Civil Eng, Univ of Strathclyde, Glasgow, UK.

Foster G R (1990). Process-based modelling of soil erosion by water on agricultural land. In Soil Erosion on Agricultural Land. Boardman J, Foster I D L and Dearing J A (eds). John Wiley and Sons.

Foster G R (1982). Modelling the erosion process. From Hydrologic Modelling of Small Watersheds. ASAE Monograph Number 5. Ed. C T Haan. ASAE.

Foster G R and Meyer L D (1975). Mathematical simulation of upland erosion by fundamental erosion mechanics. Proc. Sediment Yield Workshop. USDA Sediment Lab. Oxford Miss. Nov 28-30, 1972. US Agr. Res. Ser. ARS-5-40. 285pp.

Fournier R (1960). Climat et erosion, la relation entre l'erosion du sol par l'eau et les precipitations atmospheriques. Presses Universitaires de France, Paris.

Govers G (1990). Empirical relationships for the transport capacity of overland flow. Erosion Transport and Deposition Processes (Proc. of the Jerusalem Workshop, March-April, 1987) IAHS Publ. No. 189.

Gupta S K and Solomon S I (1977). Distributed sediment model for estimating runoff and sediment discharge of ungauged rivers. Parts I, II and III, Water Resources Research, 13(3) 613 (June).

Hession W C and Shanholtz V O (1988). A geographical information system for targeting non-point-source agricultural pollution. Journal of soil and water conservation. Vol 43(3), pp 264-266.

Hirschi M C and Barfield B J (1988). KYERMO - A physically based research erosion model. Part 1 Model development. Trans ASAE 31(3), pp 804-813.

Holy M H, Vrana K, Vaska J and Brazdilova B (1989). SMODERP. Simulation model of surface runoff and erosion processes (unpublished). Department of Irrigation and Drainage, Czech Technical University, Prague.

Julien P Y and Simons D B (1985). Sediment transport capacity of overland flow. Trans ASCE 28(3) pp 755-762. May-June 1985.

Kirkby M J (1974). Hydrological slope models: the influence of climate. Unpublished working paper No 89, pp 14. Geography Dept, University of Leeds, UK.

Lafflen J M, Elliot W J, Simanton J R, Holzhey C S, Kohl K D (1991). WEPP Soil erodibility experiments for rangeland and cropland soils. J Soil and Water Cons. Jan-Feb. pp 39-44.

Lea N J (1991). An aspect driven kinematic routing algorithm. Paper presented at: Workshop on the hydraulics and erosion mechanics of overland flow. University of Keele, Staffordshire, England. 6-12 July 1991.

Lenrain J (1975). Kritische studie van Universele Erosievergelijking en Laar bruikbaarheid als evaluatiemiddel van de bodemkonditioneringstechniek in der vochtige tropen. Thesis, State University Gent, Belgium.

Li R M (1977). Water and sediment routing from watersheds. In: Proc River Mechanics Institute, Chapter 9, Colorado State University, Fort Collins, USA.

Maner S B (1958). Factors influencing sediment delivery rates in th Red Hills physiographic area. Trans. Am. Geophys. Union, 39. pp669-675.

Meyer L D (1981). How rain intensity affects interrill erosion. Trans Am Soc of Agric Eng. 24 pp 1472-1475.

Meyer L D and Wischmeier W H (1969). Mathematical simulation of the processes of soil erosion by water. Trans Am Soc of Agric Eng. 12 pp 754-8, 762.

Morgan R P C, Morgan D D V and Finney H J (1986). A simple model for assessing annual soil erosion on hillslopes. In Giorgini A and Zingales F (eds). Agricultural Nonpoint Source Pollution: Model Selection and Application. Elsevier, Oxford. pp 147-59.

Moore R J and Clarke R T (1983). A distribution function approach to modelling basin sediment yield. Journal of Hydrology 65, pp 239-257.

Mou J and Meng Q (1980). Sediment delivery ratio as used in the computation of watershed sediment yield. Chinese Society of Hydraulic Engineering, Beijing.

Murota A and Hasino M (1969). Studies of a stochastic rainfall model and its application to sediment transportation. Technol. Rep. Osaka Univ. 19 pp 231-247.

Mutchler C K and Bowie A J (1976). Effect of land use on sediment delivery ratios. In Proc. of the third Federal Inter-Agency Sedimentation Conference. US Water Resource Counc., Washington DC, pp 1.11-1.12.

Negev M (1967). A sediment model on a digital computer. Tech Report No 76, Dept of Civil Engineering, Stanford University, California, USA.

Neibling W H and Foster G R (1977). Estimating deposition and sediment yield from overland flow processes. Int. Symp. on Urban Hydrology. Univ. of Kentucky, Lexington, Kentucky, July 18-21, 1977.

NIA and Engineering Consultants Inc. (1978). Draft feasibility report - Magat watershed management project. Vol I, II, III. National Irrigation Administration, Manilla, Philippines.

Philip J R (1991). Soils, natural science and models. Soil Science 151(1) pp 91-98.

Roehl J R (1962). Sediment source areas, delivery ratios and influencing morphological factors. Int. Assoc. Hydrol. Sci. Publ. 59, pp 202-213.

Russel J R (1981). Sedimentation in the proposed Kotmale reservoir, Sri Lanka. In South East Asian Regional Symposium on problems of soil erosion and sedimentation, Bangkok, Thailand, 27-19 January 1981, AIT.

Smith D D and Whitt D M (1948). Evaluating soil losses from field areas. Agric. Engineering, 29, pp349-396.

Smith R E (1977). Field test of a disturbed watershed erosion/sedimentation model. In: Soil erosion: prediction and control. Soil Conservation Society of America, Special publication No 21, Ankeny, Iowa, USA.

USDA (1980). CREAMS: A field scale model for chemicals, runoff and erosion from agricultural catchment management systems. Conservation Research Report No 26. Science and Education Admin. pp 643.

Walling D E (1983). The sediment delivery problem. J Hydrol, 65 pp 209-237.

White S M (1989). Sediment Yield Assessment using a Geographical Information System. International Symposium on River Sedimentation. IRTCES, Beijing, China, 5-9 June 1989.

White S M (1987). Estimation of sediment yield. Bandung Workshop 22-24 September 1987. Overseas Development Unit OD/P 101, HR Wallingford, UK.

Wight J R (ed) (1983). SPUR: Simulation of production and utilisation of rangelands: a rangeland model for management and research. USDA ARS Miscellaneous Publ No 1431, pp 120.

Williams J R, Dyke P T and Jones C A (1982). EPIC: a model for addressing the effects of erosion on soil productivity. In: Proc Third Int Conf on State-of-the-Art in ecological modelling. Colorado State Univ, Fort Collins, Colorado, USA, 24-28 May 1982.

Williams J R (1977). Sediment delivery ratios determined with sediment and runoff models. Int. Assoc. Hydrol. Sci. Publ. 122, pp 168-179.

Williams J R (1975). Sediment routing for agricultural watersheds. Water Resources Bulletin, Vol 11, No 5, pp 965-974.

Williams J R and Berndt, H E (1972). Sediment yield computed with universal equation. J Hydraul. Div., Proc. Am. Soc. Civ. Eng., 98(HY2): pp 2087-2097.

Wischmeier W H and Smith D D (1958). Rainfall energy and its relationship to soil loss. Trans Am Geophys Union, 39, pp 258-291.

Wischmeier W H, Johnson C B and Cross B V (1971). A soil erodibility nomograph for farmland and construction sites. J. Soil and Water Conserv. 26, pp189-93.

Wischmeier W H and Smith D D (1978). Predicting rainfall erosion losses: a guide to conservation planning. USDA-SEA Agr. Handbook 537, Agr Res Serv, pp 58, USDA, Washington DC, USA.

Woolhiser D A and Todorovic P (1974). A stochastic model of sediment yield for ephemeral streams. Proc. USDA - IASPS Symposium on Statistical Hydrology. USDA Misc. Pub.

Woolridge R (1986). Sedimentation in reservoirs: Magat reservoir, Central Luzon, Philippines - 1984 reservoir survey and data analysis. Report No OD69, HR Wallingford.

Young R A, Onstad C A, Morris M N, Bosch D D and Anderson W P (1987). AGNPS, Agriculture Non-Point Source Pollution Model. A Watershed Analysis Tool. USDA Agric Service. Conservation Research Report 35. pp 80.

List of variables

a = Coefficient in sediment delivery equation (Equation 6.3)
A = Regression coefficient used in the rainfall elevation (Equation 4.1)
b = Coefficient in sediment delivery equation (Equation 6.3)

B = Regression coefficient used in the rainfall elevation relationship (Equation 4.1)

C = Cropping factor used in the USLE (see Equation 2.1)
CP = Combined crop management and conservation practice factor or USLE (see Equation 3.1)

d = Flow depth
D_{50} = Median sediment size
DI_p = Delivery index for an individual pixel
DR = Delivery ratio
DR_p = Delivery ratio for an individual pixel (Equation 1.1)

E = Annual kinetic energy of rainfall
E_a = Average annual soil loss estimated using an erosion predictor such as USLE

f = Used to denote some unspecified function of a given variable
F = Flow path score (number of paths which cross a given pixel)

g = Gravitational constant

I_{30} = Maximum intensity of a 30 minute rain storm in a particular year

k = Scaling constant used in the calibration of transported erosion in CALSITE
$k_1 ... k_i$ = Other scaling constants specified in particular equations
K = Soil erodibility factor used in the USLE (see Equation 2.1)

L = Slope length
LS = Slope length and steepness factor used in the USLE (see Equation 2.1)

n = Manning's coefficient

O = Observed sediment yield

p = Channel welted perimeter
P = Conservation practice factor used in the USLE (see Equation 2.1)
P_a = Annual precipitation (rainfall)
P_r = Predicted sediment yield

Q = Liquid discharge
Q_p = Peak runoff (Equation 2.3)

r = The difference in elevation across a surface (the 'relief')
R = Rainfall erosivity factor used in the USLE (see Equation 2.1)

R_c = Annual rainfall at Consuelo (in Magat catchment)
R_h = Hydraulic radius of flow
RC = Crop type and cropping practices factor used in SLEMSA (see Equation 2.2)
RK = Soil loss estimation from bare soil used in SLEMSA (see Equation 2.2)
RX = Slope steepness and length factor used in SLEMSA (see Equation 2.2)

s = Saturation value of DI_p in the delivery function
S = Slope of land surface or river channel
SE = Annual 'source erosion' from a pixel

t = Threshold value of DI_p in the delivery function
T = Sediment transporting capacity
TE = Annual 'transported erosion' from a pixel to a specified catchment outlet

$\overline{u}$ = Mean flow velocity
u_* = Shear velocity

V_a = Total annual volume of discharge (overland flow)

w = Channel width

X = Sediment concentration
X_f = Sediment concentration transporting capacity along a flow path

Y_a = Estimated annual sediment yield

Appendices

Appendix 1

Results of sedimentation surveys of Magat reservoir

Appendix 1 Results of sedimentation surveys of Magat reservoir

A1.1 Methods for computing sedimentation rates from survey data

Rates of reservoir sedimentation are generally monitored by means of hydrographic surveys by means of which the current storage capacity of the reservoir is estimated. The differences between two or more such surveys, or between a single survey and a design capacity calculated from a pre-impoundment map provide estimates of the deposited volume of sediment in a given period. In the early years of a reservoir's life, when the volume of deposited sediment is small, this method of measurement introduces large potential errors in the estimated sedimentation rate since it is a small number obtained as the difference between two large numbers.

A second difficulty in estimating long-term sedimentation rates from both sediment monitoring in rivers and hydrographic survey of reservoirs is the magnitude of inter-annual variations: the sediment load in a single year has often been known to exceed the combined load in the previous ten years or more. The calculated average rate of sedimentation will, therefore, be strongly influenced by whether a year of heavy sediment transport occurred during the period under study.

A further difficulty in obtaining reliable estimates of sedimentation rates from reservoir survey data is the inaccuracy of some computational procedures used to estimate volume changes from range line survey results. Faraji and Bolton (1987) and Bird (1988) reviewed available computational methods and showed that the Constant Factor method of Burrell (1951) was superior to other methods because it used information derived from the pre-impoundment contour map to guide the interpolation. The original volume of the reservoir between survey lines is calculated by planimetry of the contour areas from the original map and is adjusted to give the new volume by reference to the sediment accumulated on the upstream and downstream survey lines.

Lea (1991) developed an improvised computational method, the Stage Width Modification Method, which uses contour areas to guide interpolation, as with the Constant Factor Method, but instead of taking information from the survey lines at increments according to the contour spacing, provides a method of continuous integration over the full depth of each section. This method produces a significant increase in accuracy particularly for the deepest parts of the section, below the lowest contour elevation, and upstream of the first survey line on the headreaches of the main reservoir and tributary arms. In a comparison between the Stage Width Modification Method and Constant Factor Method for data from a reservoir in Zimbabwe errors were typically halved by the new method and greater stability in volume estimates was produced when data were sparse (increased range line spacing or increased contour interval). The Stage Width Modification Method program called SWIMM which includes on-screen editing facilities to correct errors in survey data.

A1.2 Sedimentation rates for Magat Reservoir

Survey beacons were established on 35 range lines across the reservoir basin prior to impoundment and were surveyed by land-survey methods in 1977 and 1978. Reservoir impoundment began on 7 March 1982 and an initial hydrographic survey of the reservoir was conducted by NIA in collaboration with HR Wallingford beginning in October 1984. Part of this survey was completed by land survey at a later date because reservoir levels were low. The analysis of these data suggested a total sediment deposition of approximately 22 x 10^6 m^3 out of an initial volume below a storage level of 193m of 1346 x 10^6 m^3 (1.6%), see Wooldridge, 1986. The errors in survey technique are large in relation to this small quantity of sediment being measured with the result that errors of the order of 20-30% in the final result might be expected. The 1984 analysis was done prior to the development of SWIMM, using the Constant Factor Method, but in this the additional error introduced was negligible. However, in interpreting the result, a significant error was made in that it was assumed that the reservoir had been in operation for only two years. In fact, since the main river discharges occur in September and October and since the land survey of the range lines in the head reaches, where initial sedimentation is greatest, were completed after October, the reservoir had received three seasons of monsoon inflows when the critical sections were surveyed. The sediment yield figure published by Wooldridge (1986) as 38 t ha^{-1} yr^{-1} should, therefore, have been closer to 25 t ha^{-1} yr^{-1} using his assumptions about trapping efficiency and density of deposited sediment.

In the latter part of 1988 and early 1989 NIA conducted a second reservoir survey. The results of this survey have been processed using SWIMM and at the same time the 1984 results have been re-analysed using SWIMM. The sediment volumes from the two surveys estimated from the two sets of survey result are set out below.

Year of survey	No. monsoon seasons	Volume sediment below 193m (x 10^6 m^3)	Proportion of total capacity lost
1984	3	22	1.6
1988/89	7	49	3.6

The sediment yield can be calculated assuming that the deposited sediment has a mean density of 1320 kgm^{-3}, that the Magat has a trapping efficiency of 92% and that the basin area is 4123 km^2.

Period	Years	Mean annual sediment yield (t ha^{-1} yr^{-1})
1981/2-1984/5	3	25.5
1984/5-1988/9	4	23.5
1981/2-1988/9	7	24.4

The above figures are, however, subject to errors, as explained above, due to the difficulty of achieving high survey accuracy with small differences in

reservoir capacity. As estimates of long-term sediment yields they should be viewed with caution due to the inter-annual variability of sediment loads in rivers such as the Magat. Much longer periods of monitoring would be required before a reliable figure could be deduced.

References

Bird, J D (1988). Digital Terrain Models for volume measurement of reservoir sedimentation and accuracy assessment of range line computational methods. Technical Note OD/TN/38. HR Wallingford.

Burrell, G N (1951). Constant Factor Method aids computation of reservoir sedimentation. Civil Engineering, ASCE 21(7), p 51-52.

Faraji, S A S and Bolton, P (1987). Methods for the computation of reservoir capacity and the volume of sediment deposits using range line survey data. Technical Note OD/TN/24, HR Wallingford.

Lea, N J (1991). Analysis of reservoir range line surveys using the Stage Width Modification Method. Technical Note OD/TN/56, HR Wallingford.

Woolridge, R (1986). Sedimentation in reservoirs: Magat reservoir, Central Luzon, Philippines - 1984 reservoir survey and data analysis. Report No OD69, HR Wallingford.

Appendix 2

Preparation of the elevation image from a contour map

Appendix 2 Preparation of the elevation image from a contour map

Elevation, slope and aspect are three of the important controlling variables in erosion risk assessment. However, elevation is only known at discrete intervals (contours and spot heights) from topographic maps. Slope and aspect maps were not available for Magat and are normally not available. Therefore in order to assess slope and aspect and to obtain an estimate of elevation for each pixel, a digital elevation model (DEM) is needed. The topographical map used was a 1:500 000 Tactical Pilotage Map (TPM) of Northern Luzon. Data were available at much larger scales, but it was felt that little accuracy would be gained in using these, although the workload would have vastly increased. Use of the TPM meant that this map could be electronically scanned rather than using the slightly less accurate video grabbing techniques. Any larger map would have made scanning prohibitively expensive, and data extraction extremely time-consuming.

The data needed to use a DEM are a series of spot heights covering the whole catchment. This can be achieved by tracing contours on the screen using a mouse, and recording points along the mouses' journey. In practice this is achieved by typing an elevation value for a certain contour into the computer via the keyboard. The mouse cursor is then used to follow that contour on the screen, drawing a line as it goes. Each time the contour changes direction a button on the mouse must be pressed to end one segment of the line and start the next one. The co-ordinates of the mouse cursor at the point where the button is pressed are recognised by the computer and can be stored in an output file together with the elevation of the contour concerned and other identifying features. The same sort of procedure can be followed for spot heights, only in this case it is only necessary to type in elevation, locate the mouse cursor and push the button for the data to be stored. This operation was carried out for all contours and spot heights on the TPM.

Digital elevation models (DEM's) work by fitting a smooth surface between a series of points of given elevation. There are several techniques available to achieve this, of which the following were tried:-

1. Bi-linear interpolation

   (a) Linear interpolation between adjacent data points in the X direction, followed by the same procedure in the Y direction. This gave two sets of estimates of elevation for each pixel, which were averaged to give the final DEM.

   (b) Linear multi-quadratic interpolation in the X and then the Y directions, followed by averaging of the two sets of results. This technique considers a whole horizontal or vertical line of pixels at one time, fitting a profile to all of the data points at once.

2. Multi-quadratic areal interpolation (Hardy, 1974)

Here information from blocks surrounding the pixel of interest is used to predict the elevation of the pixel. By using more of the surrounding data, instead of simply adjacent points it is possible to fit a more realistic surface to the DEM.

This type of analysis does, however, take longer to run and tends to be strongly influenced by the concentration of data on the contours. The result of this can be an extremely stepped profile for the DEM.

3. Lest squares fit to the surface

These techniques are all based on data from the area surrounding the pixel of interest. The computer searches for the 'n' nearest points in each direction out from the pixel. There is a limit on how far away from the pixel can be searched to find the 'n' points, as data from further away obviously does not have an influence. When the 'n' points have been found a surface is fitted to all of the selected points, with data from further away being weighted to have less influence.

(a) Plane fit - using a function of the form f(1, x, y)

(b) Hyper-surface fit - f(1, x, y, xy)

(c) Polynomial surface - f(1, x, y, xy, x^2, y^2)

All six of these methods were tried with mixed results. Most of the techniques were heavily influenced by the concentration of data on the contours and corresponding lack of data between them. This resulted in very stepped profiles for the DEM.

Because of these high concentrations of data, use of any interpolation techniques becomes difficult. It was therefore decided to compress the data file onto a smaller grid thus effectively reducing the number of points on the contours and the number of points needing interpolation. A DEM is produced at this smaller scale, and then this is used as input to another interpolation technique to expand the map to full size again. Elevations on the resultant map are scaled such that numbers between 0 and 255 can be used to represent height.

The standard way of checking the effectiveness of an interpolation procedure such as these is to check the root mean square error (RMS error). This checks how well the fitted surface has maintained the original data points. All of the above techniques have an RMS error of less than 1 pixel, indicating a good fit. Maximum errors were also only around 2 to 3. However, these checks are rather inadequate in assessing the goodness-of-fit of a DEM, as it is possible to entirely maintain the original data set whilst fitting unrealistic elevations to other data points. This is just what happens for the DEM's which produce stepped profiles. There has therefore to be some element of qualitative assessment of the DEM's produced as well as checks on RMS errors.

Using qualitative and quantitative procedures to check the DEM's produced by the six techniques described above, it seemed that the plane least squares fit to the elevation data gave the best representation of the catchment surface, and maintained the original contour and spot height data. T his interpolation was carried out on the small scale data file with the result being expanded to full size by bi-linear interpolation. The resultant elevation model was used for all further work.

Reference

Hardy, Rolland L (1974). Multiquadratic equations of topography and other irregular surfaces. Journal of Geophysical Research, Vol 76, No 8, p1905-1915.

Appendix 3

Aspect, slope and flow path algorithms

Appendix 3 Aspect, slope and flow path algorithms

A3.1 Overland flow on a planar surface

With respect to the behaviour of overland flow on a planar surface, consider a point source on a uniform hillslope and the direction which water will flow from it. The hillslope can be modelled as a plane in three-dimensional cartesian co-ordinates with the z-ordinate representing elevation. The equation of an arbitrary plane intersecting the origin is:

$$z = Ax + By \qquad \text{Equation A3.1}$$

Consider a unit path beginning at the origin in the XY plane and described by the angle θ. The projection onto the plane of the end of the unit path is:

$$z = A\cos\theta + B\sin\theta \qquad \text{Equation A3.2}$$

Water will flow along the path leading to the lowest point on the plane (i.e. along the steepest downhill gradient). This path will have direction θ when Equation A3.2 above is at a minimum.

We can rewrite Equation A3.2 in the form:

$$z = R\cos(\theta + \alpha) \qquad \text{Equation A3.3}$$

where $\alpha = -\arctan(B/A)$ and $R = \sqrt{(A^2 + B^2)}$

Since R is positive, the minimum value of z occurs when:

$$\theta + \alpha = \pi \qquad \text{Equation A3.4}$$

giving: $\theta = \pi + \arctan(B/A)$ Equation A3.5

The cartesian unit vector in the direction of θ in the XY plane $(\cos\theta,\sin\theta)$ is equal to $(-A/\sqrt{(A^2 + B^2)}, -B/\sqrt{(A^2 + B^2)})$. Thus flow proceeds across a plane defined by the equation, $z = Ax + By$, in the direction of the vector $(-A,-B)$.

The *aspect vector* is defined as the projection of the normal to the surface onto the XY plane. The normal to a surface is the 3-dimensional vector defined in terms of the directional derivatives $(-\delta z/\delta x,-\delta z/\delta y,1)$ and its projection onto the XY plane is the 2-dimensional vector $(-\delta z/\delta x,-\delta z/\delta y)$. Since A and B are the coefficients of x and y respectively, they are also the directional derivatives, $\delta z/\delta x$ and $\delta z/\delta y$. Thus the vector describing the direction of flow is equal to the aspect vector.

Given that flow proceeds in the direction of the aspect vector, the routing algorithm determines flow paths using only aspect information. Elevation data is used solely in the initial determination of aspect. The basis of the algorithm developed below is to model the entry and exit points of flow on the perimeter of each pixel and to consider flow within a pixel as a point source moving in the direction of the aspect vector. This overcomes the inaccuracies encountered with 'lowest neighbour' algorithms and has proved to be suitable for the prediction of sub-catchment boundaries.

A3.2 Aspect Calculation

Before defining the flow algorithm, it is necessary to consider the problem of deriving aspect values from the matrix of elevation points that comprise the Digital Terrain Model. Since the aspect vector is derived from a surface and the DTM specifies spot heights at the centre of pixels, the first task is to fit planes representing the surface of each pixel.

Suppose the DTM uses a three dimensional cartesian co-ordinate system with the z-ordinate representing elevation. Without loss of generalization it is possible to shift onto a co-ordinate system where the SW corner of the pixel is at (0,0) in the XY plane, and the NE corner has co-ordinates (1,1). A plane is then required of the form:

$$z = \alpha x + \beta y + \gamma \qquad \text{Equation A3.6}$$

For the purpose of calculating the aspect vector (which only requires α and β), we neglect the spot height defined at the centre point and fit a plane to the co-ordinates of the four corners. Since three linearly independent points in three dimensions uniquely define a plane, a "best fit" plane must be found to fit the four points given.

Using the principle of least squares, the best fit plane is obtained when:

$$\alpha = ((c_{ne} - c_{nw}) + (c_{se} - c_{sw}))/2 \qquad \text{Equation A3.7}$$

$$\beta = ((c_{ne} - c_{se}) + (c_{nw} - c_{sw}))/2 \qquad \text{Equation A3.8}$$

where c_{ne}, c_{se}, c_{nw}, c_{sw} are the estimated elevations of the four corners of the pixel.

Since α and β are the estimated coefficients of x and y in the equation of the plane, the aspect vector, as already discussed, is simply $(-\alpha,-\beta)$. Equivalently it can be defined as the angle θ which is equal to $\pi+\arctan(\beta/\alpha)$.

For the purposes of overland flow routing, it is necessary for the aspect to be defined at every pixel. It is quite possible that α and β are both computed to be zero in which case the aspect, θ, would remain undefined. Since this would never happen on real terrain - there is always a direction of greatest slope no matter how shallow it is - an estimate must be made of the aspect under these conditions.

Suppose the aspect vector is undefined, i.e. $\alpha=0$ and $\beta=0$. By solving Equations A3.7 and A3.8 simultaneously, it can be seen that the situation only occurs when:

$$c_{se} = c_{nw} \qquad \text{Equation A3.9}$$

$$\text{and, } c_{ne} = c_{sw} \qquad \text{Equation A3.10}$$

that is, when both pairs of opposite corners have equal elevations. In such cases, the estimated elevations of the corner pixels can be re-calculated using wider consideration of the terrain data. Initially the estimated elevation of each corner (C_{se}, C_{sw}, C_{ms}, C_{ne}) is calculated as the mean of the four surrounding

spot heights. This process can be expanded and the mean of a three by three square of spot heights with its corner on the centre pixel may be used for the new estimate. If these estimates cause the same problem, a four by four square is used and so on (see Figure A3.1).

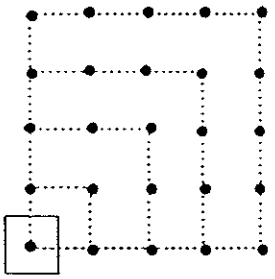

Figure A3.1 Iterative estimation of corner elevations.

By this means, the angle of the aspect vector may be calculated for each pixel. The routing algorithm defined in the next section makes use of only this parameter since it contains all the information needed to derive flow paths.

A3.3 Slope calculation

In deriving the aspect vector for the arbitrary plane $z = Ax + By$ in Section A3.1 it was shown that the unit vector in the direction of greatest slope is:

$$\left(\frac{-A}{\sqrt{A^2+B^2}} , - \frac{B}{\sqrt{A^2+B^2}} \right)$$

The change in elevation, z, in moving from the origin (which is on the plane) to the point on the sloping plane with the coordinates, $\left(\frac{-A}{\sqrt{A^2+B^2}} , - \frac{B}{\sqrt{A^2+B^2}} , h \right)$ is:

$$h - O = \left[A. \frac{-A}{\sqrt{A^2+B^2}} + B. \frac{-B}{\sqrt{A^2+B^2}} \right] - O$$

$$= - \frac{A^2+B^2}{\sqrt{A^2+B^2}}$$

$$= - \sqrt{A^2+B^2}$$

Slope is the change in z divided by the distance moved in the horizontal plane; the latter is 1 because the point in the horizontal plane, $\left(- \frac{A}{\sqrt{A^2+B^2}} , - \frac{B}{\sqrt{A^2+B^2}} , O \right)$ is on the unit circle; therefore:

$$\text{Slope} = \sqrt{A^2+B^2} = R = \sqrt{\left(\frac{\partial z}{\partial x}\right)^2 \left(\frac{\partial z}{\partial y}\right)^2} \qquad \text{Equation A3.11}$$

In the generalised form of the equation of the plane, A equates to α and B to β (Equations A3.7 and A3.8) so the slope image can be created as part of the same calculations used to create the aspect image.

A3.4 Flow routing

Flow is assumed to originate at the centre of the source pixel and travel kinematically as a point source. In the following analysis the co-ordinate system defined above is used with the SW corner of the source pixel having co-ordinates (0,0) and the NE corner having co-ordinates (1,1). Consider the source pixel. Flow originates at the point (0.5,0.5) and proceeds in the direction of the aspect, θ, until it reaches the perimeter.

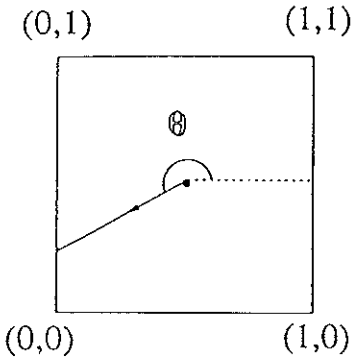

Figure A3.2 Initial flow path from the centre point of a pixel.

The co-ordinates (x_o,y_o) are defined to be the 'outlet point' i.e. the intersection of the pixel's perimeter with the flow path. The relationship between the outlet point and the aspect is derived by simple trigonometry and is given by:

$(x_o,y_o) = (1, (1+\tan\theta)/2)$ for $-\pi/4 < \theta \leq \pi/4$:eastern exit
$= ((1+\cot\theta)/2, 1)$ for $\pi/4 < \theta \leq 3\pi/4$:northern exit
$= (0, (1-\tan\theta)/2)$ for $3\pi/4 < \theta \leq 5\pi/4$:western exit
$= ((1+\cot\theta)/2, 0)$ for $5\pi/4 < \theta \leq 7\pi/4$:southern exit

The outlet point (x_o,y_o) translates to an inlet point (x_i,y_i) on the perimeter of the neighbouring pixel that shares the edge on which the outlet point lies.

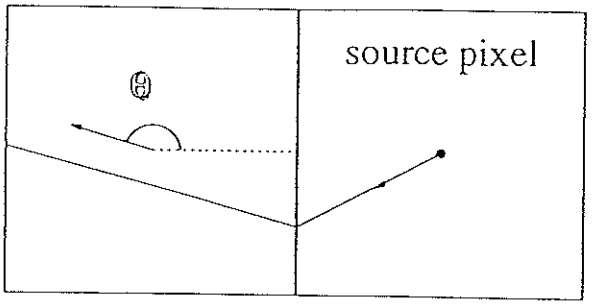

Figure A3.3 The flow-path across adjacent pixels.

The inlet point is also defined with respect to co-ordinates whose origin lies on the SW corner of the new pixel. The relationship between the outlet and inlet points is thus:

Outlet	(1,t)	flows to eastern pixel with inlet	(0,t)
"	(t,1)	flows to northern pixel with inlet	(t,0)
"	(0,t)	flows to western pixel with inlet	(1,t)
"	(t,0)	flows to southern pixel with inlet	(t,1)

where t is an arbitrary parameter defining position along an edge and $0 \leq t < 1$.

Unlike in the previous example where flow originates at the centre of the source pixel, there is a chance that flow starting at the perimeter of the new pixel will not be routed across the pixel at all. Flow will cross a pixel when the aspect vector has a negative component in the direction of the inlet edge (i.e. points away from it). For example if the inlet point is on the eastern edge, as in the diagram above, flow will cross to another edge if $\pi/2 < \theta < 3\pi/2$. In the cases when this does not happen, the slopes of the two pixels face each other and effectively form a valley. Since the inlet edge forms the valley floor, flow is routed along the inlet edge to neighbouring pixels.

When flow is known fully to cross a pixel, it travels along the line from the inlet point in the direction θ. Arbitrary points on this line of the form (x,y) satisfy the equation:

$$(y-y_i)\cos\theta = (x-x_i)\sin\theta \qquad \text{Equation A3.12}$$

The outlet point is defined as the intersection of this line with the edges of the pixel except the inlet edge. Since a line can only intersect the perimeter of a square twice, and it is know that this line intersects the inlet edge, it must intersect precisely one of the other three edges. The edges of the pixel lie on the lines: x=0, y=0, x=1, y=1. Intersecting Equation A3.12 with these lines gives the possible outlet points:

x=1 (Eastern edge)	$(1 , y_i + (1-x_i)\tan\theta)$
y=1 (Northern edge)	$(x_i + (1-y_i)\cot\theta , 1)$
x=0 (Western edge)	$(0 , y_i - x_i\tan\theta)$
y=0 (Southern edge)	$(x_i - y_i\cot\theta , 0)$

Unless $\theta=0$ or $\theta=\pi/2$, each one of these intersection points will be defined, but an intersection with an edge requires the point (x_o,y_o) to be such that $0 \leq x_o, y_o \leq 1$. Intersection points outside of this range are discarded, leaving one legitimate outlet point. As before, this outlet point is translated to the inlet point of the appropriate neighbouring pixel and the process repeated.

In the case where the aspect has positive component in the direction of the inlet edge and a full crossing is not possible, then a prediction can still be made of the flow path. Consider the example illustrated by Fig 5.

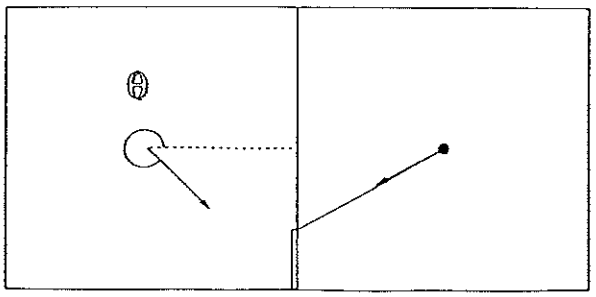

Figure A3.4 An example where full crossing is not possible.

The adjacent pixels have slopes facing each other. From the inlet point of the left pixel, flow is neither possible eastwards nor westwards, but since the aspect has a positive southern component, flow is routed to the most easterly point on the southern edge. In the computer implementation of this algorithm, this point is represented as (0.999999,0). The procedure described here can be generalised to hold for the whole perimeter in the following way. Flow unable to cross a pixel is routed to the edge adjacent to the inlet in the direction with positive aspect component. The outlet point is the point on this edge nearest to the inlet edge.

The algorithm outlined above describes the routing of flow across individual pixels. Flow paths are constructed by the repeated application of the algorithm until the catchment outlet is reached, or a hollow prevents the continued progress of flow. Hollows are represented by groups of pixels whose aspects prevent flow from escaping. This is illustrated by the two examples in Figure A3.5.

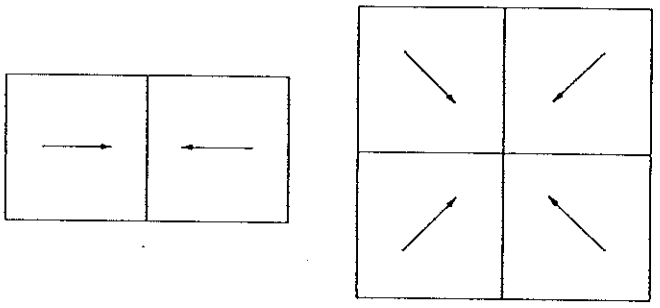

Figure A3.5 Aspect vectors that represent typical hollows.

When constructing flow paths it is therefore necessary to record pixels already in the flow path so that when hollows are reached, flow is prevented from sloshing indefinitely backwards and forwards or round and round.

Appendix 4

Transporting capacity of overland flow based on equations for alluvial channels

Appendix 4 Transporting capacity of overland flow based on equations for alluvial channels

In Section 6.2 of the report a formula is sought which relates the transporting capacity of overland flow to the variables Q (discharge or runoff) and S (land slope) in order to derive a sediment delivery function. The basic equation (given as Equation 6.3) is:

$$T = k_1 Q^a S^b$$

where T = sediment transporting capacity (possible units; tyr^{-1}).

A relationship of this form can be derived directly from empirical formulae used to describe the behaviour of alluvial channels. The deviation is given below in order for the results to be compared with the empirical data obtained by Govers (1990) which are discussed in the main text.

There are a large number of theoretically based, empirically calibrated, sediment transport equations. In general they relate sediment load (or concentration) to such variables as slope, discharge, sediment size and density and channel dimensions (such as depth and cross-sectional area). Since we are seeking a unique relationship between sediment load and the variables Q and S, channel dimension variables must be excluded from the equation since channel depth and width are, themselves, related to Q and S. Before presenting the transport equation it is, therefore, necessary to provide two independent equations which relate channel dimensions to Q and S. The equations describe the 'regime' flow of alluvial channels and are both derived from a large number of field observations. The first is the equation of Lacey for wetted perimeter (p) which states:

$$p = k_3 Q^{½}$$

For channels which are wide relative to their depth (such as will occur in overland flow) we can equate p to w (width). Hence.

$$w = k_3 Q^{½} \qquad \text{Equation A4.1}$$

The second equation is that of Manning which relates mean velocity ($\bar{u}$) to hydraulic radius (R_h) and slope:

$$\bar{u} = n^{-1} R_h^{0.67} S^{0.5}$$

Again for flow which is wide and shallow the hydraulic radius and depth (d) are approximately equal giving

$$\bar{u} = n^{-1} d^{0.67} S^{0.5}$$

Substituting $\bar{u} = Qwd$ and $w = k_3 Q^{0.5}$ gives

$$Q^{0.5} k_3^{-1} d^{-1} = n^{-1} d^{0.67} S^{0.5}, \text{ so}$$

$$d^{1.67} = nk_3^{-1}Q^{0.5}S^{-0.5}$$

$$d = k_4Q^{0.3}S^{-0.3} \qquad \text{Equation A4.2}$$

One of the simplest sediment transport equations which has also been shown to have a fairly high degree of validity over a range of conditions is that of Engelund and Hansen (1967) which can be written as:

$$X = k_5\overline{u}u_*^3d^{-1}$$

where X is sediment concentration
k_5 is a constant for given sediment, and
u_* is the shear velocity = $(gdS)^{0.5}$

so $T = XQ = k_5\overline{u}\ u_*^3d^{-1}Q$

Substituting for u_* and $\overline{u}$ ($=Q^{0.5}k_3^{-1}d^{-1}$ as above) gives

$$T\ k_3^{-1}k_5Q^{1.5}d^{-2}(gdS)^{1.5} = k_3^{-1}k_5gQ^{1.5}d^{-0.5}S^{1.5}$$

Substituting d from Equation A4.2 gives

$$T = k_6Q^{1.5}S^{1.5}(Q^{-0.15}S^{0.15})$$

$$= k_6Q^{1.35}S^{1.65}$$

Hence the values for the coefficients in Equation 6.3 deduced from these regime and sediment transport equations for an alluvial channel are:

a = 1.35
b = 1.65

This report is one of a series on topics of water resources and irrigation, prepared by HR Wallingford Limited and funded by the British Overseas Development Administration.

Others in the series include :

OD 115 Socio-economic parameters in designing small irrigation schemes for small scale farmers : Nyanyadzi case study. Report II : Net agricultural incomes and plot sizes.
M Tiffen & M Glaser

OD 116 Socio-economic parameters in designing small irrigation schemes for small scale farmers : Nyanyadzi case study. Report III : Managing water and group activities; implications for scheme design and organisation.
M Tiffen

OD 117 Socio-economic parameters in designing small irrigation schemes for small scale farmers : Nyanyadzi case study. Report IV : Summary and conclusions.
M Tiffen

OD 118 Workshop on sediment measurement and control, and design of irrigation canals : Digest of technical sessions.
T E Brabben & R Wooldridge

OD 119 Performance of Porac Gumain Rivers Irrigation System : Summary report.
J A Weller

OD 120 A rapid assessment procedure or identifying environmental and health hazards in irrigation schemes : Initial evaluation in northern Nigeria.
P Bolton, A M A Imevbore & P Fraval

OD 121 Socio-economic parameters in designing small irrigation schemes for small scale farmers : The Exchange case study.
F M Chancellor-Weale

OD 122 Sediment discharge measurements - Magat catchment summary report : 1986-1988.
A Dickinson, M B Amphlett & P Bolton

OD 123 Schistosomiasis control measures for small irrigation schemes in Zimbabwe : Results from three years of monitoring at Mushandike irrigation scheme.
M Chimbari, R J Chitsiko, P Bolton & A J Thomson

OD 124 The design of sluiced settling basins : A numerical modelling approach.
E Atkinson